Università degli Studi di Firenze

Scuola di Ingegneria

DIEF - Department of Industrial Engineering of Florence

PhD School: *Energetica e Tecnologie Industrali ed Ambientali Innovative*

Scientific Area: ING-IND/08 - *Macchine a Fluido*

NUMERICAL ANALYSIS OF THE DYNAMIC RESPONSE OF PRACTICAL GASEOUS AND LIQUID FUELLED FLAMES FOR HEAVY-DUTY AND AERO-ENGINE GAS TURBINES

PhD Candidate: ING. ALESSANDRO INNOCENTI

Tutor: PROF. ING. BRUNO FACCHINI

Co-Tutor: DR. ING. ANTONIO ANDREINI

Academic Supervisor: PROF. ING. SERGIO MARIO CAMPOREALE

PhD School Coordinator: PROF. ING. MAURIZIO DE LUCIA

XXVIII PhD School Cycle - 2012-2015

Università degli Studi di Firenze

Scuola di Ingegneria

DIEF - Department of Industrial Engineering of Florence

PhD School: *Energetica e Tecnologie Industrali ed Ambientali Innovative*

Scientific Area: ING-IND/08 - *Macchine a Fluido*

NUMERICAL ANALYSIS OF THE DYNAMIC RESPONSE OF PRACTICAL GASEOUS AND LIQUID FUELLED FLAMES FOR HEAVY-DUTY AND AERO-ENGINE GAS TURBINES

PhD Candidate: Ing. Alessandro Innocenti

Tutor: Prof. Ing. Bruno Facchini

Co-Tutor: Dr. Ing. Antonio Andreini

Academic Supervisor: Prof. Ing. Sergio Mario Camporeale

PhD School Coordinator: Prof. Ing. Maurizio De Lucia

XXVIII PhD School Cycle - 2012-2015

A chi ha creduto ed a chi continua a credere in me...
a chi mi ha insegnato ed a chi continua tuttora ad essere un
esempio di umiltà...
a chi ha instillato in me la curiosità e la volontà.

Ringraziamenti

Arrivati al termine di questi anni di Dottorato finalmente ho l'occasione di ringraziare le persone che mi hanno accompagnato, consigliato e sostenuto durante tutto il mio percorso.

In primo luogo desidero ringraziare il Prof. Bruno Facchini che mi ha dato la possibilità di intraprendere questa intensa esperienza di studio, ricerca ma anche e soprattutto di vita. Grazie anche per la cordialità e la fiducia dimostratemi. Un ringraziamento particolare va all'Ing. Antonio Andreini che mi ha seguito ed indirizzato passo passo durante questi anni: preziosissima guida!

Ringrazio con piacere anche il Prof. S.M. Camporeale del Politecnico di Bari per il lavoro di controrelazione alla presente tesi.

Desidero inoltre ringraziare l'Ing. Matteo Cerutti di GE Oil & Gas e l'Ing. Antonio Peschiulli di GE Avio, che hanno seguito costantemente gli sviluppi del mio lavoro e per le stimolanti conversazioni avute.

Non possono poi mancare i ringraziamenti ai miei colleghi, compagni di avventura e amici con i quali ho condiviso momenti indimenticabili.

Infine, voglio ringraziare mia madre, che da sempre mi sprona ed è per me un modello di energia ed intraprendenza e fonte inesauribile di serenità, e la mia Francesca per essere al mio fianco, sopportarmi e sostenermi in ogni momento.

Fatelo! E se lo fate, fatelo bene.

Sergio Scifo

(Professore al Liceo scientifico G. Castelnuovo, Firenze)

Do it! And if you do it, do it well.

Sergio Scifo

(Professor at the scientific High school G. Castelnuovo, Florence)

Abstract

Lean premixed combustion technology is regarded as the most effective one to achieve the recent legislation limits on NOx emissions. One of the most critical issues affecting this kind of technology is the occurrence of combustion instabilities that may compromise the combustor life and integrity so that the prediction of the thermo-acoustic behaviour of the system becomes of primary importance.

This research activity is aimed at developing reliable tools to be used in the industrial design process, which are able to describe the complex interaction between the system acoustics and the turbulent flame. The results, in terms of Flame Transfer Function, will be then exploited for the thermo-acoustic linear stability analysis on lean-burn combustors, with Finite Elements codes. The flame response is computed exploiting Unsteady-RANS simulations of the reactive case and System Identification techniques.

The procedure is then applied to the study of a practical GE Oil & Gas gas turbine combustor, in the framework of a collaboration with the industrial parten GE Oil & Gas and in part within ATENE (Advanced Technologies for ENergy Efficiency) project funded by Regione Toscana, with the aim of giving more physical insight on the dynamic response of the real flame and understanding the driving mechanism of thermo-acoustic instability onset as well. A reliable numerical model has been generated and assessed through comparisons with results from full-annular combustor experimental campaign carried out by GE Oil & Gas. The inclusion in the final model of several driving mechanisms (air and fuel mass flow

fluctuations) constitute a novel aspect in FEM studies of industrial gas turbine combustor configurations.

Furthermore, the methodology is then employed, in the framework of LEMCOTEC (Low Emissions Core-Engine Technologies) EU project, to understand the driving mechanisms that regulate the coupling between heat release rate fluctuation and the acoustic field in aero-engines, in an innovative way. Great attention has been devoted to the impact of liquid fuel evolution and droplet dynamics. For this purpose the GE-AVIO advanced PERM (Partially Evaporating and Rapid Mixing) lean injection system has been analysed focussing the attention on the effect of several modelling parameters on the processes involved in liquid fuel evolution and heat release. A set of advanced post-processing tools has been also set-up and exploited to get even more insight on the complexity of such kind of the flames and pointing the way for further enhancements. The application is one of the few in literature where the liquid flame dynamics is numerically investigated providing a description in terms of FTF and detailed information on the physical phenomenon. Therefore, it constitutes and important step forward in the numerical methodology developed for analysing the thermo-acoustic response of GE AVIO lean burn combustor equipped with PERM injection system family.

Contents

List of Figures

List of Tables

Nomenclature

A	Area	$[m^2]$
	Zimont's model constant	$[-]$
	Amplitude	$[-]$
c	Sound speed	$[m\ s^{-1}]$
	Reaction progress variable	$[-]$
c/C	Cross correlation vector	$[-]$
c_p	Spec. heat capacity (constant pressure)	$[J\ kg^{-1}\ K^{-1}]$
c_v	Spec. heat capacity (constant volume)	$[J\ kg^{-1}\ K^{-1}]$
C_r	Crest factor	$[-]$
d	Diameter	$[m]$
D_{32}	Sauter Mean Diameter	$[m]$
e	Internal energy	$[J\ kg^{-1}]$
f	characteristic wave amplitude	$[-]$
F	Transfer function	$[-]$
	Flame identifying function	$[-]$
FAR	Fuel to Air Ratio	$[-]$
g	characteristic wave amplitude	$[-]$
G	Stretch factor	$[-]$
h	Unit impulse response vector	$[-]$
k	Kinetic energy	$[m^2\ s^{-2}]$
	Wave number	$[m^{-1}]$
	Thermal conductivity	$[W\ m^{-1}\ K^{-1}]$
L	Vector length	$[-]$
	Length	$[m]$
LHV	Lower Heating Value	$[J\ kg^{-1}]$
$\mathcal{L}$	Losses	
M	Model order	$[-]$
n	interaction index	$[-]$

OPR	Overall Pressure Ratio	$[-]$
p	Pressure	$[Pa]$
PFR	Product Formation Rate	$[s^{-1}]$
q/Q	Heat release	$[J\ kg^{-1}]$
q	Spread parameter in Rosin-Rammler distribution	$[-]$
Q	Measure of identification quality	$[\%]$
R_g	Gas constant	$[J\ kg^{-1}\ K^{-1}]$
S	Entropy	$[J\ K^{-1}]$
S_c	Source of progress variable c	$[kg\ m^{-3}\ s^{-1}]$
S_L	Laminar flame speed	$[m\ s^{-1}]$
S_T	Turbulent flame speed	$[m\ s^{-1}]$
t	time	$[s]$
T	Temperature	$[K]$
	Period	$[s]$
TKE	Turbulence Kinetic Energy $[m^2\ s^{-2}]$	
u/U	Velocity	$[m\ s^{-1}]$
V	Volume	$[m^3]$
WF	Weighting function	$[-]$
x	Input signal	$[-]$
$\mathbf{x}$	coordinate vector	$[-]$
X	Mean droplet diameter	$[m]$
y	System output (response)	$[-]$
Y_k	Mass fraction of the k-th specie	$[-]$
Z	Mixture fraction	$[-]$
Acronyms		
$ACARE$	Advisory Council for Aeronautics Research in Europe	
BC	Boundary condition	
BTM	Burner Transfer Matrix	
$CAEP$	Committee on Aviation Environmental Protection	
CFD	Computational Fluid Dynamics	
CTA	Constant Temperatuer Anemometry	
$DACRS$	Dual Annular Counter Rotating Swirl	
DES	Detached Eddy Simulation	
DLN	Dry-Low NOx	
DNS	Direct Numerical Simulation	
EU	European Union	
FEM	Finite Element Model	

FGM	Flamelet Generated Manifold
FFT	Flame Transfer Function
FR	Finite Rate
FTF	Flame Transfer Function
GGI	General Grid Interface
GIS	Grid Induced Separation
HT	High Turbulence
$KIAI$	Knowledge for Ignition, Acoustics and Instabilities
$ICAO$	International Civil Aviation Organization
LDI	Lean Direct Injection
LES	Large Eddy Simulation
$LEMCOTEC$	Low Emissions Core Engine Technologies
LPC	Lean Premixed Combustor
$LODI$	Local One-Dimensional Inviscid
$LP(P)$	Lean Premixed (Prevaporised)
LTI	Linear Time Invariant
LTO	Landing Take-Off
$MISO$	Multi-Input Single-Output
$NEWAC$	NEW engine Architecture core Concepts
$NRBC$	Non-Reflective Boundary-Conditions
$PERM$	Partial Evaporation Rapid Mixing
PDF	Probability Density Function
PIV	Particle Image Velocimetry
PMX	Premixer/d
PIL	Pilot
POD	Proper Orthogonal Decomposition
PVC	Precessing Vortex Core
$RASW$	Random Amplitude Square Wave
RB	Random Binary
RN	Random Number
$RANS$	Reynolds Averaged Navier-Stokes
RQL	Rich-Quench-Lean
SAC	Single Annular Combustor
SAS	Scale Adaptive Simulation
SI	System Identification
$SISO$	Single-Input Single-Output
SMD	Sauter Mean Diameter

TAB	Taylor-Analogy Breakup
$TAPS$	Twin Annular Premix System
TFC	Turbulent Flame speed Closure
TM	Transfer Matrix
UHC	Unburned Hydro-Carbons
UIR	Unit Impulse Response
ULN	Ultra Low NOx
$URANS$	Unsteady RANS

Greeks

γ	Heat capacity ratio	$[-]$
ϵ	Energy of the periodic flow component	$[J\ kg\ m^3]$
ε	Turbulence eddy dissipation	$[m^2\ s^{-3}]$
Γ	Auto-correlation Matrix	$[-]$
λ	Eigenvalue	$[rad]$
	Air to Fuel ratio	$[-]$
Θ	Phase difference	$[rad]$
	Model constant in Eckstein FTF model	$[-]$
ρ	Density	$[kg\ m^{-3}]$
σ	Model constant in Eckstein FTF model	$[-]$
	relaking parameter in the NRBC	
$\sigma_{i,j}$	Stress tensor	$[Pa]$
τ	Delay time	$[s]$
μ	Dynamic viscosity	$[Pa\ s]$
ω	Angular pulsation	$[rad\ s^{-1}]$
Δ	Spacing	$[m]$
ϕ	Equivalence Ratio	$[-]$
	Phase	$[rad]$
Ψ	General flow variable	
χ_u	Thermal diffusivity of unburnt gasses	$[W\ m^{-1}\ K^{-1}]$

Subscripts

A	Air
b	Burner
CF	Choked Fuel line
F	Fuel
k	Kinetic
p	Potential
r	Reference
w	Wall

Superscripts

a	Periodic flow component
eq	Equilibrium
t	Turbulent flow component

Miscellaneouss

$\vec{\widetilde{\cdot}}$	Density-weighted Average
$\bar{\cdot}$	Time Average
$\cdot'$	Fluctuation over the mean quantity
$\hat{\cdot}$	Complex amplitude
$\lvert\cdot\rvert$	Modulus
$\triangle$	Difference

Introduction

Context of the Present Research

The stringent regulations of these last years on gas turbines pollutant emissions for both heavy-duty and aero-engine applications, in particular on NOx, have led gas turbine producer and engineers to optimise the combustors concept design, adopting advanced combustion technologies. Lean premixed combustion technology is nowadays regarded as the most promising one, allowing it a drastic reduction of nitrogen oxides emission [1, 2]. Nowadays, lean premixed technology is the state of the art for heavy-duty gas turbine combustion systems and the one aero-engine producers count on to achieve stricter and stricter legislation limits. NOx formation rate, in fact, drastically depends on the composition and temperature levels within the combustion chamber. In particular, if a mixture composition that is instantaneously or locally close to stoichiometric values (to which are associated high temperature levels), NOx production increases rapidly, with a marked impact on the overall emission levels. Therefore, great efforts are devoted to the attainment of a homogeneous mixture before entering the combustor in order to limit the mentioned non-uniformities and in turn, pollutant formation.

In case of heavy-duty practical burners which operates with gaseous fuels, the fuel and air are pre-mixed in the injection system before the combustor. Dedicated designs are exploited where high turbulence levels, swirled flows and cross flow-jet configurations are realised within the injector with the main aim of intensifying the mixing between fuel and

oxidant. In case of aero-engine combustion systems operating with liquid fuels, a mixture as much uniform as possible is generated through a proper design of the injection system which has to realise a very fine atomization of the injected fuel and to promote a rapid mixing with the air. In this way the combustion process can be moved towards lean premixed-like modality [3].

One of the most critical issues of lean combustion technology is the occurrence of combustion instabilities related to a coupling between pressure oscillations and thermal fluctuations excited by unsteady heat release. Such instabilities may damage combustor's components and limit the range of stable operating conditions so that the prediction of the thermo-acoustic behaviour of the system in the early design phase becomes of primary importance. Among the methods used to predict thermo-acoustic instabilities in a combustor, such as the solution of full three-dimensional unsteady Navier-Stokes equations or low-order methods as 1D-acoustic elements networks, Finite Element Methods (FEM) may be used to solve for the complete 3D problem. Because of the reasonably low computational cost, the numerical study of thermo-acoustic instabilities using FEM is of great interest for industrial applications. The set of linear transport equations for the perturbations of velocity, temperature and density can be derived by linearising the Navier-Stokes equations [4]. It is often assumed that the mean flow is at rest so that a wave equation for the acoustic perturbations can be derived, where the local unsteady heat release appears as a forcing term.

The effect of the flame presence and of a fluctuating heat release on the system acoustics is concentrated in this term which necessitates of an accurate formulation. To model the effect of a fluctuating heat release on the acoustics, a deep understanding and a proper description of the flame dynamics are necessary.

The flame can be considered a black-box input-output system, with the driving mechanisms as inputs and the unsteady heat release as output. For sufficiently small levels of perturbation, the flame response can be considered linear. Therefore usually, each input is related to the output

through a so-called Flame Transfer Function (FTF). A perfectly premixed flame can be described as a Single-Input Single-Output system and its response is governed by air mass flow fluctuations only. However, in a real combustion system, together with air mass flow rate fluctuations, also fuel mass flow fluctuations can contribute to the dynamic response of the flame. More in general, a flame system can be regarded as a Multi-Input Single-Output system. For liquid fuel flames the situation is even more complex due to the effects that acoustic perturbations have on the liquid fuel related processes such as atomization, evaporation and successive gas phase evolution and mixing. Simple Flame Transfer Function formulations are very often adopted that, in many cases, are inadequate to represent the complex physics lying behind the flame dynamic response. Moreover, sometimes the used models need a proper calibration of the model constant to be adapted to the particular application [5], that is usually done empirically. Otherwise, the FTF may be obtained experimentally but it can be very difficult, expensive and requires very careful experimental work (especially in the presence of turbulent flows and complex geometries or flame configurations) together with sophisticated post-processing and long test runs [6]. An alternative attractive way to determine the FTF is its computation from computational time series data generated with unsteady CFD simulations where the flame dynamics is reproduced.

A simulation is performed exciting the system with a carefully designed broadband signal while recording the time series of the system inputs and heat release fluctuations. Exploiting System Identification (SI) post-process techniques it is possible to obtain the FTFs relating each input to the output of the system thus completely characterising the flame response.

Aim of the Work

The main objective of this research is the development of numerical tools for the study of the dynamic flame response of practical burners typical of industrial and aero-engine applications.

A methodology has been set-up and simulation practices given in order to perform an unsteady reactive simulation of the flame response when acoustically forced. The SI tools for the CFD results post process and the FTFs computations have been implemented starting from what available in literature and validated on relatively simple test case of a perfectly-premixed experimental flame.

Since numerical tools are intended to be used in an industrial design context, particular attention has been dedicated to find a trade-off between the computational cost and a meaningful representation of the physical phenomena, in the numerical procedure development.

The assessed numerical tools are then exploited to study a practical flame for heavy-duty gas turbine with the main aim of providing greater insight of the coupling mechanisms responsible for the flame dynamic response. The effect of fuel mass flow fluctuations is also introduced as further driving input, describing the flame as a Multi-Input Single-Output system. The obtained results are implemented into a finite element model of the combustor, realized in COMSOL Multiphysics, with the main aim of developing an affordable numerical modelling tool to analyse the system stability and to be used in GE Oil & Gas since the early phases of the design and development of a heavy-duty gas turbines. Usually, in industrial studies of combustor stability fuel mass flow fluctuations as driving mechanism are neglected, considering a chocked fuel line. Therefore, the presented application is one of the few cases in literature where the model is refined in this way and to the author's knowledge, the first one to be applied to FEM study of thermo-acoustic stability of real combustors. Precise indications are given on the role of fuel mass flow fluctuations on the physics of the practical flame and on the erroneous predictions deriving by neglecting them. Further in-depth studies are carried out on pilot flames aiming at replicating the dynamic response of the real flame and understanding the driving mechanism of thermo-acoustic instability onset as well.

As further goal, the methodology is applied to numerically study a liquid fuel flame dynamics. The investigated combustor is equipped with

a GE-AVIO PERM (Partially Evaporating and Rapid Mixing) advanced injection system. The understanding of liquid fuel flame dynamics still represents a quite uncharted problem area, so that the main aim of this application is to be able to get more information on the flame response to acoustic perturbations and its relation with the liquid fuel evolution within the combustor. Such an application to liquid fuel combustion together with the information derived constitute one of the few numerical study aimed at the understanding of the flame dynamic for aero-engine applications and provide a description of it in terms of FTF. The impact of the several modelling parameters together with the main modelling strategies needs to be accurately investigated and assessed. Moreover, a series of advanced post-process instruments are to be set up, to enhance the understanding of the complex physics of such configurations, and eventually used as a further investigation instrument. The obtained results are an important step forward in the numerical modelling of the dynamics of liquid fuel flame and towards the fulfilment of the objective of developing more suitable FTF formulations to be used in lean burn aero-engines analyses.

The activity that led to the results presented in this dissertation carried out thanks to the collaboration with the industrial partners GE Oil & Gas and GE AVIO and in the framework of two main projects: ATENE (Advanced Technologies for ENergy Efficiency) project founded by Regione Toscana, concerning the heavy-duty gas turbine application, and LEMCOTEC (Low Emissions Core-Engine Technologies) EU project in the context of aero-engine application.

Thesis Outline

The present work is structured as follows:

Chapter 1 Technical Background The context into which the work has been carried out, of low emission engines is presented. The chapter is focused on the limitations that characterize standard heavy-duty and aero-engine combustors and that motivate the efforts aimed at

the implementation of the lean burn technology, with all the related the issues. Moreover, the basics of the theory of combustion instabilities are given at the end.

Chapter 2 Numerical Study of Combustion Instabilities Commonly used approaches to predict thermo-acoustic instabilities in a combustor are presented. Following, theoretical notions on premixed and technical flames dynamics and modelling exploiting important results from the literature are given, with particular focus on Flame Transfer Function estimation from CFD/SI coupled approach.

Chapter 3 Numerical Methods for Flame Dynamics Investigation and Thermo-acoustic Stability Analysis Details on the numerical methods, strategies, post-processing techniques used in this work are presented in this chapter. The basics of the System Identification theory are also presented herein.

Chapter 4 Application to a Perfectly-Premix Lean-Burn Combustor The procedure described in previous chapters is applied for the study of a perfectly premixed experimental flame. Results that allowed the validation of the methodology are discussed in this chapter.

Chapter 5 Numerical Analysis of the Dynamic Flame Response of a Technically-Premixed Gaseous Flame for Heavy-Duty Applications In this chapter the application of the methodology and a stability analysis of a lean-premixed gas-turbine full-annular combustor for heavy-duty gas turbine are presented. Further refinement of the model have been proposed analysing the effects of several driving mechanisms on the flame response and on the stability of the system. Valuable design indications emerged in the analyses are also presented here.

Chapter 6 Numerical Study of the Dynamic Response of a Liquid Fuel Flame for Aero-Engine Applications The dynamics of a spray flame generated by a PERM injector has been numerically studied in this chapter. The CFD/SI method, successfully applied at perfectly and technically premixed gas flame, has been used to investigate a liquid fuelled flame dynamics. The main findings are discussed in this chapter

together with the results of advanced post-process investigations.

Chapter 7 Conclusions In the last chapter, a summary of the main achievements of this research is given together with conclusions and recommendations for future research.

Chapter 1

Technical Background

1.1 Recent Development of Low-Emission Gas Turbine Combustors

The development of gas turbine engines for power generation and propulsion applications has been driven for years by the goal of increasing performance and efficiency, which are greatly dependent on turbine inlet temperature. Therefore, great efforts have been put in rising this parameter without any particular attention at the combustion regime or modality. Typically, diffusion-flame combustors were used, because of their reliable performance and reasonable stability characteristics [7]. However, high levels of pollutant emissions, in particular thermal NOx, are usually produced with this type of combustors so that the stringent regulations of these last years on gas turbines pollutant emissions have led engine manufacturers to develop combustors concept designs that meet various regulatory requirements ([8] [1]).

All major international environmental authorities (US EPA, European Commission, local environmental ministries) are introducing increasingly stringent limits to the amount of pollutants emitted by industry. Gas turbines are an important contributor to pollutants such as NOx, CO, UHC, and as such, they are subject to regulatory restrictions applicable

to new installations and, in many cases, also to units already installed
and running for a long time [9]. For commercial aircraft, nitrous oxides
(NOx) abatement is considered a mayor target in this effort; the ICAO-
CAEP standards (see Figure 1.1) imposed the reduction of such pollutant
emissions, leading to the improvement of combustion processes to meet
the prescribed constrictions.
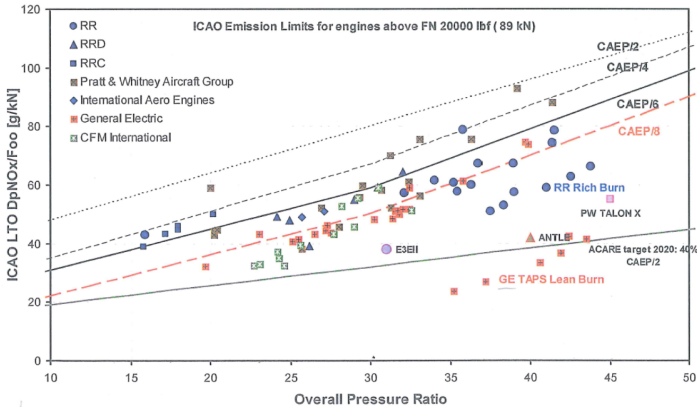
Figure 1.1: NOx emission limits for engines above FN 20000 lbf (89 kN)
as a function of OPR [10].

Among all the factors influencing pollutant emissions from gas tur-
bine combustors, the most important is by far the temperature of the
combustion zone [2].

The typical ranges of temperature reached with conventional combus-
tors are indicated in Figure 1.2. At low-power operations, temperature
decreases at around 1000 K so that too much CO is produced, while, at
full-load conditions, temperature rises to 2500 K and excessive amounts of
NOx are formed. Only in the fairly narrow band of temperatures between
1670 and 1900 K the levels of CO and NOx are below 25 and 15 ppmv,
respectively.

Due to the tough dependency of NOx formation rate on temperature,
a precise control of reactants composition is mandatory. It has been
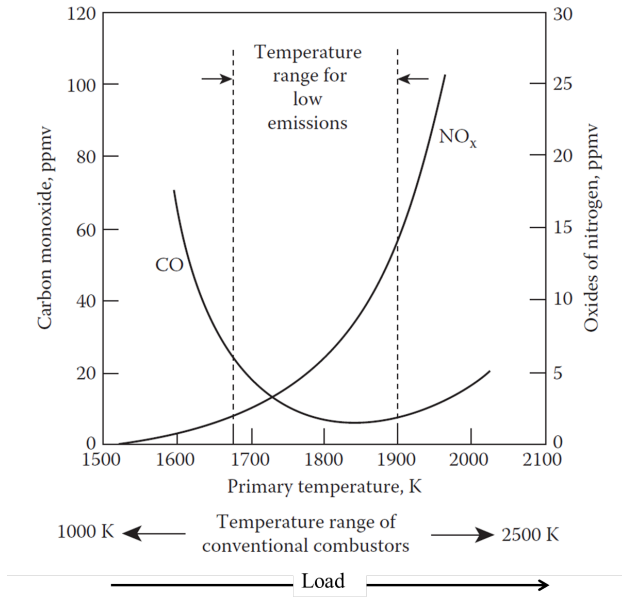
Figure 1.2: Influence of combustion zone temperature on CO and NOx emissions [2].

observed that both spatial and temporal variations in the fuel/air mixing will impact emissions of NOx [11, 12]. NOx production increases rapidly whenever a pocket of mixture, instantaneously or locally richer than the average, is consumed, and the impact on overall NOx emissions can be severe even if the deviation from the mean equivalence ratio is small [13]. Therefore, the level of premixing begins to take on a critical role in the performance of the combustor and additional efforts have been put in strategies to rapidly and completely mix the fuel and air prior to combustion [14]. Lean Premixed Combustion (LPC) nowadays can be considered the most effective solution to control CO production rising the residence time in combustion chamber, without impact on NOx emissions, thanks to the lower temperatures [1, 2]. Extremely well premixed flames exhibit ultra-low NOx, CO, and UHC emissions if the flame temperature

is maintained below 1900 K and a sufficient residence time is guaranteed [15]. It is worth pointing out that the definition "lean" refer to a local level of equivalence ratio. For gas turbine combustion, it is insufficient to consider an overall lean combustion situation. What is meant by lean herein is operation at locally lean conditions in the combustion zone. This is accomplished only when the fuel and air are premixed.

1.1.1   Industrial Low-Emission Combustors

As far as heavy-duty gas turbine combustors are concerned, lean premixed technology is nowadays the state of the art. In a practical LPC, the fuel and air are premixed within the injector to achieve a lean, uniform mixture inside the combustor. In order to improve the mixing process, premixer designs that enhance turbulence levels in the nozzle, against increased pressure losses are often employed. Typical lean combustion strategies basically involve mixing the fuel and air far upstream of the reaction zone. Various approaches are used in swirl-stabilized combustion systems including fuel injection through the swirl vanes. With gaseous fuels, hundreds of injection points can be used to distribute the fuel over the injector exit plane [14]. As an example, in Figure 1.3 is shown a GE burner for heavy-duty lean-premixed gas turbine. In particular the configuration presents a Dual Annular Counter Rotating axial Swirl (DACRS) nozzle, where the fuel is injected from the outer annuls and the mixing with the feeding air is enhanced by the interaction of the two swirled flows and is completed through the converging nozzle.

However, the intense search for highly premixed mixtures makes the flame more prone to thermoacoustic instabilities.

Moreover, in case the flame temperature is kept low, operations can be limited by lean blow-out occurrence.

In order to provide operability for lean premixed gas turbines, it is very common to rely on a *pilot* injector of some sort. The pilot often consists of a discrete injection of either pure fuel or of a relatively rich fuel/air mixture. The pilot is generally directed into a specific location in the combustor to enrich a region that will help sustain the reaction[14].
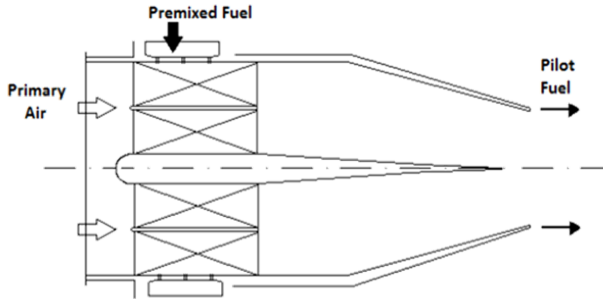
Figure 1.3: GE Double Annular Counter Rotating Swirl Nozzle for heavy-duty lean premixed combustor.

Another proposal involves staged combustion, meaning both fuel staging operations or staged combustor architectures in which combustion chamber is divided into smaller chambers with each zone controlled separately and optimally [16].

With this technique, fuel is supplied only to selected combinations of fuel injectors at different operating conditions as illustrated in Figure 1.4 illustrates typical partial load staging operations where the fuel is supplied only to selected combinations of fuel injectors. Only at the highest level of power is the full complement of fuel injectors employed. The objective of this modulation technique is to raise the equivalence ratio and hence also the temperature of the localized combustion zones at low-power operation thus reducing CO and UHC emissions, and realizing the added advantage of extending the lean blowout limit to lower equivalence ratios [2].

A typical staged architecture, instead, has a lightly loaded primary zone, which provides all the temperature rise needed to drive the engine at low-power conditions, operating at equivalence ratio of around 0.8. At higher power settings, its main role is to act as a pilot source of heat for the main combustion zone, which is supplied with a fully premixed fuelair mixture. When operating at maximum power conditions, the equivalence ratio in both zones is kept low at around 0.6 to minimize NOx and smoke [2].
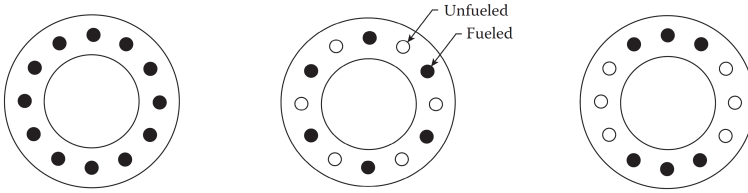
Figure 1.4: Illustration of the use of selective fuel injection [2].

An example of staged combustor is the GE DLN1, employed in several MS5002 series machines. For a detailed description of the device refer to [17]. Fuel flow is injected in each combustion zone through the primary and secondary fuel nozzles so that the combustion system is arranged as a two-staged architecture.

The operation of the DLN1 technology is based on four different modes activated in sequence from ignition to base-load premix conditions (Figure 1.5). The description for each is briefly reported below according to Thomas et al. [19]:

- *Primary mode*: Only primary nozzles are fuelled. Flame is in the primary zone only. This mode of operation is used to ignite, accelerate, and operate the machine over low to mid-loads, up to a pre-selected combustion reference temperature.

- *Lean-Lean mode*: Both the primary and secondary nozzles are fuelled. Flame is in both the primary and secondary zones. This mode of operation is used for intermediate loads between two pre-selected combustion reference temperatures.

- *Secondary mode* Secondary nozzle only is fuelled. Flame is in the secondary zone only. This mode is a transition state between lean-lean and pre-mix modes. This mode is necessary to extinguish the flame in the primary zone, before fuel is reintroduced into what becomes the primary pre-mixing zone.
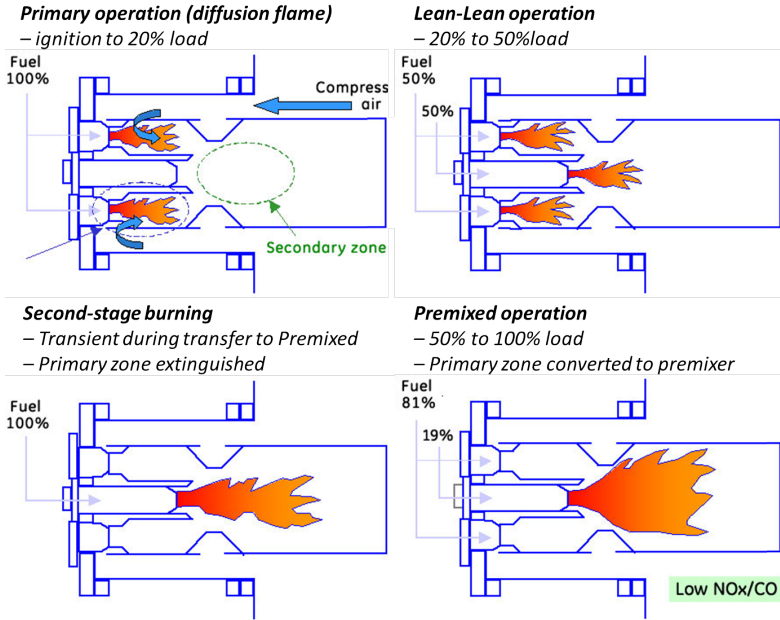
Figure 1.5: DLN1 modes of operation [18].

- *Premixed mode*: Both the primary and secondary nozzles are fuelled. Flame is in the secondary zone only. This mode of operation is achieved at and near the combustion reference temperature design point. Lower emissions are generated in premixed mode.

Another well established low-emission burner design is the Alstom EV burner in Figure 1.6. The EV burner is the standard burner for the GT13E2 fleet and for all Alstom gas turbines. The burner is a dual fuel burner system for dry low NOx natural gas combustion and for liquid fuel combustion with water injection. During startup of the GT13E2 gas turbine, pilot fuel gas is injected over the central lance and leads to a fuel enrichment of the burner core flow. A broad stable range is therefore guaranteed under this condition. At higher load, the burner is operated

in the full premix mode in order to achieved the lowest emission. A sketch
of these different modes is shown in Figure 1.6.
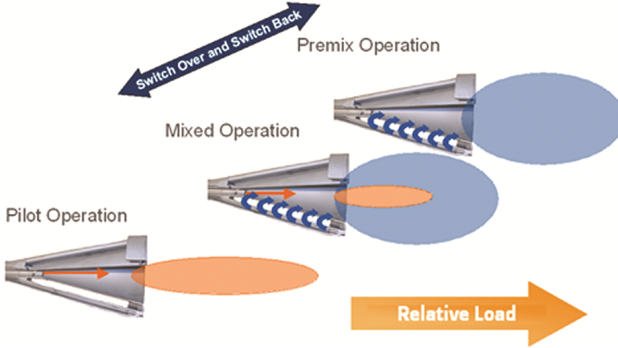
Figure 1.6: Alstom EV burner: operation modes [20].

An example of an aero-derivative gas turbine can be found in the
LM6000 combustor in Figure 1.7 that employs a triple annular design for
fuel staging to achieve an ultra-lean flame with a reduced temperature.
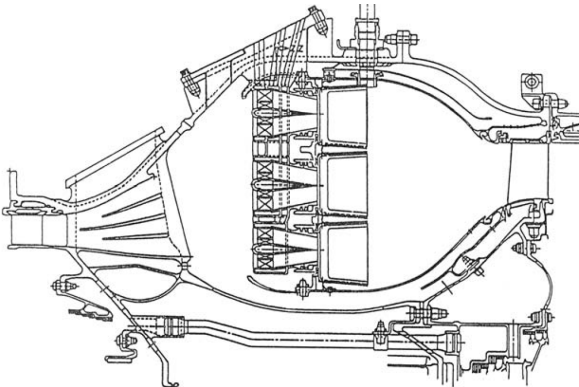
Figure 1.7: GE LM6000 Dry-Low NOx combustors [2].

However, a disadvantage of splitting the combustor in more than one
zone is that the overall size and the number of parts increase significantly,

thus leading to serious penalty on cost and weight. Also due to their geometrical complexity these combustors have relatively large surfaces to be cooled, leaving, for a given cooling technology, less air available for the lean injectors and so limiting partially the expected gain in NOx emissions. This drawback can be overcome with advanced cooling systems but to detriment of cost [21].

1.1.2   Combustors for Aeroengines

Most of the aeroengines currently employed in the civil aviation sector, which are subjected to the mentioned ICAO standards (Foo > 26 kN), employ the Rich Quench Lean (RQL) combustion technology. The latter, in fact, offers the optimal trade-off between emissions, safety and stability.

(a) RQL concept   *(b) RQL combustor scheme (RR Trent XWB)*
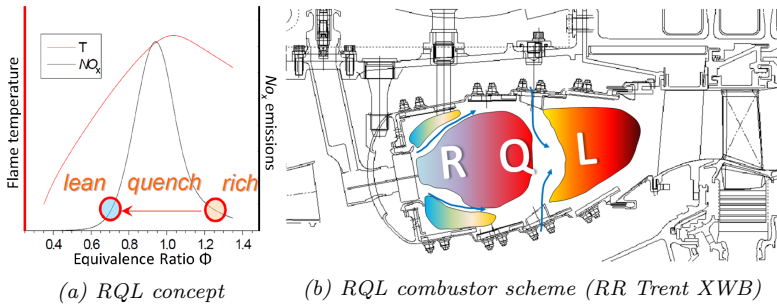
Figure 1.8: Rich-Quench-Lean combustor concept.

The scheme is shown in the scheme in Figure 1.8. A rich primary combustion is realized to guarantee stability. Moreover, at $\phi = 1.2 - 1.6$ NOx emissions are kept at low levels due to the relatively limited temperature levels and the limited concentration of oxygen. Successively, a rapid mixing is realized injecting dilution air realizing a quenching of the reactions. The operation point is then suddenly moved to lean$-$burn conditions ($\phi = 0.5 - 0.8$) where, nevertheless, gas mixture is hot enough to complete the reaction and burn out smoke. The main focus and the technological issues lie in ensuring rapid mixing to minimize the residence

time at the stoichiometric condition, at which is associated the maximum NOx production [22].

In order to meet the next emissions standards and regulation limits, the main aero-engines manufacturers are developing alternative combustion technologies. If, on the one hand, Pratt & Whitney has continued to evolve RQL strategies for its commercial engines, on the other hand, GE and Rolls-Royce have focused on lean combustion approaches [14].

The implications for lean operation include several design modifications as a consequence of the different combustion strategy. Figure 1.9 illustrated the main differences between a conventional RQL and lean premixed combustors. In the conventional approach, the fuel is injected directly into the combustion chamber along with approximately 30% of the total air entering the combustor. In the lean combustion strategy shown, the fuel is premixed with about 60% of the combustor air flow. Hence, much more air enters the primary zone in the lean premixed case. This also reduces the amount of airflow available for cooling which can be a concern for maintaining liner integrity and can also impact the opportunity to properly tailor temperature profiles to meet the requirements of turbine materials at the turbine inlet [14]. As it is possible to see from the same Figure (1.9) also LPC design is modified if compared to RQL ons. In particular, the increase of residence time in the combustor, necessary to complete the combustion, in lean premixed combustor is realised increasing the volume of the device. Modern combustors has, in fact, a volume twice the conventional one and, in general, there is no a subdivision in a primary and a secondary (dilution) zone. The mixture enters the combustion chamber already at low equivalence ratios.

Staged combustors can be found also in aeroengine applications, though the trend in the aeroengine development is the realization of internally staged injectors in single annular combustors.

Before entering the reaction zone a premixing between fuel and oxidant has to be obtained. Even if it is relatively simple to obtain premixed mixture in case of gaseous fuels, it is a more difficult task using liquid fuels. Moreover, the process is deeply influenced by the operating conditions, e.g.
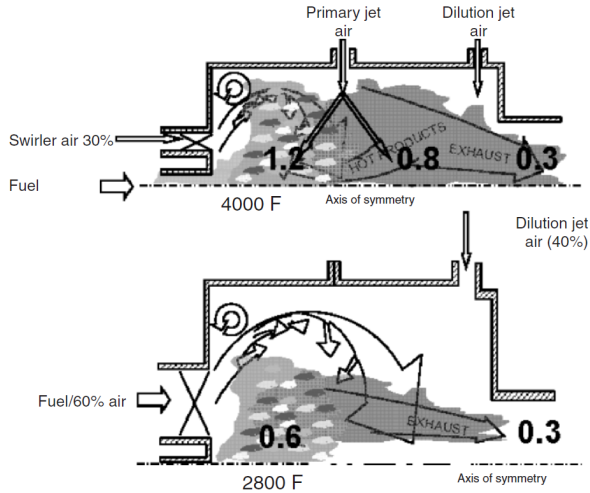
Figure 1.9: Comparison of the main features for conventional (top) and lean premixed (bottom) combustor design [14].

air temperature and pressure and it is difficult to scale to various engine sizes due to various non-linear effects. A change in aero-engine size then, results in changes of engine cycle, combustor inlet pressure, temperature and nominal FAR with a direct impact on low NOx injector performance. Therefore, the injection system technology should be adapted to the specific application.

At the moment, General Electric is the only manufacturer to produce lean injectors for civil aero-engines: the TAPS (Twin Annular Premix System) injector, currently used on the GEnx engine, entered in service in 2010. The TAPS combustor concept is a lean burn system where each fuel injector contains a center pilot and concentric outer main as shown in Figure 1.10. The central pilot flame is a rich burn configuration, where 100% of the fuel is directed at starting and low power operation. At higher

power approximately 70% of the air flow passes through the injector and most of the fuel is injected through the main swirler, thus providing a lean combustion.
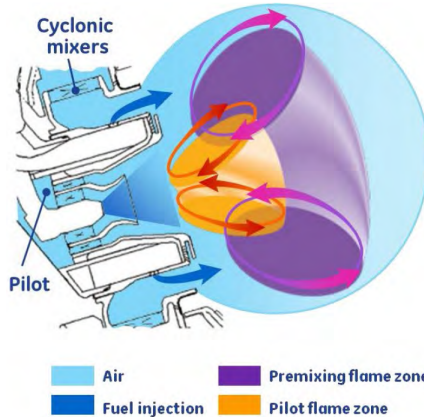
Figure 1.10: TAPS Fuel Injection Concept [23].

In the European Union context, several research programmes have been funded with the main aim of developing lean combustion technology. As an example, in NEWAC (NEW Aero-Engine Core Concepts), an Integrated Project co-funded by the European Commission within the Sixth Framework Programme, two different combustion technologies were investigated (see Figure 1.11): LPP (Lean Premixed Pre-vaporized) and LDI (lean direct injection) concepts.

- LPP concept is based on the action of several air flows, one devoted to the fuel atomization and the second dedicated to the mixing and fuel evaporation. The combination of the two acts also as a promoter for the flame stabilization in the combustion chamber [21]. The LPP concept has been shown to have the lowest NOx emissions, but for advanced high-pressure-ratio engines, the possibility of autoignition or flashback precludes its use. It is targeted for an Overall Pressure Ratio (OPR) lower than 25.
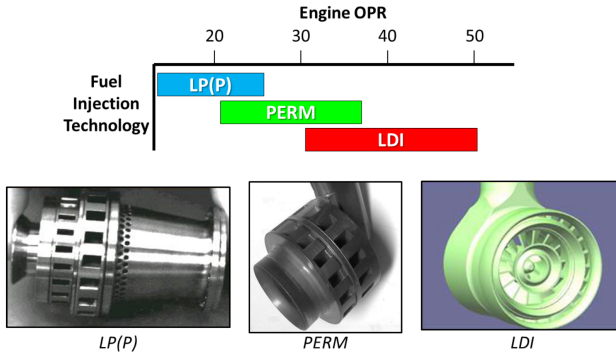
Figure 1.11: LP(P), PERM and LDI injectors and relative operating OPR ranges.

- LDI differs from the other as the fuel is injected atomized directly into the flame zone, and thus, it does not have the potential for autoignition or flashback and should have greater stability. It can be used at higher OPRs ($25 \div 50$). However, since it is neither premixed nor pre-vaporized, a good atomization is necessary to limit NOx formation and the fuel must be mixed quickly and uniformly, so that flame temperatures are kept low. In the context of the same project, GE AVIO developed a particular LDI injector: the PERM injector. With the purpose of overcoming flashback issues at OPRs in the range of $25 \div 35$, the PERM injector has been developed aiming at achieving a partial evaporation of the fuel within the swirler and the rapid mixing within the combustor. PERM design is based on a double swirler airblast with a pilot fuel injection located in the inner swirler, whereas the main one is sustained through the formation of a liquid fuel film on the lip that separates the two swirled flows. As the lip edge is reached, the liquid film breakups into droplets. The fuel is then injected at a very fine atomization level providing a rapid and intense mixing. Atomization increases the vaporization surface guaranteeing a suitable distribution inside the flame region.

The technology developed in NEWAC (mainly component and / or

breadboard validation in a laboratory environment) will be driven further
in LEMCOTEC research project. The main technological objective will
be the improvement of the core-engine thermal efficiency by increasing
the overall pressure ratio to up to 70 (NEWAC was < 50 OPR). This
will lead to a further reduction of CO2 emissions. However, as in return
NOx increases with pressure (OPR), combustion technologies have to be
further developed at the same time to at least compensate for this effect.
LEMCOTEC aims to provide technological solutions to reduce CO2 and
NOx emissions, which can be implemented in the next generation of aero
engines to be introduced around 2020, as shown in Figure 1.12 [24].
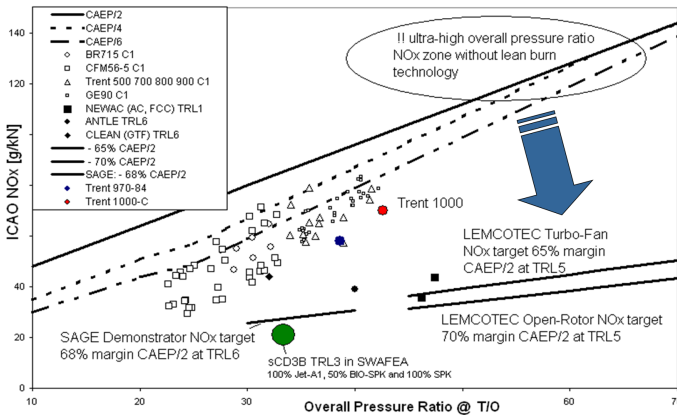
*Figure 1.12: Potential NOx reduction for the engine concepts (engine
alone) [25].*

1.1.3   Low-Emission Combustors: The Thermo-acoustic
Issue

The remarkable improvements on pollutant emissions achieved with
Lean Burn technology make it the state of the art of industrial gas turbine
and the next technology for aero engines. One of the main drawbacks and
critical issues of such a technology is the onset of combustion instabilities

related to the coupling between pressure oscillations and thermal fluctuation induced by unsteady heat release. Although combustion instability is not considered to be an issue for diffusion flames, in lean-premixed combustion system it becomes a substantial challenge for designers.

There are several features that make lean premixed combustor prone to flow oscillations. In the first place, they typically operates near lean blowout limit where even a small perturbation in the equivalence ratio can lead to high heat release oscillations. A possible explanation to such a susceptibility can be given in terms of the relationship between equivalence ratio and chemical reaction time.
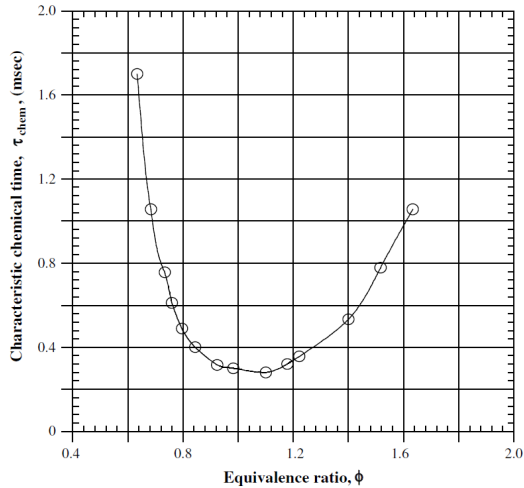
Figure 1.13: Experimentally obtained chemical reaction time as a function of the equivalence ratio [26].

As reported by experimental data of Zukoski [26], shown in Figure 1.13, the gradient of chemical reaction time with respect to equivalence ratio, $\partial\tau_{chem}/\partial\phi$, increases significantly as the flame gets leaner. Being the chemical reaction time inversely proportional to the reaction rate, a small variation in ϕ can create large fluctuations in the reaction rate at lean conditions, as compared to the stoichiometric condition.

Moreover, the reduced amount of cooling air available at the liner surface reduces the beneficial effect of acoustic damping of the cooling system.

Finally, in premixed combustor a short flame is generally present if compared to the longitudinal acoustic wavelength. Such an acoustically compact configuration facilitates the interaction between between oscillatory heat release and flow motion [7].

The occurrence of thermo-acoustic instabilities in LPC systems needs to be carefully anticipated and prevented in the design phase. A comprehensive understanding of combustion instability is therefore mandatory and extensive efforts have been made by industrial and academic communities to investigate the unique stability characteristics of low-emission lean-premixed gas turbine engines.

1.2   Combustion Instabilities

Generally, in a fluid in motion, an instability can be observed whenever a small perturbation of one of the variables characterizing the flow or of a boundary condition is amplified. Consequently, the system responds with drastic changes of its variables or with very large amplitude oscillation of the latter. In particular, a thermo-acoustic instability is originated by the interaction of system acoustics and unsteady heat release. Such instabilities may damage combustor components and limit the range of stable operating conditions so that they are definitely undesirable phenomena.

Unlike other flow instabilities, thermo-acoustic instabilities are not a local phenomenon as the stability properties are not determined solely by the dynamics of the heat source and the flow field in the immediate surrounding. Acoustic waves travel forth and back the combustion system and as a consequence acoustic boundary conditions far from the heat source may strongly affect stability properties [27].

In general, the fluctuations of heat release in a flame, induced by turbulent fluctuations in the velocity field, produce sound. Such a combustion

noise exhibits a broad band frequency distribution, due to the multi-scale and chaotic distribution of turbulent eddies giving rise to the fluctuations. When the flame is enclosed in a chamber, as in gas tubines, the sound can be reflected and the chamber acts as a resonator. If a positive feedback is established between heat release fluctuations and acoustic wave, the perturbation grows till saturation is reached and oscillation amplitude does not change any more (limit cycle). The resulting frequency spectrum, generally, exhibit pure tones peaks close to the system eigenfrequencies.

A basic classification of instabilities has been proposed in the work of Barrère and Williams [28]:

- The *low frequency* are also called *chugging* and are related to the coupling of the combustion chamber with the feeding system. The related frequency is of some tenths of Hz. They occur during the starting or shut-down transient phase and have a short lifetime of few seconds [29].

  Another phenomena carachteristic of this frequency range ($50 \div 150Hz$) is the so-called *rumble*. Rumble has been observed in the context of liquid-fuelled diffusion burners operated at low inlet temperature ($T < 500K$) and low combustor pressure ($p_{30} < 4bar$), typical of idle and sub-idle conditions [30].

- *Intermediate-frequency* also called *buzz* or *system instabilities*, are associated with the processes taking place in the flame front itself. The entire system is involved, anyway, and the wave motion inside the combustion chamber is, generally, longitudinal and can be described int terms of planar modes [29].

- The *higher frequency instabilities* are also reffered as *screeching* or *streaming* refers to acoustic instability of resonant combution, with the frequency and phase of the wave oscillation corresponding to those for the acoustic resonance of the chamber. Any type of wave may be present: longitudinal, radial, tangential, standing or spinning modes [29].

Once understood how do instabilities appear, it is important to understand which are the main pathways for the energy exchange in a flow that feed instabilities and which are the conditions for the instabilities to occur. Moreover, which are the feedback mechanism for the growth of the instabilities?

1.2.1   Energy Transfer Mechanisms

To better understand the first issue, recently, Heang et al. [31] studied the energy transfer mechanisms between mean, periodic and turbulent motions, considering also heat release influence on flow dynamics in a turbulent reacting flow, by means of triple decomposition technique. In general, in practical turbulent flows random and periodic (coherent) motions co-exists. When the triple decomposition is applied to a compressible flow, each flow variable ψ can be expressed as sum of density-weighted long-time-averaged $\vec{\psi}$, periodic (coherent) ψ^a and turbulent (stochastic) ψ^t, as follows:

$$\psi(\mathbf{x}, t) = \overrightarrow{\psi}(\mathbf{x}) + \psi^a(\mathbf{x}, t) + \psi^t(\mathbf{x}, t) \qquad (1.1)$$

The decomposition is achieved using the density-weighted long-time and ensemble-phase averaging techniques. For details refer to [7].

The average kinetic energy per unit volume is defined, e.g. as follows:

$$k = \overline{\rho u_i u_i}/2 = \overline{\rho \overrightarrow{u_i}\,\overrightarrow{u_i}}/2 + \overline{\rho u_i^a u_i^a}/2 + \overline{\rho u_i^t u_i^t}/2 \qquad (1.2)$$

The energy associated with periodic motion, ϵ, contains both kinetic (k^a) and potential (ϵ_p) energies, in accordance with acoustic theories.

$$\epsilon = k^a + \epsilon_p = \overline{\rho u_i^a u_i^a}/2 + \overline{(p^a)^2}/(2\overline{\rho} \cdot \overline{c}^2) \qquad (1.3)$$

In their work, Huang et al. applied the triple decomposition technique to mass, momentum and energy equation for an ideal gas mixture and derived the equations for the three component of the kinetic energy ($\overrightarrow{k}, k^a, k^t$) and an equation for the potential energy of the periodic motions.

The equation for the total energy of periodic motion $\epsilon = k^a + \epsilon_p$ is then defined.

The main energy exchanges in a turbulent reacting flow can be summarized in the schematic diagram in Figure 1.14.
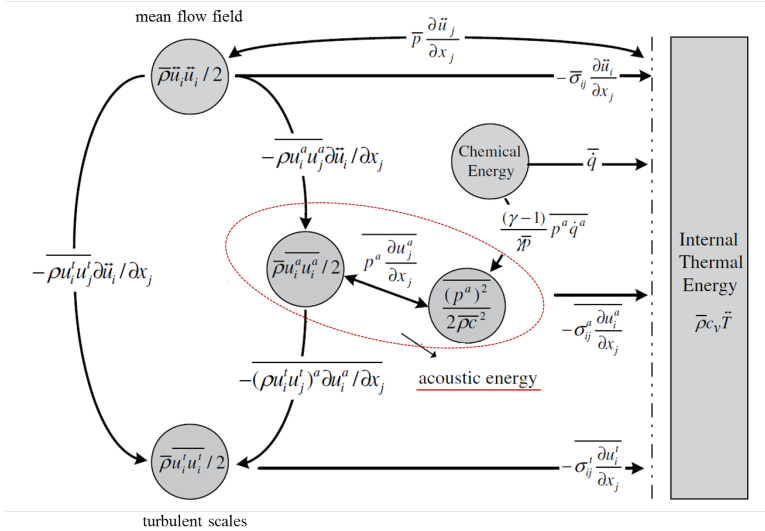
Figure 1.14: Diagram of energy exchange among mean, periodic, and stochastic motion in turbulent reacting flows (adapted from [31]).

The oscillatory motions can acquire energy through two main pathways: They may extract energy from the mean flowfield $(-\overline{\rho u_i^a u_j^a} \partial \overrightarrow{\tilde{u}_i}/\partial x_j)$ or chemical reactions $(\frac{\gamma-1}{\gamma \overline{p}} \overline{p^a \dot{q}^a})$. They can also exchange energy with background turbulent motion $(-\overline{(\rho u_i^t u_j^t)^a} \partial \overrightarrow{\tilde{u}_i^a}/\partial x_j)$, or dissipate it into thermal energy through viscous damping effects $(-\overline{\sigma_{ij}^a \partial u_i^a /\partial x_j})$.

In case of absence of chemical reactions, the primary energy source for periodic motions is the mean flowfield and/or boundary effects. With combustion, heat release from chemical reactions is the major source for driving periodic motions. It is interesting to notice that, the introduction of organized flow oscillations provides an additional pathway to transfer

energy from the mean flowfield to turbulent motion, in comparison with stationary flow conditions.

The source term, $\frac{\gamma-1}{\gamma\overline{p}}\overline{p^a\dot{q}^a}$, appearing in the equation of total acoustic energy, representing the contribution of energy from unsteady heat release, can assume both positive or negative sign, depending on the phase difference between pressure and heat release oscillations. Let θ be the phase difference, then:

$$(\gamma-1)\overline{p^a\dot{q}^a}/\gamma\overline{p} = (\gamma-1)|p^a\dot{q}^a|\cos\theta/\gamma\overline{p} \tag{1.4}$$

If the oscillations of pressure and heat release are in phase ($-\pi/2 < \theta < \pi/2$), this term is positive, and energy is supplied to the oscillatory flowfield. Otherwise, energy is subtracted from the system. This result is closely related to the Rayleigh criterion (see section 1.2.2).

1.2.2   Rayleigh Criterion

As far as the second question is concerned, that is, which are the conditions for the instabilities to occur, an answer is provided by Lord Rayleigh in 1878 who stated the so-called Rayleigh's criterion [32] with the following words:

"If heat be periodically communicated to, and abstracted from, a mass of air vibrating (for example) in a cylinder bounded by a piston, the effect produced will depend upon the phase of the vibration at which the transfer of heat takes place. If the heat be given to the air at the moment of greatest condensation, or be taken from it at the moment of greatest rarefaction, the vibration is encouraged. On the other hand, if heat be given at the moment of greatest rarefaction, or abstracted at the moment of greatest condensation, the vibration is discouraged".

This statement can be summarized using the following mathematical expression and gives the necessary conditions because, following the energy exchanges described in section 1.2.1, an instability occur [33]

$$\int_V \int_T p'(x,t)q'(x,t)dtdV \geq \int_V \int_T \sum_i \mathcal{L}(x,t)dtdV \tag{1.5}$$

where $p'(x,t)$, $q'(x,t)$ and $\mathcal{L}_i$ are the combustor pressure oscillations, periodic heat addition process, and i-th acoustic energy loss process, respectively. Eq. 1.5 allows us to highlight two important aspects. First of all, in order to have combustion instabilities it is necessary a coupling between the acoustic field and heat release fluctuations in such a way that energy is added to the acoustic field. Furthermore, in order to make the combustor unstable, the net rate of energy addition to the acoustic field should exceed the net rate of damping provided by inherent dissipation processes (perforated liners, Helmholtz resonators etc.), usually employed gas turbine combustors.

1.2.3 Feedback Mechanisms

Combustion instabilities are excited by feedback between the combustion process and the acoustic oscillations in the system and they need a positive closed loop to grow, as depicted in Figure 1.15.
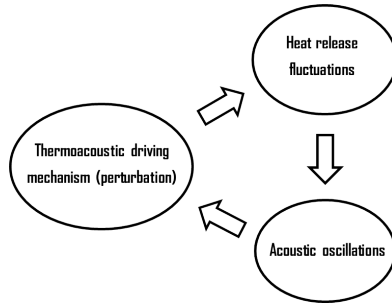
Figure 1.15: Scheme of the feedback process responsible for combustion instabilities.

The analysis presented in 1.2.1 suggests that the dominant physical processes or mechanisms responsible for driving unsteady flow oscillations in a combustion system arise from either heat release or gasdynamic fluctuations, or both . The latter include acoustic motions in the chamber, evolution of large-scale coherent structures, and other flow phenomena. Heat release is largely related to local equivalence ratio and mass flow

rate[7].

In a gaseous premixed flame, heat release fluctuations may result from flame surface variations, equivalence ratio fluctuations, mass flow rate oscillations, and vortex shedding processes due to hydrodynamic instabilities. In systems using liquid fuel, atomization and droplet vaporization are additional participating mechanisms.

The main feedback mechanisms are listed below.

- **Velocity perturbation:** It is the typical thermo-acoustic feedback mechanism. Basically a perturbation in the acoustic velocity causes a heat release fluctuation when it reaches the flame. The generated sound wave travels along the combustor forth and back after being reflected at the domain boundary and again perturbs the velocity field at the burner. The acoustic perturbation travels at the local speed of sound influencing also the local turbulent flow field which, in turn, modulates the turbulent burning velocity and thus the fuel consumption rate [34, 35, 36, 37, 38, 39]. In case of gaseous premixed flame, this is the main mechanism driving combustion instabilities. As shown by Cho and Lieuwen [40], in this case, a change in the turbulent flame speed moves the flame surface and causes change in the area available for the reaction (see Figure 1.16).

Figure 1.16: Process generating heat release oscillation caused by acoustic velocity perturbation (adapted from [40]).

- **Equivalence ration fluctuation:** Pressure oscillations in the combustor propagate in the injector affecting the mixing process between air and fuel. The fuel and/or the air supply is altered and the resulting equivalence ratio varies periodically in time [40, 41]. The mixture is transported convectively to the flame front and burnt, so that a heat release fluctuation is generated which drives the instability [42, 43, 44, 45, 46, 47].

Looking at Figure 1.17, it is possible to see how the flame surface area is, in this case, an indirect effect of a change in the flame speed due to a local change in ϕ.
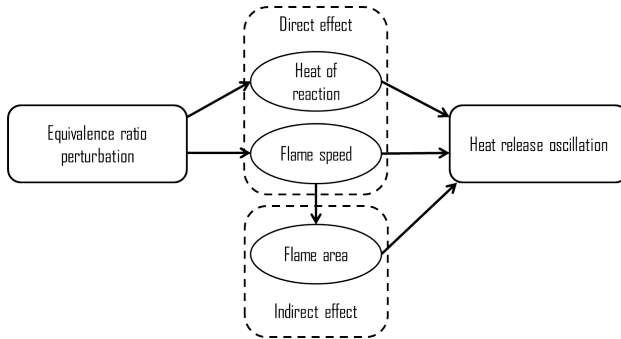
Figure 1.17: Process generating heat release oscillation caused by equivalence ratio perturbation (adapted from [40]).

- **Oscillatory atomization, evaporation and mixing:** In case of liquid fuel, the interaction with the acoustic field with the fuel spray can produce periodic variation of the spray shape, droplet size distribution and, in turn, a variation in the evaporative [48, 49] and mixing processes [50]. These periodic variation in fuel supply rate and/or periodic variation of the equivalence ratio at the flame location produce heat release oscillations that drive the acoustic field [51, 52, 53]. The physical processes involved are very complex and not completely understood and very few investigations can be found in literature especially for the interaction between acoustics and droplet primary breakup [5].

- **Entoropy waves:** An entropy wave is a perturbation in the temperature of the gas mixture. In particular, it is associated to local hot spot of temperature generally due to the combustion of a locally richer pocket of mixture. The feedback mechanism is generated when the perturbation is convected into a choked nozzle at the combustor exit. Being associated to low convective time from the flame

to the combustor outlet, low frequencies are typically associated with this mechanism [30, 54, 55, 56].

Together with the mentioned feedback mechanisms, also a possible interaction is established with the turbulence noise and vortex shedding phenomena:

- **Turbulence noise** is intrinsic in turbulent combustion phenomena. As already mentioned, such combustion noise has a broadband spectrum and selective amplification might be generated due to resonance effects.

- **Vortex shedding**: Acoustic perturbation at the burner or flame-holders can generate large-scale, coherent vortical structures due to flow separation effects or vortex-breakdown in swirled burners, often present in gas turbine combustors. The formed vortex can interact with the flame varying its surface or transport richer pocket of mixture to the flame front, thus causing heat release variation that can drive acoustic oscillations [51, 57, 58]

Chapter 2

Numerical Study of Combustion Instabilities

In the first part of the chapter the commonly used approaches to predict thermo-acoustic instabilities in a combustor are presented, starting from the solution of the full three-dimensional unsteady Navier-Stokes equations in a CFD simulation, to FEM approach, acoustic network and analytical methods. Attention will be dedicated to FEM approach as it is the one adopted in this thesis to study the system stability in the various applications.

Following this part, in section 2.2, an in-depth on premixed and technical flames dynamics and modelling is presented where the main theoretical and physical concepts are discussed exploiting important results from the literature.

In section 2.3, attention will focus on the Flame Transfer Function concept and a brief review of the numerical methods to obtain a Flame Transfer Function as well as some of the main analytical formulation are presented. A more detailed review is proposed in the last part for those works were a coupled approach, exploiting CFD and System Identification (SI) post process, as it is functional to the following application of this thesis.

2.1   Numerical Methods for the Analysis of Thermo-acoustic Stability

As already described in the previous chapter 1.2, when an instability occurs, a perturbation in one of the flow variable or boundary condition is amplified and grows in time till a limit cycle and amplitude saturation is reached. The first part of the process exhibit a linear trend that develop in the growth of the dominant mode, non-linear saturation and, finally, the limit cycle [44, 59]. The phenomenon can be described by the Navier-Stokes conservation equations for mass, species, momentum and energy. Depending on the different degree of simplification of the previous equations or if the solution is performed in the time or frequency domain, several mathematical method can be used to determine the thermo-acoustic behaviour of the system considered.

In the following a description of the main approaches to the study of thermo-acoustic problem are presented. CFD approaches are described at first. Then, de simplification made to arrive at the so-called wave equation are discussed before FEM approach, used to solve for the latter in the frequency domain is described, together with some works where this approach is exploited. Successively low-order and analytical methods are briefly presented as they are not exploited in the following of this work.

2.1.1   The study of thermo-acoustic instabilities by means of CFD

The most straightforward method to investigate the problem is the use of unsteady simulations to solve for the complete Navier-Stokes equation set for a compressible, turbulent reactive flow. A small perturbation is introduced in the domain and the evolution of the system is observed. The main advantage of this method is the low degree of simplification of the original equations that avoid modelling of the coupling between the acoustics and combustion process. It is also not restricted to the linear behaviour nor to the compactness assumption of the flame [42]. On the

other hand, the level of complexity is the highest among all the possible methods and a tremendous computational cost can be associated to them. Moreover, several drawbacks affect such a method. In general, the solution allow to identified only the most unstable modes while those with lower growth rate cannot be observed [27]. It is not easy to distinguish spurious numerical instabilities from a physical one and the solution can severely depend on the initial condition (the introduced initial perturbation can influence the system evolution) and on the boundary conditions assignment (definitely a non-trivial problem) [27].

Three different modelling approaches can be found:

- *Direct Numerical Simulation (DNS)* consists in the direct solution of the Navier-Stokes equations on a very fine mesh and with sufficiently small time step to catch the whole spectrum of the spatio-temporal scale of the problem.

- *Large Eddy Simulation (LES):* Only the largest scales are solved directly while the smallest ones are identified after a spatial filtering operation, generally based on the mesh size, and a model is provided for them.

- *Reynold-Averaged Navier-Stokes (RANS):* The average values are computed with this approach, without solving any turbulent quantity. Turbulence effects need, therefore, to be modelled.

As far as DNS approach is concerned, it could, in general, be used to represent the flame dynamic and its interaction with acoustic waves. However, its use is practically limited as it is extremely computationally expensive and infeasible.

Several works have, instead demonstrated Large Eddy Simulations capabilities to deal with thermo-acoustic issues in both laboratory and industrial configurations. Just to mention few works, Martin et al. [60] analysed self-excited combustion instablities in a laboratory-scale, swirl-stabilized combustion system using LES. Selle et al. [61] analysed self-excited oscillations with Large Eddy Simulations of a partially-premixed industrial gas turbine burner.
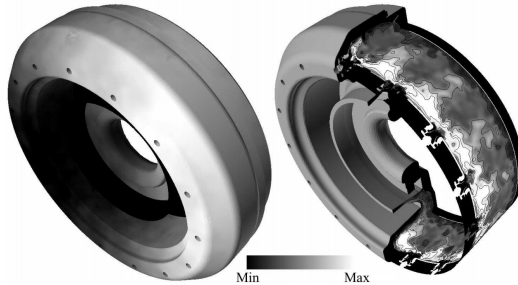
Figure 2.1: Full helicopter combustion chamber flow visualization. Left: pressure field on the combustor skin. Right: temperature field with temperature isocontours on a cylindrical plane [62].

Bourdier et al. [63] performed fully compressible reacting LES computations of a single sector of a helicopter combustion chamber, while in [64, 65] Wolf et al. simulated the full combustion chamber comprising all sectors, exploiting massively parallel computers (see Figure 2.1). Emphasis was placed on the azimuthal mode that often appears in real configurations. The current LES are shown to capture these self-excited modes well. The Flame Transfer Function (FTF) is then extracted from the full multi-burner LES results and compared to both Proper Orthogonal Decomposition (POD) analysis and a pulsated single sector LES.

As far as RANS use for the study of thermo-acoustic instabilities are concerned, few example can be found in literature.

In [66] RANS simulations are exploited to draw some guideline to lower the computational effort (i.e. by restraining domain boundaries or by increasing cell dimensions and time steps) without a particular impact on the reproduced physics of the thermo-acoustic phenomena.

In [67] ENEL Produzione Research Centre of Pisa carried out a CFD analysis by means of an in-house Reynold Averaged Navier Stokes code, of a 3D geometrical model of their experimental test-rig, with satisfactory agreement with experimental data. A similar example can be found by the same research group where RANS simulations are employed for the study of combustion instabilities, with the target of a very low computational

costs [68].

2.1.2 Solution of the Helmholtz equation with Finite Element Method

The Navier-Stokes equations can be simplified linearising the main physical quantities such as density, pressure velocity, in the presence of a generic mean flow. The procedure involve the decomposition of each variable in a steady mean quantity and a fluctuating one. Under the hypothesis of small perturbation the *Linearised Navier-Stokes equations* are obtained. Viscous losses and thermal losses are included. The equations can be further simplified neglecting viscous effects thus obtaining the so-called *Linearised Euler equations*. Combining the linearised Euler equations and neglecting mean flow effects leads to the *inhomogeneous wave equation* that, expressed in the frequency domain is also called *Helmholtz equation.*

Among the approaches to solve for the Helmholtz equation (*Galerkin method*, *Green's function technique* etc.) *Finite-Element Method (FEM)* is commonly employed.

One advantage of this method is that it can be used for the solution of the complete 3D problem and that the geometrical details of the combustor can be accounted for. It also does not need for any assumption about the coupling of different modes and longitudinal as well as tangential and radial modes are predicted. On the other hand, additional flow effects or driving mechanisms for oscillations, like equivalence ratio fluctuations, or pressure losses and damping in the system can only be determined indirectly or a model needs to be provided. Also a model is required for the description of the source term of the equation, representing the unsteady heat release, that is, the flame effect.

FEM based method have been successfully employed to compute linear stability analysis of simple experimental configuration as well as of more complex full-annular combustors. Despite of being of great interest, only few works can be found in literature regarding the numerical study

of thermoacoustic stability of annular combustors using finite element method.

Walz et al. [69] assessed the reliability of the Finite Element Method in the prediction of resonant frequencies by studying a cylindrical configuration and comparing numerical results with analytical ones. Then, they analysed an annular combustion chamber proving the great influence of boundary conditions on the eigenfrequency spectrum.
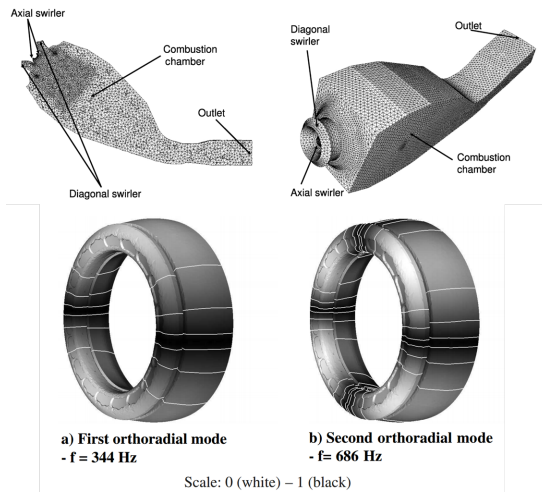
Figure 2.2: Mesh for the acoustic analysis of the Siemens combustor and first two modes of annular the combustor studied in [70].

Nicoud et al. [70] developed a finite element based methodology to determine thermoacoustic modes of industrial systems and applied it to annular combustors, as shown in Figure 2.2. The strategy they introduced requires a coupling with RANS/LES codes to provide the input data for the thermoacoustic analysis.

In [71] Camporeale et al. adopted the FEM approach to solve for equation for the acoustic waves in the frequency domain, coupled with a flame heat release model. The analysis has been applied at first to several

test cases of simple geometries, where analytical solution were available
[72], such as simple cylindrical combustors in different configurations.
Then a simplified annular combustion chamber was studied, analysing
the effects of the flame transfer function parameters on the stability
properties of the acoustic modes, allowing the the identification of pressure
fluctuations in both plenum and combustion chamber.
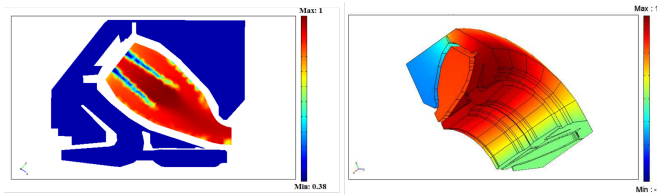
*Figure 2.3: Temperature distribution from CFD and results from FEM
analysis by Campa et al. [73].*

The analysis was then extended to a full annular combustion chamber
by the same research team in [73, 74] as shown in Figure 2.3. The influ-
ence of the flame shape on the thermoacoustic solution was investigated
comparing a spatially distributed flame, obtained by means of a RANS
simulation of the combustor, with a compact idealized flame sheet.

In [75] Andreini et al. investigated a tubular combustor with an
advanced lean injection system. A criterion was presented to simplify the
geometry of the double swirler injector thus allowing the reduction of the
number of elements necessary to model this component. Moreover, the
influence of flame region shape on the eigenfrequencies computation was
investigated together with the effect of two different expressions for the
unsteady heat release term.

The same authors in [76, 77], performed a thermoacoustic analysis of
a full annular combustor for aero-engine applications, shown in Figure 2.4.
The system is equipped with an advanced PERM (Partially Evaporating
and Rapid Mixing) injection system and combustor walls are based on
multi-perforated liners to control metal temperature. The acoustic effect
of multi-perforated liners was introduced by modelling the corresponding
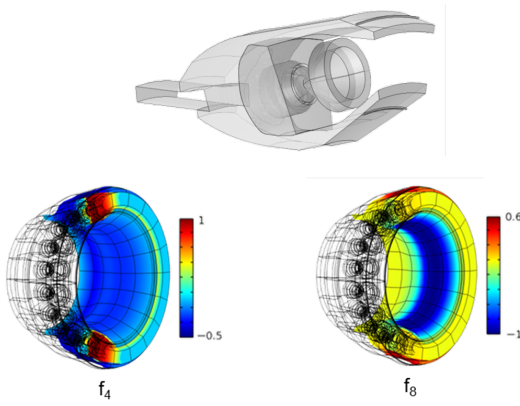
Figure 2.4: Sector of the full-annular combustor and results from FEM analysis obtained by Andreinii et al. in [76].

surfaces with an equivalent internal impedance. Different simulations with and without the presence of the flame were performed analysing the influence of the multi-perforated liners on the acoustic damping inside the combustion chamber.

2.1.3   Low-order and analytical methods

A further simplification of the methods to study the thermo-acustic stability, consists in dividing a complex system (such as a combustor) into a network of simple elements. In *acoustic network model technique* or *low-order methods*, the geometry of the combustor is modelled by a network of homogeneous (constant density) 1D acoustic elements where the acoustic problem can be solved analytically [78]. A transfer matrix relates the acoustic variables, pressure and velocity, at the inlet and outlet of each element. As an advantage, mean flow effects can be brought back thanks to the simplified form that the solved equations assume. The main drawback is that the geometrical details of the combustor cannot be accounted for and, due to the (quasi)-1D assumption, only the first longitudinal modes, below the cut-off frequency of the element are solved.

While in FEM models a spatial distribution can be assumed for the flame, in network models it is commonly assumed to be a discontinuity of negligible thickness and can be represented by a dedicated model.

In literature a multitude of applications can be found where acoustic networks are used as design tool and for the estimation of the thermoacoustic behaviour of simplified, experimental as well as industrial combustion system. Just to mention few applications for the shake of completeness, network approach has been adopted to analyse the effects of different flame models in [79] or to investigate the effects of entropy waves interaction at the exit nozzle [55]. Application to annular gas turbine combustor for industrial application can be found in [80, 81] where also the effect of acoustic dampers has been investigated.

Finally, *analytical methods* can be used to analyse combustion system. However, only very simplified geometry with equally simplified combustion mechanisms and flow physics can be investigated. Examples of application in literature can be found in [46, 72, 81, 82, 83].

Among the numerical methods, both FEM and acoustic network approach needs a model for the term representing the unsteady heat release. This term can be considered the heart of the thermo-acoustic problem: it represent the flame behaviour and its effect on the acoustic of the whole system. As already touched on discussing literature works, several approaches can be used to express the flame term, ranging from simple analytical relations or more complex forms exploiting unsteady CFD simulations.

Before a review of the method to identify the Flame Transfer Function is presented in section 2.3, the flame dynamics is discussed in section 2.2 for both perfectly premixed flame and technically premixed flame.

2.2 Flame Dynamics Analysis of a Low Emission Combustion Systems

The flow and flame evolutions and the underlying mechanisms for driving instabilities, discussed in 1.2 evidenced how complex the coupling between flow motions and flame is in determining the characteristics of turbulent combustion.

Unsteady heat release has been shown in section 1.2.1 to be the most important source term providing the energy that drives combustion instability.

For a lean-premixed combustion system, this term depends on a variety of physical processes, such as flame surface and equivalence ratio fluctuations, hydrodynamic instability, and liquid fuel atomization and droplet evaporation. None of these processes can be modelled in sufficient detail [7]. With basic considerations that links the instantaneous heat release of the flame Q' to the consumed fuel mass flow at the instant and further decomposition of the latter into a flame propagation speed S_T, the flame area A and the mixture density ρ and equivalence ratio ϕ, the flame dynamics of such a combustion system can be described as follows:

$$\frac{\dot{Q}'}{\bar{\dot{Q}}} = \frac{S_T'}{S_T} + \frac{A'}{A} + \frac{\phi'}{\phi} + \frac{\rho'}{\rho} \tag{2.1}$$

It is interesting to notice that also applying the triple decomposition technique, where the random and periodic motions are separated from each other, is employed, the same result is obtained. In [84] this technique is applied to investigate the effects of acoustic oscillations and turbulence on the periodic behaviour of a turbulent flame. Within the flamelet assumption, the rate of heat release per unit volume can be given as, $Q' = q\rho S_L A$. When the triple decomposition technique is applied, the following expression for heat release fluctuation is obtained:

$$\frac{\dot{Q}^a}{\bar{\dot{Q}}} = \frac{q^a}{\bar{q}} + \frac{S_T^a}{S_T} + \frac{A^a}{A} + \frac{\rho^a}{\bar{\rho}} \tag{2.2}$$

The superscript a denotes the periodic (coherent) component of a fluctuating quantity. Thus, the fluctuation of heat-release rate contains contributions from the fluctuations in heat of reaction q, density, flame speed, and flame surface area.

The fluctuation of heat of reaction is attributed to the changes in the mixture-equivalence ratio resulting from flow disturbances. Therefore, equation 2.2 assumes a similar for to 2.1.

The oscillation of flame speed, similar to that of heat of reaction q, is caused by equivalence ratio fluctuation, for a given chamber and flow condition.

The mechanisms of flame surface-area fluctuation are relatively complex and primarily dictated by local velocity perturbations.

The density fluctuation, mainly arising from pressure perturbation, has a negligible effect on unsteady heat release as compared to other three factors [84]. With this simplification, valid for low Mach number, equation 2.1 becomes:

$$\frac{\dot{Q}'}{\bar{\dot{Q}}} = \frac{S_T'}{S_T} + \frac{A'}{\bar{A}} + \frac{\phi'}{\bar{\phi}} \tag{2.3}$$

2.2.1 Dynamics of a Perfectly Premixed Flame

If a perfectly homogeneous mixture with $\phi' = 0$ is considered, equation 2.3 further reduces to:

$$\frac{\dot{Q}'}{\bar{\dot{Q}}} = \frac{S_T'}{S_T} + \frac{A'}{\bar{A}} \sim \frac{u_r'}{u_r} \tag{2.4}$$

A heat release perturbation resulting from a modulation of the flow upstream the flame u_r can thus be interpreted as a combination of a fluctuation of the propagation speed and the associated flame surface area. Generally, the reference location for the velocity fluctuations u_r is chosen at the burner exit [42, 85]. A perturbation in the flow field comes from the burner, is transported downstream with the speed of flow, reaching the flame. The surface area and the turbulent flame speed are

then modified. The strength of the disturbance is directly related to that of the velocity fluctuation at the burner.

The dynamic response of a flame to a perturbation can be represented in the frequency domain by its Flame Transfer Function $FTF(\omega)$ (also "frequency response").

$$F_u(\omega) = \frac{\dot{Q}'(\omega)/\overline{\dot{Q}}(\omega)}{u_r'(\omega)/\overline{u_r}(\omega)} \tag{2.5}$$

The above relation represent a Single-Input Single-Output system (SISO) with the velocity just upstream the flame as input and the heat release rate as output (see Figure 2.5).
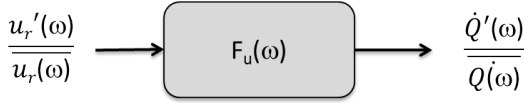
Figure 2.5: Scheme of the SISO model of a perfectly premixed flame.

The defined model structure have a great importance and introduce great simplifications in the definition of the strategy to identify the FTF of such kind of flames.

Considering a harmonic behaviour, the perturbations can be expressed in terms of amplitude, denoted by ˆ and phase:

$$\dot{Q}'(\omega) = \hat{Q}(\omega)e^{i(\omega t + \phi_Q)}$$
$$u'(\omega) = \hat{u}(\omega)e^{i(\omega t + \phi_u)} \tag{2.6}$$

The FTF can then also be written in the same form:

$$F_u(\omega) = \hat{F}_u e^{i\phi_{F_u}} = \frac{\hat{Q}(\omega)}{\hat{u}(\omega)}e^{i[\phi_Q - \phi_u]} \tag{2.7}$$

In Figure 2.6 and example of FTF for a perfectly premixed flame is reported.

The considered heat release is the global one all over the domain.
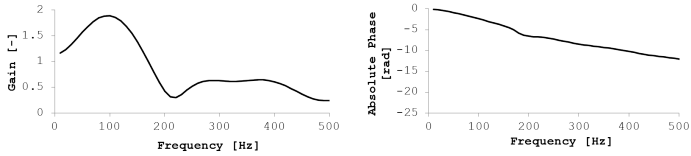
Figure 2.6: Example of FTF for a perfectly premixed flame: gain (left) and absolute phase (right).

Consequently, the FTF phase is a global characteristic and the flame is considered as a discontinuity [86]. Such a global characteristic is an important basis for the many analytical expressions of the FTF based on the concept of time-delay τ in the heat-release response with respect to the excitation, as will be described in section 2.3. Basically, the flame is considered to react at a time t to a perturbation at the burner occurred at a time $t - \tau$.

As far as the theoretical limits for the FTF of a perfectly premixed flame are concerned, in the low frequency limit, the amplitude and phase approach 1 and 0, respectively. This is due to the quasi-steady response of the flame so that any fluctuation in the mixture flow is translated into an equal fluctuation of heat release [87].

At the other limit for $\omega \to \infty$, the dispersion of the perturbation is large, so that the flame do not follow the perturbation any more, and the amplitude of the FTF tends to 0.

For intermediate frequency it is possible to observe one ore more peaks where the amplitude exceeds unity (see i.e. Figure 2.6). Even if this point is still topic of discussion, it is generally attributed to vorticity transport by swirl number fluctuations ([43, 88, 89, 90, 91]).

In [88] Hirsch proposed a mechanism of how the presence of swirl fluctuations can induce a secondary velocity fluctuation: the fluctuation in axial velocity associated with the acoustic wave travels with speed of sound, the fluctuation in tangential velocity is transported convectively by the flow field. Komarek and Polifke [43] investigated experimentally and numerically the impact of the variations of swirl number on the flame

response.
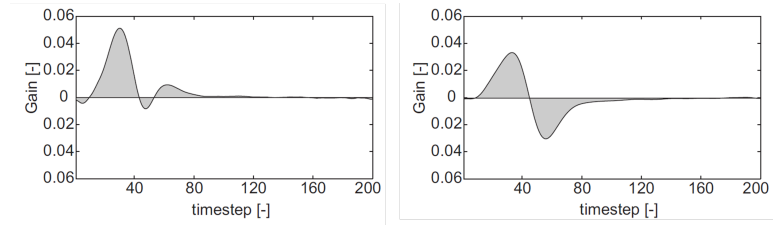
Figure 2.7: Unit impulse responses to an axial excitation (left) and to a tangential excitation (right) [43].

In Figure 2.7 is shown the the response of the flame to a Unit Impulse (UIR) in the axial and tangential velocity respectively. The perturbation in the axial velocity introduce more mixture flow in the reaction zone, inducing a rise in the heat release, proportional to the augmented fuel mass flow supplied. The response to the tangential velocity perturbation show a different behaviour: the perturbation is transported in the flame region as well but at an initial enhancement of the heat release it follows an undershoot of comparable entity. The provided explanation is that a perturbation in the tangential velocity leads to an increase in the flame surface (increased burning rate) not sustained by an increased fuel mass flow: the first increase in the heat release is not followed by fresh mixture so that the flame is contracting, thus reducing its surface (reduced burning rate).

Following the explanation provided by Polifke in [92] the under shoot of the Unit Impulse Response and the excess gain of the flame transfer function $|F(\omega)| > 1$ for a range of frequencies ω, are actually strongly related to each other.

As will be described in more detail later in section 3.2.3, the response of a linear, time-invariant system (e.g. the flame) can be characterized completely by its Unit Impulse Response, h_k for a discrete-time system, in the time domain or by its equivalent description in the frequency domain, the frequency response (e.g. the FTF). The the frequency response $(F(\omega))$

is calculated from the UIR by a z-transformation:

$$F(\omega) = \sum_{k=0}^{M} h_k e^{-i\omega k \Delta t} \tag{2.8}$$

If the UIR h_k has all positive coefficients then, with the increasing frequency ω there will be increasingly destructive superposition between the contribution of the individual coefficients of the overall flame response due to phase factors $\exp -(i\omega k \Delta t)$ that appear in the z-transform, Eq. 2.8. In this, case the gain $|F(\omega)|$ can never be larger than the gain $|F(0)|$. If, on the other hand, a UIR exhibits positive as well negative peaks, than it is possible that the phase factors lead to constructive superposition between the contributions of the individual coefficients, resulting in a gain $|F(\omega)| > 1$ for a range of frequencies.

The same conclusion is obtained looking again at the limit for $\omega \to 0$, considering that, as mentioned above, an increase in the flow rate of mixture results in a corresponding increase in heat release. The transfer function between fluctuations of flow rate (MF) and heat release of a perfectly premixed flame must be unity in the limit of zero frequency:

$$\lim_{\omega \to 0} F_{MF}(\omega) = \sum_{k=0}^{M} h_{k,MF} e^{-i\omega k \Delta t} = 1 \tag{2.9}$$

On the other hand, as fluctuations of swirl (S) do not supply additional mixture to the flame:

$$\lim_{\omega \to 0} F_S(\omega) = \sum_{k=0}^{M} h_{k,S} e^{-i\omega k \Delta t} = 0 \tag{2.10}$$

which implies that some coefficients $h_{k,S}$ must be negative.

2.2.2 Dynamics of a Technically Premixed Flame

In practical flames the assumption that fuel and air are perfectly premixed is an idealization of what happens and the mixing is very often far from being perfect, though efforts in premixer designs have been put

in place strategies to rapidly and completely mix the fuel and air prior to combustion. In such burners, fluctuations of velocity at the fuel injection location or at the premixer air will generate fluctuations in the equivalence ratio that, in turn, has a significant impact of the flame dynamics.

These effects have been often discussed separately and the flame dynamics is then described as a SISO system. Generally the interaction mechanisms between flow, mixing, heat release and acoustics may be acst simultaneously and the flame response should be considered a super-position of individual contributions [92]. Huber and Polifke in [93, 94] have argued that for practical premixed flame a SISO structure might be inadequate as equivalence ratio fluctuations ϕ' are not related in a straightforward manner to velocity fluctuations at the burner exit u'_b but, instead, they should be related to the entire system acoustics. Therefore, they suggested a Multi-Input Single-Output model structure as the most suitable description for the such flames.
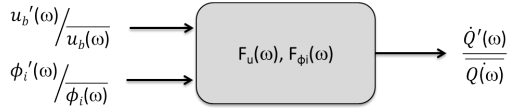
Figure 2.8: *Scheme of the MISO model of a technically premixed flame.*

With a MISO structure, schematically represented in Figure 2.8, the flame dynamics is described by multiple Flame Transfer Functions, relating the acoustic velocity fluctuations at the burner outlet ($F_u(\omega)$) and fluctuations of equivalence ratio at injector $i - th$ ($F_{\phi_i}(\omega)$) to the overall heat release:

$$F_u(\omega) = \frac{\dot{Q}'(\omega)/\overline{\dot{Q}}(\omega)}{u'_b(\omega)/\overline{u_b}(\omega)} \qquad and \qquad F_{\phi_i}(\omega) = \frac{\dot{Q}'(\omega)/\overline{\dot{Q}}(\omega)}{\phi'_i(\omega)/\overline{\phi}(\omega)} \qquad (2.11)$$

Equivalence ratio fluctuations can also be expressed in terms of acoustic variables (generally resolved in numerical codes), after Taylor expansions and neglecting higher order terms:

$$\frac{\phi'_i}{\overline{\phi}} = \left(\frac{u'_{F,i}}{\overline{u}_{F,i}} - \frac{u'_{A,i}}{\overline{u}_{A,i}} \right) \frac{\overline{\dot{m}}_{F,i}}{\sum_{i=1}^{N} \overline{\dot{m}}_{F,i}} \tag{2.12}$$

Where subscripts F ans a stands for fuel and air respectively. Therefore, for a technically premixed burner with N injectors, the global heat release fluctuations can be expressed as follows:

$$\frac{Q'(\omega)}{\overline{Q}} = F_u(\omega) \frac{u'_b(\omega)}{\overline{u}_b} + \sum_{i=1}^{N} F_{\phi_i}(\omega) \left(\frac{u'_{F,i}(\omega)}{\overline{u}_{F,i}} - \frac{u'_{A,i}(\omega)}{\overline{u}_{A,i}} \right) \frac{\overline{\dot{m}}_{F,i}}{\sum_{i=1}^{N} \overline{\dot{m}}_{F,i}} \tag{2.13}$$

To get more insight on the flame response to equivalence ratio perturbation, compared to acoustic velocity perturbation, Huber and Polifke [93, 94] analysed the flame behaviour in terms of Unit Impulse Response. In Figure 2.9 are reported the UIRs of acoustic velocity (left) and of equivalence ratio (right).
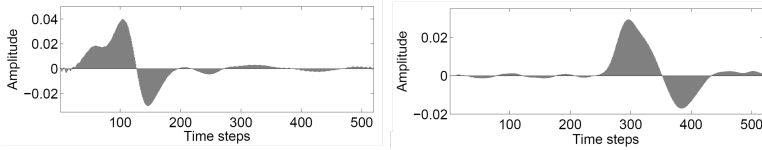
Figure 2.9: Unit impulse responses to a velocity excitation (left) and to an equivalence ratio excitation (right). Adapted from [42].

As far as the first is concerned, the two peaks are interpreted as the adjustment to mass flow perturbation the first and to a swirl wave the second, in referece to the discussion in 2.2.1. Looking at the UIR to equivalence ratio perturbation, in Figure 2.9 right, a peak is observable after approximatively the convective time from the injector to the flame, followed by an undershoot. The explanation provided by the authors in [93, 94] for this behaviour is the following: As a richer mixture arrives at the flame and it is burnt. The heat release grows and, due to the consequent increase in the flame speed S_T, the flame propagates upstream, reducing its surface. Once that the richer mixture is consumed the flame

surface results too small so that the heat release experiences an undershoot while the flame is convected downstream to its original position.

As discussed, the complex mechanisms governing the dynamic response of a flame to fluctuations of one ore more of the so-called driving mechanism, is expressed in terms of Flame Transfer Function . In the next section the numerical approaches used to give a form to the FTF are presented.

2.3   Identification of Flame Transfer Functions

The Flame Transfer Function may be obtained experimentally, e.g. using chemiluminescence to evaluate heat release combined with velocity or pressure sensors [95]. The experimental determination of FTFs can be difficult, very expensive and requires very careful experimental work (especially in the presence of turbulent flow or combustion), sophisticated post-processing and long test runs [6].

However, as the present work deals with numerical method to evaluate the flame behaviour and the stability properties of gas turbine combustors, the experimental methods are not discussed in the following.

Alternatively, numerical methods can be used in a variety of approaches, ranging from steady CFD to characterize empirical constant of simple analytical formulation or exploiting unsteady simulation to reproduce the flame dynamics and generate computational time series to be post-processed to extract a Flame Transfer Function.

A brief review of numerical methods to obtain a Flame Transfer Function and analytical formulation is presented herein.

One global characteristic of the Flame Transfer Function is a time delay τ in the heat release response to an excitation. The flame reacts at a time t to a perturbation at the burner occurred at a time $t - \tau$.

A general form of Flame Transfer Function is given in the frequency domain in terms of amplitude $A(\omega)$, and phase $\phi(\omega)$. The former relates the intensity of the heat release response relatively to the perturbation

which caused it, while the latter determines the time lag of the flame response.

$$F(\omega) = A(\omega)e^{i\phi(\omega)} \tag{2.14}$$

Generally, the time delay has a convective behaviour: the acoustic perturbation at the burner mouth follows the flow and is convected into the flame.

A simple and widely used formulation of the Flame Transfer Function was proposed by Crocco and Chen [96], the so-called $n - \tau$ model:

$$F(\omega) = ne^{-i\omega\tau} \tag{2.15}$$

In this formulation, the time delay should consider all the physical processes involved in the transport mechanism, ranging from convection time to chemical delay time. However, it is usually represented only by the convection time, i.e. the time required by velocity oscillations at the injection plane to be convected in the flame region. The constant amplitude is definitely not consistent with the flame response observed experimentally and described in sections 2.2.1 and 2.2.2: the gain above unity for the low frequency range as well as the low-pass filter behaviour are neglected with this formulation.

In order to describe such a low-pass filter behaviour and the influence of time delay variation due to flow dispersion, other authors modelled the time delay with a distribution. Sattelmayer [46], for example, derived a rectangular probability distribution of $\Delta\tau$ around the time delay; Polifke [97] proposed a Gaussian time delay probability distribution (see Figure 2.10).

If the dispersion at higher frequency is modelled, the amplitude peak above unity is still not reproduced by the proposed models. To represent this behaviour, an extension to higher order polynomial model is proposed (i.e. Dowling [37] or Pankiewitz [99]) but, in general, the higher the order, the lower the physical understanding of the model associated parameters.

In other cases the Flame Transfer Function formulations consider other
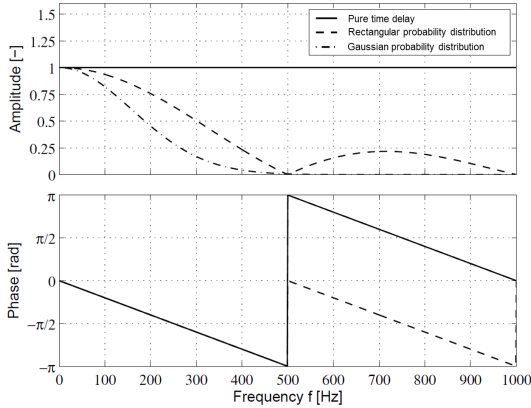
Figure 2.10: Example of time delay distribution models (Adapted from [98]).

physical mechanisms that can affect the flame response such as swirl-induced velocity fluctuations or, in case of liquid fuels, the fluctuation of droplet diameter caused by the fluctuation of air velocity.

As far as the swirl-induced velocity fluctuations are concerned, Hirsch et al. [88] developed a formulation to take into account the modulation of the flame heat release by a velocity perturbation along the flame front that results from a fluctuation of the azimuthal vorticity in the combustor flow-field. The latter is generated from swirl perturbations within the burner that are caused by the acoustic excitation and subsequently transported into the flame by convection.

An important parameter is the swirl delay τ_S describing the convective time delay between swirl generation at the tangential slots (S) and its arrival at the burner exit (E) in the sketch of the combustor used in their anaysis in Figure 2.11.

The swirl time delay is responsible for the decoupling of the swirl fluctuation from the axial velocity fluctuation at the burner exit and does thus strongly influence the vortex dynamics. Note that a dispersion of the swirl wave during convection to the flame is not taken into account in
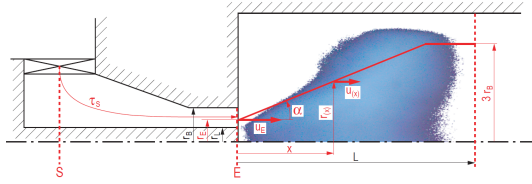
Figure 2.11: Sketch of the TD1 burner used in [98] to apply the swirl model
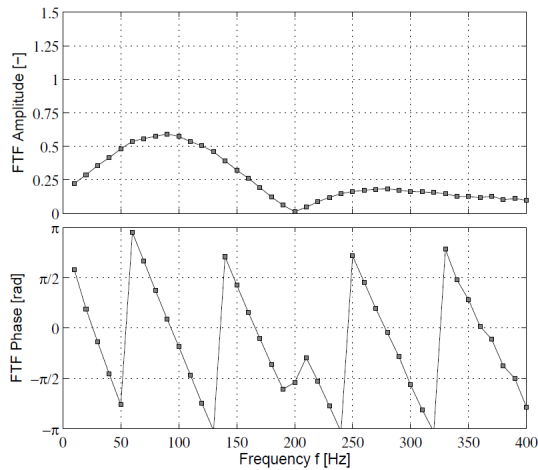
Figure 2.12: Example of the swirl model transfer function FTF [98].

this model, since the degree of dispersion is difficult to determine [98].

The model does only predict the heat release fluctuation resulting from a vorticity perturbation (see Figure 2.12). Therefore, the typical global transfer function behaviour is not yet produced since the direct influence of the burner velocity perturbation - the supply of the flame with combustible mixture - is not included in the presented modelling approach. Vorticity perturbations can be considered to "ride on top" of a velocity perturbation generated within the burner.
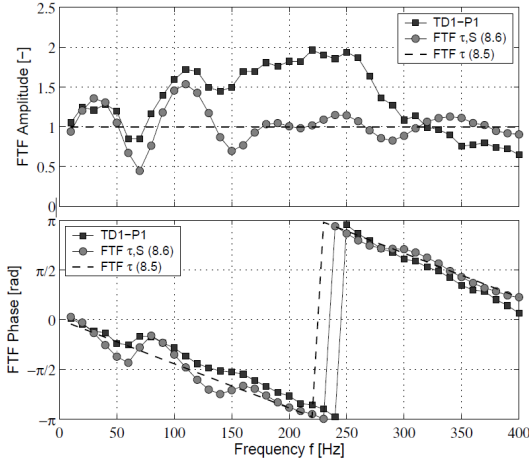
Figure 2.13: n-τ model, n-τ + Swirl model and experimental FTFs [98].

The final model can be then derived from an additive superposition of the two parts as can be seen in the example of Freitag [98], where a simple time delay model and the swirl model are summed and compared with experiments in Figure 2.13.

Concerning liquid fuel dealing Flame Transfer Function formulations, Eckstein and Sattelmayer [100] proposed a FTF for diffusion flames generated by an airblast injection system. The fluctuation of droplet diameter caused by the fluctuation of air velocity is considered the main driving mechanism: Assuming a negligible pre-vaporization [30, 100], the heat release rate is directly proportional to droplet evaporation rate and thus a relation between heat release fluctuations and droplet diameter can easily be found. Eckstein et al. [50] proved that for low-frequency combustion oscillations a quasi-steady description of the airblast atomizer is appropriate and droplet diameter fluctuations can be directly related to air velocity fluctuations at the injection plane:

$$\frac{Q'(\omega)}{\overline{Q}} \propto \frac{d'_r(\omega)}{\overline{d}_r} \propto \frac{u'_r(\omega)}{\overline{u}_r} \tag{2.16}$$

Positive air velocity fluctuation leads to a positive oscillation of the heat release rate because a higher velocity causes a reduction of droplet mean diameter and so a greater heat release rate. The proposed FTF is therefore:

$$F(\omega) = \sigma\Theta e^{-i\omega\tau} \tag{2.17}$$

Where σ is a constant derived from experimental correlations for the Sautern mean diameter of droplet population generated by the airblast system. Eckstein [30] for his injection system obtained a value of $\sigma = 1.6$; however recent correlations [101] suggest that this constant could be less than 1.

An assessment of analytical Flame Transfer Function applied to the analysis of modern lean-burn aero-engine combustors can be found in [5]. Simple FTFs formulations have been applied to the thermo-acoustic analysis of a tubular combustor equipped with a PERM injection system, developed by GE-AVIO, with the main aim of assessing their capabilities in the prediction of thermo-acoustic instabilities. As regards thermodynamic mean properties, two different operating conditions have been considered. The first one, which will be referred to as Case A, is a low pressure case (representative of idle conditions) in which about 20 % of fuel is supplied through the pilot injector whereas in the second one (Case B) a high pressure condition is considered.

Three FTF formulation have been tested (see Figure 2.14) the classical n-τ model with constant amplitude (FTF-1), the model proposed by Sattelmayer in [46] (FTF-2), discussed before and the one proposed by Eckstein et al. [50], just mentioned and specifically dedicated to airblast atomisers (FTF-3).

In Figure 2.15, the obtained results in terms of normalised frequency and growth rates for the three FTF formulations are shown, that evidenced the effect of the FTF formulation on the solution and that lead to the conclusion that finding a proper formulation for the FTF for liquid fuel combustor is essential in this case.

An alternative method to describe the flame behaviour and derive a
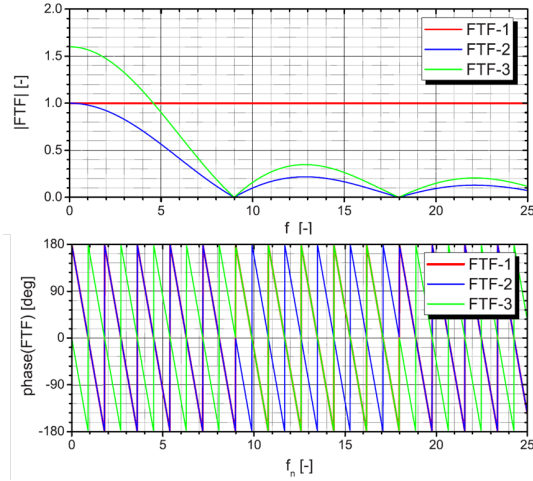
Figure 2.14: Comparison between the FTFs analysed in [5].
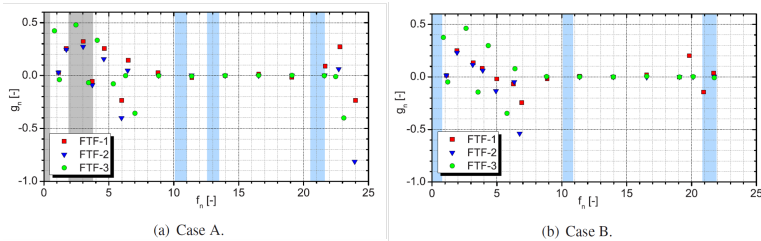
Figure 2.15: Effect of the different FTF formulation on predicted modes stability for the two cases tested in [5].

time leg distribution is using numerical simulations. Steady state RANS simulations can be used combined with a Lagrangian approach to derive a time-lag distribution. Once the steady solution of the flame front is computed, particles are injected in the domain and their flying times from the injection point to the flame front are measured. There could be found several example in literature where this approach is used (see i.e. Giauque et al. [102], Flohr et al [103, 104], Campa [74]). In Figure
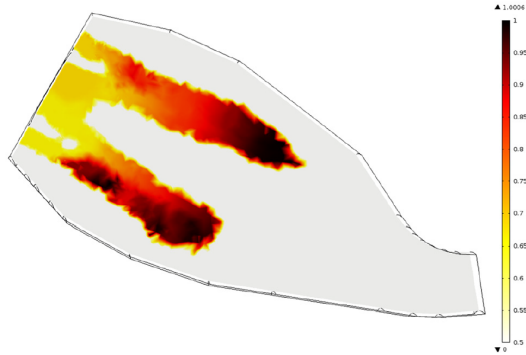
Figure 2.16: Example of a (normalized) time delay distributions obtained from RANS simulations [74].

2.16 an example of a time lag distribution within and industrial annular combustor, obtained from RANS simulations, is shown. In particular, in a postprocessing of CFD calculations, the trajectories of 4480 particles, randomly starting from the fuel injection point, are followed to the flame front and the time delay for each particle computed [74].

As discussed in section 2.2.2, the dynamics of the flame response to equivalence ratio perturbation is described by the shape of the Unit Impulse Response; in particular the undershoot in the late stages of the response can be explained by an interaction of changes in the heat released per mass of premixture and burning velocity with perturbations of flame position and surface area. Therefore, as pointed out by Polifke in [92], approaches using steady state CFD simulation to determine F_ϕ simply as "fuel transport time lag distributions" are not able to capture this effect: these methods assume a fixed position of the flame ("frozen flame") and therefore a constant flame surface area. The reduction in flame surface due to "front kinematics", which is responsible for the undershoot in the UIR_ϕ and therefore also for the excess gain of F_ϕ, cannot be properly described with such modelling strategies.

In Krebs et al. [105], instead, a transient CFD is used solving for a

passive scalar thus adopting an Eulerian approach. The advantage of the latter, compared with a Lagrangian one is that it allows the determination of a time lag distribution not only for the flame location but in the whole combustor [42].

Despite an improved time lag definition, through a time lag distribution, in all these approaches the amplitude term, the interaction index n, is still unsolved and a constant, empirical value is to be used.

To describe both the Flame Transfer Function amplitude and the time lag as a function of the frequency, many approaches exploit unsteady CFD to analyse the dynamic response of the flame to a forcing of the acoustic variables.

To investigate the flame response at a specific frequency, the system can be excited with harmonic forcing at the frequency of interest (as it is commonly done in experimental procedures). This approach is particularly suitable when the interest is focused on the response to a single frequency or to get more insight to the flame front kinematic response. Successful application of this method can be found in literature, when applied to a methane jet-flame [106] or to a more complex configuration as a swirled premixed burner [102, 107], industrial configuration [108, 109, 110, 111]. Obviously, if the flame response has to be obtained over a wide range of frequencies, such a method need for many CFD computations and, in case of complex configurations, this might become infeasible for industrial purposes (especially if LES/SAS/DES modelling approaches are adopted).

To compute the Flame Transfer Function in a single computation an impulsive excitation can be used [112] as it contains multiple frequencies. The system response is recorded an Laplace-transformed to obtain the Flame Transfer Function .

Alternatively, a way to determine the FTF is its computation from computational time series data generated with unsteady CFD simulations, where the flame dynamics is reproduced, coupled with the digital signal post-processing methods from System Identification (SI).

A simulation is performed exciting the system with a carefully designed broadband signal, so that the whole range of frequency of interest is excited

at the same time. From the time series of the input excitation and of its response, it is possible to calculate the Unit Impulse Response using a well-established procedure (see i.e. [113]) based on a linear least-square optimization and exploiting correlation functions (Wiener-Hopf method). The computed UIR is then Z-transformed to obtain the FTF.

2.3.1 Literature Rewiew of CFD/SI Applications

Some application of CFD/SI at non reactive context can be found in literature (e.g.[108, 114, 115]) to obtain the transfer matrix of acoustic elements.

Concerning reactive application of the methodology, in [43] Komarek and Polifke and in [95, 116] Chong et al. investigated an experimental turbulent premixed swirl flame. In particular, in [43] the authors analysed impact of fluctuations of swirl number and swirler position on flame dynamics using URANS simulations, providing the interesting results presented in section 2.2.1 and insight on premixed flames dynamics.
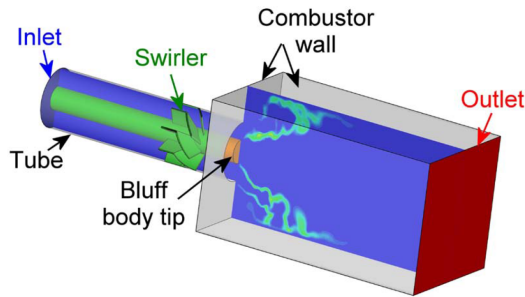
Figure 2.17: Burner studied in [95, 116].

Chong et al. [95] compared results from CFD/SI using URANS and LES simulations with experiments, for the same burner (see Figure 2.17). The FTF identified from LES, as seen in Figure 2.18, shows quantitative agreement with experiment for amplitude and phase. At higher frequencies, the gain of the FTF is underpredicted. URANS results
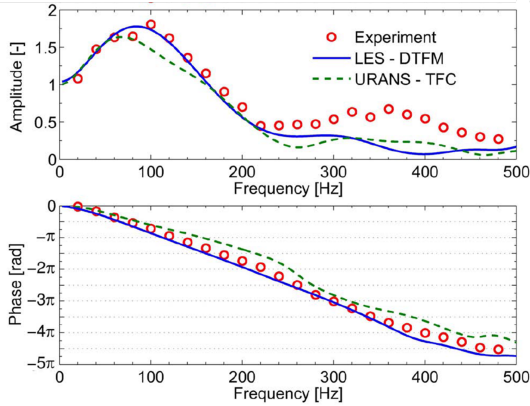
Figure 2.18: Comparison between experimental and numerical FTFs from
LES and RANS simulations [116].

show good qualitative agreement, capturing the main features of the flame
response.

Moreover, heat losses at the combustor walls were found to have a
strong influence on computed flame shapes, spatial distributions of heat
release, and frequency response.

As already discussed in sections 2.2.1 and 2.2.2, if a premixed flame
can be described by a SISO model, in case of practical premixed flame
a MISO model would be more representative, as the interaction mech-
anisms between flow, mixing, heat release and acoustics may be active
simultaneously. Huber and Polifke in [93] extended the CFD/SI approach
in the case of practical premix flames with a MISO model structure.
URANS simulation were used to study a generic practical premixed swirl
burner with two and three fuel injection stages upstream of the swirler.
Compared to a SISO model with only one signal channel, identification
of a MISO model should be more difficult, especially in the presence of
noise (turbulence related noise, spurious numerical effects, etc.), because
several input signals, usually partly correlated with each other, must be
"disentangled" [92].

Application of the CFD/SI approach to industrial combustor configurations can be found in [117] where Yang et al. performed LES simulations of and Flame Transfer Function analysis of an Alstom reheat combustor, validating against full-scale engine measurements. In this case, the flame is modelled as SISO system despite being a practical burner. Physical insight of the coupling mechanisms responsible for the dynamic response of the flame is therefore studied under such an assumption.
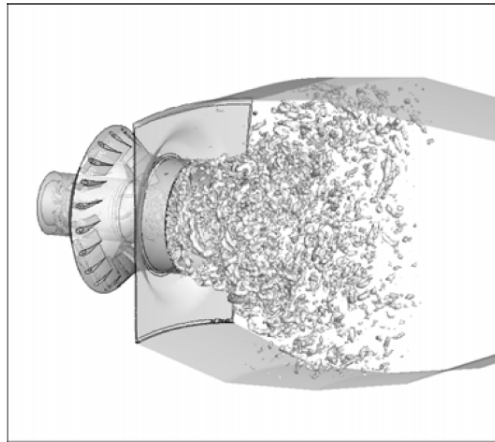
Figure 2.19: Image of the investigated combustor in [109], with Q-criterion isosurface.

Hermeth [109] performed LES simulations of a Siemens/Ansaldo industrial gas turbine in Figure 2.19, for two different burner geometries and operating conditions. The FTF is only slightly influenced for the two operating points but slight modifications of the swirler geometry do modify the characteristics of the FTF, showing that a simple model taking only into account the flight time is not appropriate and additional mechanisms are at play: Inlet velocity, the swirl and the inlet mixture fraction fluctuations. An example of the results for the computed FTF is shown in Figure 2.20.

Another FTF approach linking heat release rate to inlet velocity and
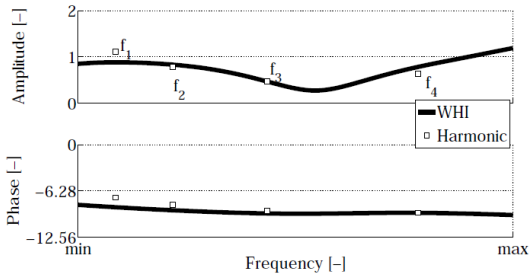
Figure 2.20: Comparison between the FTF obtained with SI (WHI) and that obtained with harmonic forcing [109].

mixture fraction fluctuation (MISO model) has been identified as a further solution for complex systems, to be developed in the future.

Finally, applications to liquid fuel-spray atomizers can be found in Zhu et al. [118] where they focussed on the low frequency oscillation (in the range 50-120 Hz) commonly called "rumble." They performed RANS simulations of a simplified domain and computed the system transfer function by determining the coefficients of an IIR filter (Infinite Impulse Response) for which the output signal is the downstream heat release rate and the input signal is the inlet flow rate (SISO system). Information has been provided distinguishing two forms to the low-frequency quasi-steady response. In the primary zone, the rate of combustion was found to be enhanced when the inlet air velocity is large while near the edge of combustion zone, the rate of combustion depends on the mixture fraction and is high when the mixture fraction is close to the stoichiometric value. At higher frequencies, the combustion lags this quasi-steady response through simple lag-laws.

In the present work, the CFD/SI procedure has been applied to a lean premixed swirl-stabilized combustor, experimentally studied at Technische Universität of Munich in order to validate it and perform some sensitivities to the main parameter. The results are presented in Chapter 4. After assessing the whole methodology, two applications at practical

configurations are presented in Chapters 5 and 6, where a technically-premixed lean methane heavy-duty gas turbine combustor and a liquid fuel combustor for aero-engine applications are studied, respectively.

Before presenting the mentioned applications, next chapter describes the models and some of the theory required for this purpose.

Chapter 3

Numerical Methods for Flame Dynamics Investigation and Thermo-acoustic Stability Analysis

In this chapter the numerical methods and the general practices utilised in the CFD investigation of the flame dynamics, the data post processing and in the thermo-acoustic stability analysis are discussed. In the first section 3.1 the general equation of the acoustic problem which are solved in the FEM code are presented together with the main modelling strategies adopted in this phase. Following, in section 5.2 the general rules used in the CFD computations as well as preliminary analysis devoted to assess the final setup are described. The basics of the System Identification theory are presented in the following section 3.2.3, while the developed CFD post processing tool are described in section 3.2.4.

3.1 Thermo-acoustic Stability: Equations and Modelling Strategies

3.1.1 Linear Acoustics Equations

The thermo-acoustic problem, the acoustic wave propagation, the flame heat release and its coupling with the acoustics as well as entropy waves, can be completely described by the Navier-Stokes Equations. Successive simplifications are then introduced to arrive to the inhomogeneous wave equation, which is the one solved in this work to investigate the combustor stability properties.

For a compressible viscous fluid, neglecting volume forces, the conservation of mass, momentum and energy lead to the Navier-Stokes equations which assume the following form:

$$\frac{D\rho}{Dt} = 0, \qquad (3.1)$$

$$\rho\frac{D\mathbf{u}}{Dt} = -\nabla p + \frac{\partial \sigma_{ij}}{\partial t}\mathbf{n}_j, \qquad (3.2)$$

$$\rho\frac{D}{Dt}\left(e + \frac{1}{2}\mathbf{u}^2\right) = -\nabla \cdot (p\mathbf{u}) + q + \nabla \cdot (k\nabla T) + \frac{\partial \sigma_{ij}u_i}{\partial t}. \qquad (3.3)$$

Where p is the pressure, ρ the density, $\mathbf{u}$ the velocity vector, σ_{ij} the viscous stress tensor, n_i the unity vector in the direction i and e the intenal energy. With $\frac{D}{Dt} = \frac{\partial}{\partial t} + \mathbf{u} \cdot \nabla$ is indicated the material derivative. Together with the constitutive equation of the gas, the equation of state, the previous equations form a complete set. In the present work, the gas is considered to behave like an ideal gas and the equation of states reduces to:

$$p = \rho R_g T \qquad (3.4)$$

Where T is the temperature and $R_g = c_p - c_v$ is the gas constant with the specific heats at constant pressure and constant volume respectively. In particular, for an ideal gas both c_p and c_v are constant.

Rearranging equations 3.2 and 3.3 and exploiting the Second Law of Thermodynamics, Eq. 3.3 can be expressed in terms of entropy S:

$$\rho T \frac{DS}{Dt} = q + \nabla \cdot (k\nabla T) + \sigma_{ij} \frac{\partial u_i}{\partial t} \qquad (3.5)$$

This equation shows that the heat release appears as a source of entropy together with the effects of temperature gradients and viscous effects. Basically, the latter terms are strictly related to the irreversibility of a real fluid. Both these terms, in fact, disappear when an inviscid fluid ($\sigma_{ij} = 0$) is considered.

Entropy is generated unsteadily in the flame region (hot spots) and convected by the mean flow, altering the fluctuating fields. It has been observed [72] to be of importance only for the lowest-frequency modes. This is mainly due to the fact that the high-frequencies entropy disturbances are smoothed out by turbulent mixing and diffusion as they are convected downstream so that they may be negligible by the time the wave reaches the combustor exit [72]. Once the entropy wave interacts with the boundary it may be partially converted into acoustics [119] and it may enhance or damp the thermo-acoustic modes of the system.

The flow variable at the position x and at the time instant t can be considered as the superposition of a mean value (denoted with the overbar) and a fluctuating component:

$$p(x,t) = \overline{p(x)} + p'(x,t) \qquad (3.6)$$

$$\rho(x,t) = \overline{\rho(x)} + \rho'(x,t) \qquad (3.7)$$

$$u(x,t) = \overline{u(x)} + u'(x,t) \qquad (3.8)$$

The perturbation are considered small compared to their ambient state values:

$$p'/\overline{p} \ll 1; \qquad \rho'/\overline{\rho} \ll 1 \qquad (3.9)$$

and consequently also the velocity fluctuation u' of the fluid associated with the acoustic wave propagation $u'/(p'c)$ is considered to be small.

Under this assumption, a linear approximation of the conservation equations can be realized: the Linearised Navier-Stokes Equations. However, this implies that the following derivations are restricted to the application of linear acoustics. When an inviscid flow is considered the Linearised Euler Equations are obtained:

$$\frac{\overline{D}\rho'}{Dt} = \overline{\rho}\nabla \cdot \mathbf{u}' = 0, \tag{3.10}$$

$$\frac{\overline{D}\mathbf{u}'}{Dt} = \frac{1}{\overline{\rho}}\nabla p' = 0, \tag{3.11}$$

$$\overline{\rho T}\frac{DS'}{Dt} = q'. \tag{3.12}$$

Combining equations 3.10, 3.11 and 3.12 and considering the entropy fluctuation $S' = c_v p'/\overline{p} - c_p \rho'/\overline{\rho}$ and $\gamma = c_p/c_v$, the inhomogeneous wave equation can be written as follows:

$$\frac{1}{\overline{c}^2}\frac{\overline{D}^2 p'}{Dt^2} - \nabla^2 p' = \frac{\gamma - 1}{\overline{c}^2}\frac{\overline{D}q'}{Dt} \tag{3.13}$$

In gas turbine combustion systems a mean flow is generally present which brings fresh reactants in the combustion zone [72]. Typically, the Mach numbers in the plenum and flame tube regions are small (less than 0.1) while they assume not negligible values in the burner region, connecting the formers. A common assumption is to neglect mean flow leading to a simplification of the governing equations and, at the same time, introducing errors which may have a severe influence on the stability prediction of the principal modes. In general, three types of fluctuations are coupled in a combustor: acoustic waves, entropy waves and vorticity waves [120]. Acoustic perturbations propagate at the speed of sound augmented or reduced by the local mean velocity while the last two modes are simply convected by the mean flow. The main consequence of assuming a zero-Mach number is that neither the entropy nor the

vorticity mode can propagate so that a wave equation for the acoustic perturbations can be derived. That is, both dissipation and the effect on acoustic propagation are neglected.

When a mean flow at rest is considered, equation 3.13 becomes:

$$\frac{1}{\bar{c}^2}\frac{\partial^2 p'}{\partial t^2} - \nabla^2 p' = \frac{\gamma - 1}{\bar{c}^2}\frac{\partial q'}{\partial t} \tag{3.14}$$

3.1.2   The FEM Model

In this work, the thermo-acoustic problem is described by equation 3.14. The solution consists in determining the resonant frequencies of the combustor and the stability of the modes associated to them. It is possible to write the generic fluctuating quantity ψ' as:

$$\psi' = Re(\hat{\psi}exp(i\omega t)). \tag{3.15}$$

ω is a complex quantity whose real part represents the frequency of oscillations and the imaginary one the growth rate of oscillations which characterize the stability of a mode. An unstable mode will have a negative imaginary part, meaning an amplitude of the fluctuation growing with time. Substituting, the 3.14 becomes the inhomogeneous Helmholtz equation, in the frequency domain:

$$\frac{\lambda^2}{\bar{c}^2}\hat{p} - \nabla^2\hat{p} = -\frac{\gamma - 1}{\bar{c}^2}\lambda\hat{q} \tag{3.16}$$

The quadratic eigenvalue ($\lambda = -i\omega$) problem here above is solved with the acoustic module of COMSOL Multiphysics [121] by means of an iterative linearisation procedure.

This routine is based on a variant of the Arnoldi algorithm called the implicit restarted Arnoldi method [122]. An iterative procedure based on a quadratic approximation around an eigenvalue linearisation point λ_0 is adopted. Such a procedure is speeded up by using, as approximate starting eigenvalue, the value obtained through the analysis of the system without heat release fluctuations. The solver reformulates the quadratic eigenvalue problem as a linear eigenvalue problem of the conventional

form $Ax = \lambda Bx$ and iteratively updates the linearisation point until convergence is reached [73].

The actual form of the equation, solved in COMSOL is:

$$\frac{\lambda^2}{\rho c^2}\hat{p} - \frac{1}{\rho}\nabla^2\hat{p} = Q^{com} \tag{3.17}$$

so that the source term (monopole source in COMSOL) is

$$Q^{com} = -\frac{\gamma - 1}{\rho c^2}\lambda\hat{q} \tag{3.18}$$

3.1.2.1 Source term application

The key of the problem is, therefore, the expression to be given at the heat release fluctuations $\hat{q}$, generally related to the acoustic fluctuations at the injection location through the Flame Transfer Function.

If the classical $n - \tau$ model is used, for example, the $\hat{q}$ is expressed as:

$$\frac{\hat{q}}{q} = -n\frac{\hat{u}_b}{u}e^{-i\omega\tau}, \tag{3.19}$$

where $\hat{u}_b$ is the acoustic velocity fluctuation at the burner mouth.

When the Flame Transfer Function computed from the CFD is used, instead, the $\hat{q}$ is expressed as:

$$\frac{\hat{q}}{q} = |FTF(\omega)|\frac{\hat{u}_b}{u}e^{i\measuredangle FTF(\omega)} \tag{3.20}$$

Where the $|\cdot|$ indicates the modulus and the $\measuredangle$ the phase.

The source term has to be zero outside the flame location while it assumes non-zero values in the flame region.

In general, the flame location can be identified in the FEM code by means of a dedicated sub-volume inside the combustor (see Figure 3.1), where the source term is applied, or through a mathematical function. In the first case, a geometrical shape (cone, cylinder) can be adopted to model the flame region but its definition is affected by the raw approximation.

In the application presented in this thesis, the flame region is defined

exploiting the results of a reactive CFD simulation. In particular, the flame shape is imported in the FEM code with an interpolation function. In the CFD there are several possibility for the flame definitions: it can be identified by the region where the rate of reaction (Product Formation Rate) assumes non-zero values (see Figure 3.2a) or, in case of models solving for a reaction progress variable (see 3.2.2.3), as the region where this variable is comprised between 0 and 1 (see Figure 3.2b).
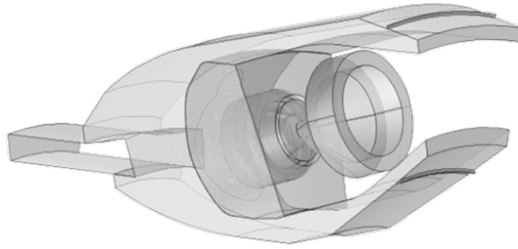
Figure 3.1: Example of flame sub-volume in a aero-engine combustor application.

(a)   (b)
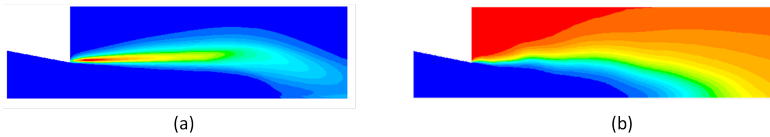
Figure 3.2: Example of fields used in the flame region definition: (a) Product Formation Rate, (b) progress variable.

Once imported in COMSOL, a mathematical function, F (flame-identifying function), which is zero outside the flame, can be defined. The source term $Q^{com} \propto \overline{q} * F$ can be defined into the whole combustor volume but, in this way, it is actually applied only in the flame region.

If a uniform monopole source is to be applied in the flame region, the term Q can be defined as the whole heat rate divided by the flame volume:

$$\overline{q} = \frac{TotalHeatRate}{\int_V F dv} \qquad (3.21)$$

Where F is defined as a step function with unity values inside the flame, zero elsewhere, as shown in Figure 3.3.
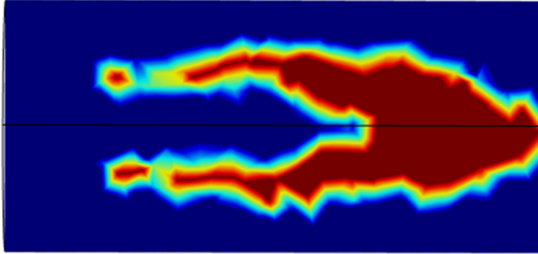
Figure 3.3: Step function to identify the flame region in the FEM model.
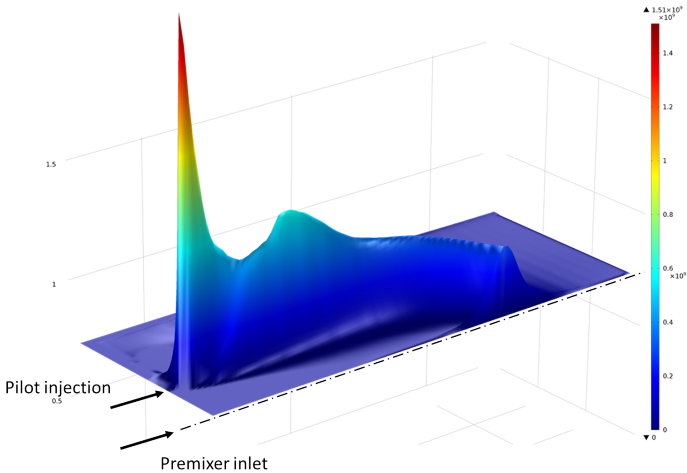
Figure 3.4: Weighting function proportional to the PFR.

To apply a non-uniform distribution of the source term, a weighting function ($WF(\mathbf{x})$), shown in Figure 3.4, can be defined in the flame region,

i.e. proportional to the Product Formation Rate (PFR). In this case the local source term is defined as:

$$\overline{q} = \frac{TotalHeatRelease}{\int_V WF(\mathbf{x})} \tag{3.22}$$

and the monopole source term as:

$$Q^{com} \propto \overline{q} * WF(\mathbf{x}) * F \tag{3.23}$$

In case of an annular combustor with N burners, the $i - th$ flame is influenced by the fluctuations u_i at the $i - th$ burner mouth only.

If in COMSOL a single volume is dedicated to the whole flame tube, the local source term can be defined as:

$$Q^{com} \propto \sum_{i=1}^{N} \hat{q} * WF_i(\mathbf{x}) * F_i \propto \sum_{i=1}^{N} \frac{\hat{u}_i}{\overline{u}} * WF_i(\mathbf{x}) * F_i \tag{3.24}$$

So that in the $i - th$ flame region F_i the only active term is the source influenced by the $\hat{u}_i$ at the mouth of the $i - th$ burner.

Alternatively, the flame volume can be divided into N sectors (see Figure 3.5) and the in each of this is applied the corresponding source term:

$$Q_i^{com} \propto \hat{q} * WF_i(\mathbf{x}) * F_i \propto \frac{\hat{u}_i}{\overline{u}} * WF_i(\mathbf{x}) * F_i \tag{3.25}$$

Even if practically identical, the two strategies differ substantially for the memory reserved by the FEM solver for the solution. In the first case, in fact, each point of the flame tube is formally a function of all the N fluctuations u_i while, in the second case, it is influenced by the fluctuation at the $i - th$ burner only. As a result, in the solution procedure, the first case produce a much more sparse matrix resulting in a high demanding memory requirement.
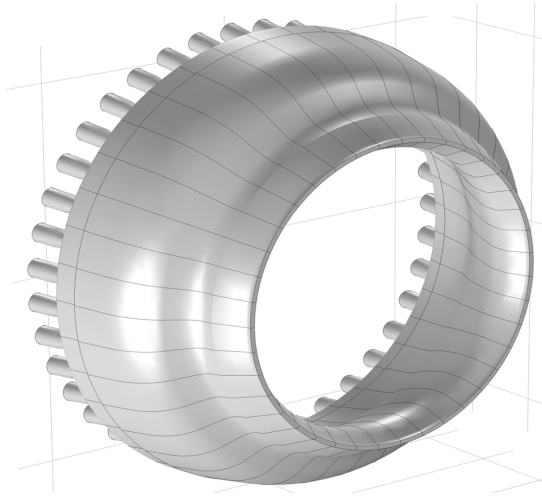
Figure 3.5: Annular combustor where the volume is divided into N sub-domains.

3.1.2.2   Temperature field import

Looking at the equation 3.14 it possible to see how the problem is governed by two main quantities : the density ρ and the sound speed c. In order to give a more physical representation, the temperature distribution is imported in the FEM model from the CFD results. Consequently, the density and the sound speed assumes local values as:

$$\rho(\mathbf{x}) = \frac{p}{R_g T(\mathbf{x})}, \qquad c(\mathbf{x}) = \sqrt{\gamma R_g T(\mathbf{x})}. \tag{3.26}$$

3.1.2.3   Burner Transfer Matrix (BTM)

An element inside of an acoustic system can be replaced by its transfer matrix (TM) linking the acoustic variables at the upstream and downstream sections (see Eq. 3.27).

$$\begin{pmatrix} \frac{p'}{\rho c} \\ u' \end{pmatrix}_d = \begin{pmatrix} T_{11} & T_{12} \\ T_{21} & T_2 \end{pmatrix} \begin{pmatrix} \frac{p'}{\rho c} \\ u' \end{pmatrix}_u \tag{3.27}$$

Where u and d stand for upstream and downstream respectively. The BTM approach involves determining four complex values (T_{ij}) from numerical simulations or experiments. Otherwise, a theoretical formulation for the BTM can be retrieved from the application of the conservation equations, i.e. the formulation proposed by Fanaca et al. [123] and Alemela et al.[124] for one-dimensional flow with low Mach number within a "compact element", variable cross section and pressure losses.

In the present work the BTM approach is not adopted in all the cases. When the BTM is used, however, it is numerically computed exploiting a numerical procedure already developed internally in case of mean flow at rest and and upgraded one where the mean flow effects are taken into account.
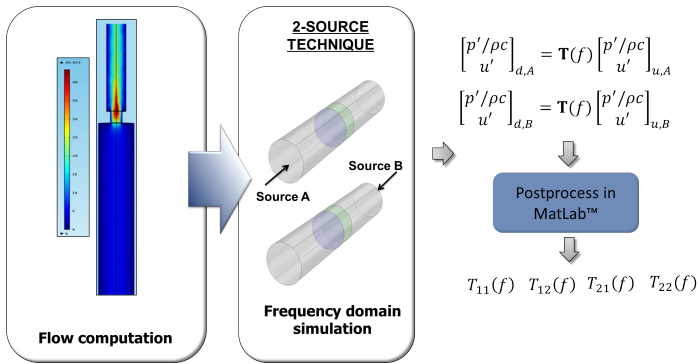
Figure 3.6: Scheme of the procedure used to compute the BTM in presence of a mean flow.

The implemented procedure to compute the TM is the numerical implementation of the experimental two-source technique [125]. Basically such experiments involve perturbing the element with an acoustic

source as an in-line siren or wall-mounted loudspeakers. Being four the coefficients to be determined, the element needs to be perturbed from both sides, once upstream and once downstream. This approach does not rely on any modelling, assuming only linear perturbations. The main drawback is the necessity of repeating the determination procedure for each operating condition, being the TM dependent on the mean thermodynamics conditions. If no mean flow is considered the TM can be computed using the *Pressure Acoustics* module in COMSOL. In order to account for local non-zero Mach number effects in the burner region, the burner is replaced with its transfer matrix, computed through the COMSOL *Aero-acoustics* module considering an assigned mean-flow, and which implicitly takes into account the mentioned effects. A flow physics is introduced in the model and solved, assigning at the inlet the desired mass flow. Once the mean flow is solved, a frequency domain simulation with acoustic forcing is performed, varying the frequency in the desired range and recording the values for pressure and velocity fluctuations at the TM interfaces. A dedicated Matlab post-process procedure is then used to retrieve the matrix coefficients (see Figure 3.6).

Following the procedure successfully adopted in [73, 126], the TM is implemented in Global Equations and a Normal Acceleration boundary conditions are applied at the matrix interfaces (upstream and downstream the element) considering the acoustic velocities. The procedure has been assessed and tested (see Appendix A.1). The effects of a mean flow have been evaluated in terms of acoustic attenuation and blockage at the premixer section as well as in terms of growth rate and mode shape of the computed eigenfrequencies. Comparisons with a 1D in-house code, theoretical BTM formulation[123, 124] and analytical solutions available in literature [72] showed a good prediction of the trends but an underestimation of the attenuation of the growth rate effect. Improvement in the BTM computation should be led by the introduction of viscous effects (i.e. solving for Linearised Navier Stokes Equations), neglected in the actual BTM computation.

3.2   CFD/SI Approach for the Flame Transfer Function Computation

In this second section, the procedure used to study the flame dynamics in the application of this work is described. The procedure is based on the coupling of a numerical simulation and the post-process technique of the System Identification.

The general practices common to all the applications are therefore discussed in the present section with particular attention to the computational code, the numerical settings and models (i.e. the combustion model). If in the study of a particular case, a dedicated model is adopted (i.e. Discrete Particle Model for liquid fuel) or in case of a comparison of the combustion model with an other one, specific details will be provided in the dedicated section.

3.2.1   Identification Strategy

The identification of the FTF by CFD/SI requires an unsteady simulation where the flow variables are excited to obtain a system response. The time series of the input variables (i.e. velocity, equivalence ratio fluctuations etc.) and heat release fluctuations are recorded in the simulation. When a MISO structure is considered to model the flame, this responds to mass flow and equivalence ratio fluctuations and two independent excitation signals are required to discern the individual effects in the post-processing identification step [42].

When extracting data from the CFD, attention should be paid to the coupling with the FEM code that solve the problem in terms of acoustic variables (p and u).

As pointed out in [42], the kinematic response to acoustic velocity perturbation F_u can be included in the FEM code in a straightforward manner extracting the velocity fluctuation at the burner exit. The CFD simulation can include only the combustion chamber if a proper inlet boundary condition is set, which takes the flow conditions upstream into account (e.g. swirling flow).
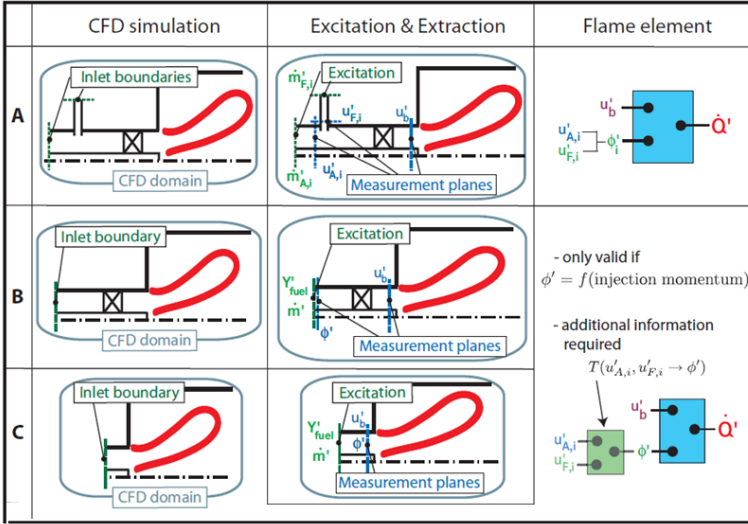
Figure 3.7: Scheme of possible identification strategies (adapted from [42])

In case of the response to equivalence ratio fluctuations, different solutions are discussed by Huber in his thesis [42] and reported here, which determine the size of the simulated domain and therefore the computational effort.

In case A the fuel ducts are included in the simulation, the fuel mass flow and the air mass flow are excited at the inlet boundary condition of the fuel line and of the mixing section, respectively. The average fluctuations are recorded upstream the fuel injection and in the mixing section upstream of the burner exit and taken as the input signals for the post-processor. The global heat release is then computed as sum of the two FTFs as in 2.13

In case B, the adduction ducts are removed from the simulation and only a part of the mixing section, the swirler and the combustion chamber are simulated. The excitation is introduced perturbing the fuel mass fraction at the inlet the assuming that the spatial distribution of

equivalence ratio fluctuations does not vary with injection momentum (not always valid as in case of jet-in cross flow whose penetration is influenced by the momentum ratio between the fuel and the mainstream). A transfer function might be necessary in the FEM code to connect the equivalence ratio fluctuations at the measurement section of the CFD simulation with the acoustic variables at the location where this fluctuations are produced. In simple configurations a constant time delay model can be chosen, which accounts for the convective transport of the fuel between both locations.

A further reduction of the computational domain is possible if also the swirler section is removed (case C). The fuel mass fraction and a fluctuation of the total mass flow rate are, in this case, both applied at the inlet boundary. The excitation signals can be used directly for the calculation. The FEM model for both cases require again a transfer function to express the equivalence ratio in terms of the acoustic fluctuations at the location of fuel injection. In contrast to case B such a transfer function should ideally also account for the dispersion due to the turbulent flow field in the mixing section and swirler.

3.2.2 CFD numerical settings

3.2.2.1 Numerics

To perform the numerical simulations the commercial Navier-Stokes solver Ansys Fluent versions 15.0 to 16.0 has been used. A second order scheme is adopted for the spatial discretization except for turbulence related quantities for which a first order upwind is adopted. A bounded second order implicit scheme is used for the time discretization together with a time step coherent with the solved case physics.

3.2.2.2 Non-Reflecting Boundary Conditions (NRBC)

In order to avoid wave reflection at the boundaries, which can affect the flame dynamic behaviour and deteriorate the identification procedure, a Non-Reflecting Boundary Condition (NRBC) is to be used. This is one of the motivations that makes the choice of Ansys Fluent more suitable

than other commercial codes: the availability of NRBC in case of reacting flow solution.

The implemented NRBC in Fluent [127] are based on characteristic wave relations derived from the Euler equations, developed for multi-dimensional viscous flow by Thompson [128, 129], and Poinsot and Lele [130].
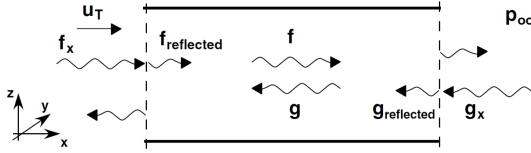
Figure 3.8: Domain with characteristic waves *f*, *g* in the interior and at the boundaries $f_{reflected}$, $g_{reflected}$: reflected waves at the upstream inlet and at the downstream outlet boundary, respectively. f_x, g_x: external forcing at inlet and outlet, respectively [131].

In the presence of a mean flow u, given that perturbation amplitudes are sufficiently small, acoustic signal components are conveniently expressed in terms of the (linearized) characteristic wave amplitudes $f = (x - (u + c)t)$ and $g = (x - (u - c)t)$ travelling in the positive and negative x-direction, respectively (see again Figure 3.8). Characteristic wave amplitudes f, g and acoustic fluctuations of pressure $\hat{p}$ and velocity $\hat{u}$ are related to each other as follows:

$$f = \frac{1}{2}\left(\frac{\hat{p}}{\rho c} + \hat{u}\right), \qquad g = \frac{1}{2}\left(\frac{\hat{p}}{\rho c} - \hat{u}\right).$$ (3.28)

A strategy for defining boundary conditions in compressible viscous flow is reformulating the latter in terms of characteristic wave relations, exploiting the quantities [130]:

$$L_i \equiv \lambda \left(\frac{\partial p}{\partial x} \pm \rho c \frac{\partial u}{\partial x}\right)$$ (3.29)

which represent time variations of wave amplitudes at the boundary.

The Local One-Dimensional Inviscid (LODI) relations to obtain approximate values for the wave-amplitude variations in terms of the primitive flow variables are obtained. As an example, for pressure and velocity the following relations are obtained:

$$\frac{\partial p}{\partial t} + \frac{1}{2}\left(L_1 + L_5\right) = 0, \tag{3.30}$$

$$\frac{\partial u}{\partial t} + \frac{1}{2\rho c}\left(L_5 + L_1\right) = 0 \tag{3.31}$$

where $\lambda_1 = u - c$ (forth-travelling wave) and $\lambda_5 = u + c$ (back-travelling wave).

A subsonic reflecting outlet ("open end") condition becomes:

$$\hat{p} = f + g = 0 \qquad L_1 + L_5 = 0. \tag{3.32}$$

A fully reflecting ("closed end") inflow boundary condition becomes:

$$\hat{u} = f - g = 0 \qquad L_5 - L_1 = 0. \tag{3.33}$$

A Non-Reflecting Boundary following Linear Relaxation Method of Poinsot and Lele [130], instead, is expressed as:

$$L_1 = \frac{\sigma c}{L}\left(p - p_\infty\right) \qquad (outlet), \tag{3.34}$$

$$L_5 = \frac{\sigma c}{L}\left(u - u_T\right) \qquad (inlet). \tag{3.35}$$

where σ is the relaxation parameter (lowering or enhancing this parameter has the same effect of moving farther or closer the boundary application point to the actual boundary) and L is representative of the domain length.

Such a condition have been tested with simple CFD toy-mode and it has been found to work quite well for the outlet-boundary. At the inlet, the NRBC can be coupled in Fluent with a velocity-inlet where

the target velocity u_T has to be assigned. In order to generate a velocity profile variable in time it is not possible to act directly on the velocity target (u_t). What happens in this case is depicted in Figure 3.11 where the resulting profile is compared to the desired one, both obtained in a simple simulation of a tube.
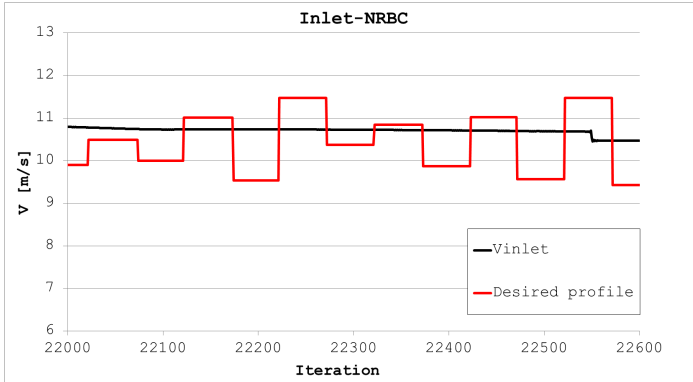
Figure 3.9: Desired (red) and resulting (blu) profile is the external excitation is applied at the target velocity in Fluent BC.

Moreover, as explained by [131] incoming excitation should be allowed to enter the computational domain and outgoing transients (g in Figure 3.8) should leave the domain without reflections. Numerical reflections at the boundaries can significantly affect the predicted flow, particularly if the geometry of the numerical domain has eigen-frequencies that match the frequencies of physical waves propagating through the flow [127].

To overcome this issue, the Non-Reflecting Boundary in case of acoustic excitation and "plane wave masking", proposed by Polifke et al. [131] has been implemented in the code by means of an User-Defined Function.

The boundary without forcing becomes:

$$L_5 = \frac{\sigma c}{L} \rho c \left(u + g - u_T \right). \tag{3.36}$$

The idea is to identify outgoing plane waves at the boundary, and then

explicitly eliminate outgoing wave contributions (g) from the linear relaxation term. In this way the contribution of the outgoing wave g to the velocity u is removed from the linear relaxation term. In other words, the "masked" outgoing wave g no longer contributes to the incoming wave and therefore should leave the domain without reflection at the boundary [131].

To construct non-reflecting boundaries with masking of outgoing plane waves and acoustic excitation, the incoming wave amplitudes f_x at the upstream inlet must be introduced (see Figure 3.10):

$$L_5 = \frac{\sigma c}{L} \rho c \left(u - (f_x - g) - u_T\right) - 2\rho c \frac{\partial f_x(t)}{\partial t}. \tag{3.37}$$

In this formulation, f_x is the desired fluctuation, u_T is the target mean velocity. When this boundary condition implementation is used, the desired velocity profile is obtained even in the presence of a Non-Reflecting inlet.

The previous formulation has been implemented in Fluent and tested on a simple tube test where an inlet profile is imposed. It is to notice how, in this formulation, the excitation is assigned through its derivative in time. Also the outgoing wave g is to be computed in the CFD. The setting of the numerical simulation is then more complicated: a plane needs to be placed close to the inlet. On this plane the average pressure and velocity, necessary to compute the g term (see Eq. 3.28), are evaluated runtime. Moreover, the definition of the time derivative for the commonly used excitation signals (see section 3.2.2.4) such as square-waves is not straightforward.

For these reasons and for the fact that such a boundary did not resulted easy to be managed, case by case the necessity of its adoption, instead of a velocity-inlet profile, was evaluated. In particular, when the input signal frequency spectrum was not altered by the matching of domain eigen-frequency, the velocity-inlet boundary condition has been preferred.
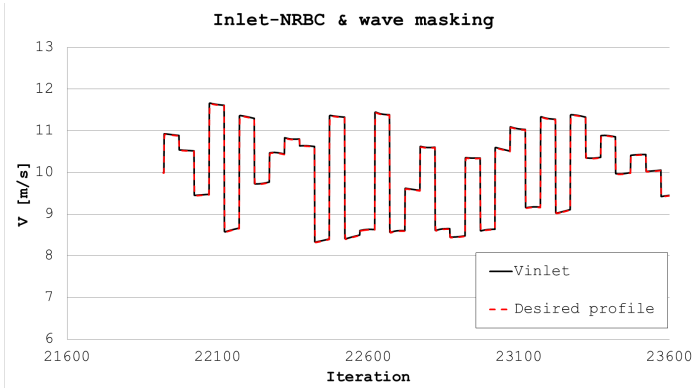
Figure 3.10: Velocity excitation applied by the implemented BC.

3.2.2.3   The FGM combustion model

As far as the combustion modelling is concerned, the FGM chemistry reduction technique has been recently employed, providing it reasonable results, for the computation of laminar [132] and turbulent partially premixed flames [132, 133], as well as for gas turbine like turbulent flames with [134, 135] and without heat losses. Moreover, reduced computational costs are generally associated with this technique, thus allowing the application of reliable and not over-simplified chemistry mechanisms in CFD simulations of combustion processes [136]. Basically, the FGM chemistry reduction method combines the advantages of chemistry reduction and flamelet models. The approach used in the latter is the idea that a multi-dimensional flame can be considered as an ensemble of one-dimensional flames, while a low-dimensional manifold is constructed solving one-dimensional flamelets [137]. As other manifolds, the number of independent control variables (manifold dimension) can be increased (i.e. reaction progress variable c, heat loss, turbulence etc.) thus improving the description of the combustion process.

In this work premixed flamelet configurations have been chosen as they have been shown to provide reasonable results for both diffusion

and premixed flames [137]. Moreover, in the latter configuration, the definition of a progress variable dimension for the flamelet tabulation becomes straightforward [138].

The progress variable is defined as:

$$c = \frac{\sum a_k \left(Y_k - Y_k^{eq} \right)}{\sum a_k Y_k^{eq}} = \frac{Y_c}{Y_c^{eq}} \tag{3.38}$$

Where Y_k is the generic specie. Generally with hydrocarbons, the species considered are CO and CO_2.

A specific kinetic mechanism is used to generate laminar flamelets databases for all the calculations and to compute laminar flame speed and mixture properties.

The laminar flamelet database all the variables are defined as a function of both mixture fraction and reaction progress variable. The added dimension makes FGM model sensitive to finite chemistry effects due to a reaction in progress and not instantaneously completed.

Due to the parametrisation by reaction progress the flame can be fully quenched, for example, by adding dilution air. No assumption of thin and intact flamelets is made by FGM, and the model can theoretically be applied to the stirred reactor limit, as well as to ignition and extinction modelling [139].

A scalar dissipation rate is also defined in Ansys Fluent FGM model as a function of Z and of the scalar dissipation of c at stoichiometric conditions (for further details see [139]). Each flamelet (different value of Z) is therefore computed at different scalar dissipation rate.

The mixture fraction and progress variable equations are solved during the calculation. The latter equation needs a closure for the source term. Typically, in the FGM model, the mean source term is modelled from the finite-rate kinetic rate obtained from the FGM, namely:

$$\overline{S}_c = \overline{\rho} \int S_{FR}(c, Z) P(c, Z) dc dZ \tag{3.39}$$

where S_{FR} is the Finite-Rate flamelet source term from the flamelet library, and $P(c, Z)$ is the joint PDF of reaction-progress (c) and mixture
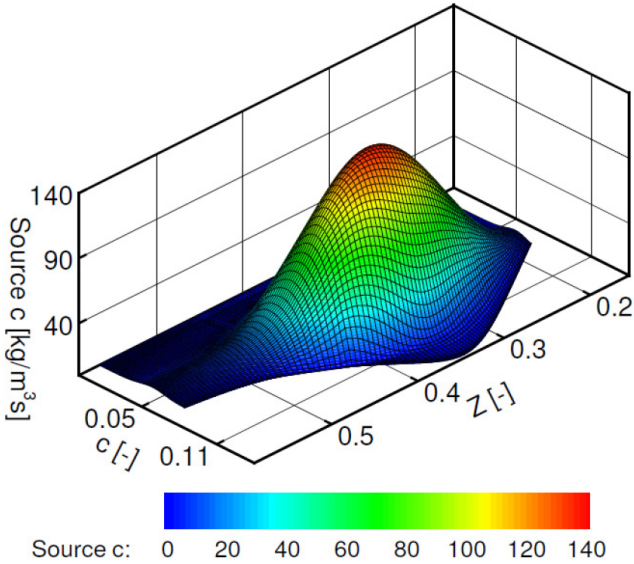
Figure 3.11: Progress variable source term parametrised as a function of mixture fraction Z and progress variable c [138].

fraction (Z).

Ansys Fluent has the option of two other turbulence-chemistry interaction models for the source term. One option is to use a Turbulent Flame speed Closure:

$$\overline{S}_c = \rho_u S_t |\nabla \tilde{c}| \tag{3.40}$$

Where ρ_u is the unburnt gases density, and S_t the turbulent flame speed. The ˜ indicates a Favre-averaged variable.

The third option is to use the minimum of the Finite-Rate and Turbulent-Flame-Speed. The idea behind is to use the turbulent flame speed model to predict the flame location and the finite-rate model to predict post-flame quenching, for example, by dilution with cold air.

A stochastic independence is generally assumed for the joint PDF $P(c, Z)$:

$$\overline{S}_c = \overline{\rho} \int S_{FR}(c, Z)P(c)P(Z)dcdZ \qquad (3.41)$$

A beta PDF shape is usually assigned to the PDFs which requires second moments to be evaluated that is, progress variable and mixture fraction variances. Two additional transport equations are, therefore, solved in the simulation.

Finally, as mentioned previously, during the simulation the quantities necessary for the system identification are recorded. The velocity fluctuations, to compute the Flame Transfer Function F_u, are recorded as mass flow average of the velocity fluctuation at the burner. Case by case, the sampling plane will be shown. The equivalence ratio fluctuations are also recorded as mass flow average at the plane of interest.

As far as the overall heat release, this is a global quantity and, using FGM combustion model, its definition is straightforward:

$$q' = \int_V S_c \cdot LHV \cdot ZdV = \int_V \rho_u \cdot PFR \cdot LHV \cdot ZdV \qquad (3.42)$$

Where LHV is the heat of reaction per unit mass of fuel and, consequently, $S_c LHV \cdot Z$ represent the heat released for unity of mixture per second.

3.2.2.4 Input signal

The input excitation is one of the fundamental aspects of the numerical identification of the FTF. Several works can be found in literature where the effect of the input signal on the result is investigated and where criteria for the quality check of the signal itself are proposed (see i.e. [42, 108, 118]). In general, the frequency spectrum is to be excited in the range of interest. Therefore, a broad-band signal that allows doing it in a single CFD simulation could be chosen. Alternatively, with a much more computationally expensive procedure, the FTF for one particular frequency can be computed at a time. An input signal with low intensity

can lead to poor results, especially in presence of noise [42]. On the other hand, the signal must be limited in amplitude to respect the linearity hypothesis lying behind the identification procedure (e.g. below the 20% of the mean velocity). A maximum utilization of this amplitude limit over a wide range of frequencies is therefore beneficial [42, 108]. A parameter to judge and quantify this aspect is the crest factor or peak-to-average ratio (see [113]).

$$Cr^2 = \frac{max_n(x_n^2)}{\frac{1}{L}\sum_{n=1}^{L} x_n^2} \tag{3.43}$$

with L number of data.

A good signal should have a low crest factor.
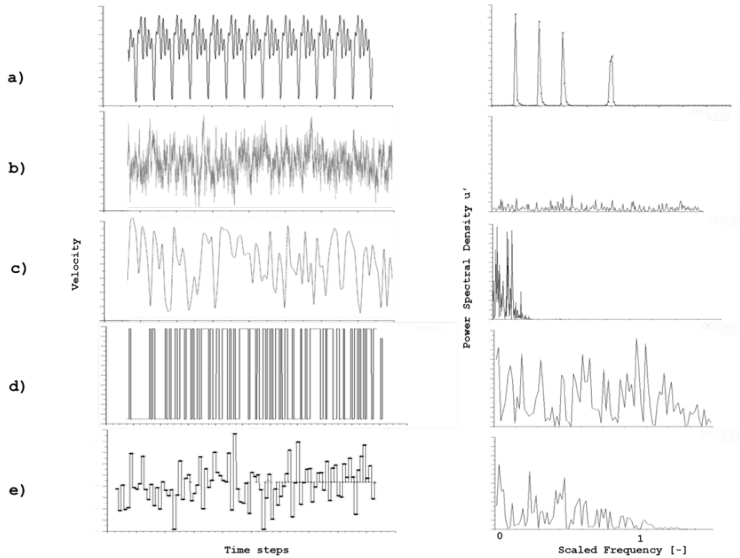
Figure 3.12: Input signals (left) and their spectra (right).

Commonly used signals, such as the composition of sine waves, a random noise signal and a random binary signal, are discussed before presenting the one adopted in this work. They are shown in Figure 3.12

together with their frequency spectra. The range of interest lies between the values of scaled frequency 0 and 1. The first signal in Figure 3.12a is formed by a number of arbitrarily chosen frequencies conveniently out-of-phase. The computed FTF will be valid in a neighbourhood of the excitation frequencies while for the other frequencies the result will be an approximation. The higher is the number of harmonics in the input signal the more accurate is the FTF over the frequency spectrum. If the frequencies of interest are known, detailed information about the system at these frequencies can be obtained from a calculation with this signal [118]. On the other hand, a broadband designed signal has the advantage that the FTF is determined as a function of the frequency in the spectrum of excitation. The random noise (RN) signal is generated from a random generated number so that all the frequencies have the same probability to be excited. If a highly uncorrelated signal, as those in Figure 3.12b, is generated part of the signal power is moved also to frequencies out of the range of interest thus limiting the signal power where needed. A filtering operation is then necessary and might be realized with standard low-pass filter operations (which may lead to a damping of the signal amplitude in the time domain, as shown in [42]) or by generating a more correlated signal as shown in Figure 3.12c. However, the control of the cut-off frequency is not straightforward. Moreover, the RN signal tends to waste power and to deteriorate easier than other signals.

The random binary signal (RB) is shown in Figure 3.12d. By varying randomly the period of the square wave within the range of interest, a broadband excitation is generated. Looking at the power spectral density of the signal, it is possible to see the tendency to act as a low-pass filter above the desired cut-off frequency (set slightly higher than scaled frequency of 1).

A further signal has been designed which combines some of the characteristics of the last two shown signals. In particular, the signal in Figure 3.12e is a Square Wave with Random variable Amplitude (RASW). The cut-off frequency is defined by the period of the square wave while the broadband characteristic is given by the variable amplitude. The

amplitude is varied in a way so that the signal mean is zero and the amplitude varies around the mean following a Gaussian distribution of imposed variance.

From the signal power spectral density it is possible to see how the filter is very effective as well as a uniform broadband excitation is achieved within the range of interest.

In order to select the most appropriate signal, tests have been run on a simple premixed flame. The discussed signals have been compare with single harmonic runs, taken as reference. For further detail refer to [140]
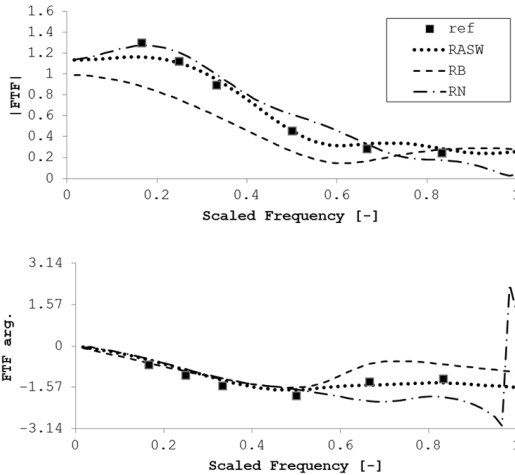
Figure 3.13: Input signals comparisons: computed FTFs module (up) and phase (down).

Figure 3.13 shows the computed FTFs. In general, it can be observed the low-pass filter behaviour of the flame. The response to acoustic excitation decreases with the frequency. All the FTFs tend to values close to 1 when the frequency tends to 0 (theoretical limit). Comparing the three FTFs with the reference computations, it is possible to see that a good agreement is obtained in terms of both absolute value and phase, with the RN and the RASW signals up to scaled frequency of

Table 3.1: *Crest factor Cr of the tested signals*

	RB	RASW	RN
Cr	1.0207	1.4137	1.5130

0.5. Above this value, the RN does not match the reference correctly. This is a consequence of a too low signal force in the second part of the spectrum due to the difficulties in controlling the cut-off frequency. A good matching is instead obtained with the RASW signal. A diffuse discrepancy between the RB signal and the reference values is instead obtained. In particular, an underprediction of the absolute values is found. In terms of phase, the RB signal gives good predictions for lower frequencies while a mismatching is found for higher ones.

In Table 3.1 the crest factor for the tested signals is reported. While RB has the best crest factor, approaching to unity, the values increase for RASW and RN. It must be noted that for RN case, the maximum admissible amplitude (set to 20 % of the mean value) is never reached but this information is not provided by such a parameter. Despite a higher Cr of the RASW signal than the RB one, probably the smoother evolution and change of the signal in time is beneficial. A possible explanation for the RB results can lie in a deviation from linearity as the jump in the change of sign is around 40 %.

Following the presented results, the FTF obtained with the RASW signal is exploited for the all the cases studied in this thesis.

3.2.3   System Identification (SI)

The time series exported from the CFD simulation are then postprocessed exploiting SI to retrieve the FTFs. A brief description of the System Identification theory is given here but for further detail please refer to specific and complete textbook ([113]).

3.2.3.1 Model structure

For small perturbation the system representing the flame can be considered a *linear time-invariant (LTI)* system: For a given input the system responds always in the same way (time-invariant) and the output is only a function of present and past inputs (causal).

For the signal theory a SISO LTI system can be fully described by the *impulse response* (h):

$$y(t) = \int_{\tau=0}^{\infty} h(\tau)x(t-\tau)d\tau \qquad (3.44)$$

Where, y is the output or response of the system and x the input signal at time t. If a noise component is present an additional term should be considered (e).

For a discrete data set, as the CFD data, the output at the instant $t_n = n\Delta t$ becomes:

$$y_n = \sum_{k=0}^{\infty} h_k x_{n-k} + e_n \qquad (3.45)$$

To avoid infinite convolution sums, the first step is the definition of the "problem dimension" (M) that is, the unit impulse h length (in time). This should be able to represent the system and, generally, it can be considered as the longest characteristic time of the system (e.g. a characteristic convective time) [92]. Sensitivity of the results to such a parameter can be found i.e. in [108]. Eq. 3.45 becomes:

$$y_n = \sum_{k=0}^{M} h_k x_{n-k} + e_n \qquad n = 0, ..., M \qquad (3.46)$$

For a flame responding to acoustic fluctuations as input ($x_n = u'/\overline{u}$), while the output is the normalized heat release rate fluctuation ($y_n = Q'/\overline{Q}$).

If the flame is modelled as a Multi-Input Single-Output system, ex-

ploiting the problem linearity, the output is determined as:

$$y_n = \sum_{k=0}^{M} h_k^{(1)} x_{n-k}^{(1)} + \sum_{k=0}^{M} h_k^{(2)} x_{n-k}^{(2)} + ... + \sum_{k=0}^{M} h_k^{(i)} x_{n-k}^{(i)} + e_n \qquad (3.47)$$

with $i = 1, ... N_{input}$, where N_{input} is the number of input of the system. If the flame responds to acoustic velocity fluctuations and equivalence ratio fluctuations then : $x_n^{(1)} = u'/\overline{u}$, $x_n^{(2)} = \phi'/\overline{\phi}$.

The $i - th$ transfer function can be determined as the Z-Transform of the Unit Impulse Response vector:

$$F^i(\omega) = \sum_{k=0}^{M} h_k^{(i)} e^{-i\omega k \Delta t} \qquad (3.48)$$

The valid frequency range for the transfer functions depends on the sampling time step Δt and the total simulation time $T = n_{tot}\Delta t$ and ranges from $f_{min} = 1/T$ to $f_{max} = f_{Nyq} = 1/(2\Delta t$), with f_{Nyq} the so-called Nyquist frequency.

Therefore, the problem consists in the determination of the UIR from CFD time series. This is accomplished exploiting a non-recursive least square method.

3.2.3.2   Identification procedure

The identification is based on the Wiener-Hopf linear least square estimator (see [113]) which exploits correlation functions.

In particular, the error $\epsilon = y_n - h_n x_n$ (difference between the measured output and the computed one), is minimised when:

$$\Gamma \mathbf{h} = \mathbf{c} \qquad (3.49)$$

Where the auto-correlation matrix Γ, between the inputs, and cross-correlation vector $\mathbf{c}$, between the inputs and the output, are calculated as:

$$\Gamma = \frac{1}{L - M + 1} \sum_{n=M}^{L} x_{n-k}^{(i)} x_{n-z}^{(j)} \tag{3.50}$$

$$c = \frac{1}{L - M + 1} \sum_{n=M}^{L} x_{n-k}^{(i)} y_n \tag{3.51}$$

For $k, z = 0, ..., M$ and $i, j = 1, ..., N_{input}$. L is, instead, the length of the data series (i.e. the length of the vectors computed from CFD).

The Eq. 3.2.3.2 is then inverted to compute the vector **h**:

$$\mathbf{h} = \Gamma^{-1} \mathbf{c} \tag{3.52}$$

A Matlab post-process routine has been implemented in to perform the identification process.

3.2.3.3   Quality checks

In order to evaluate if the identified unit impulse response describe the relationship between the measured signals and responses and if the underlying physics is correctly predicted, two quality checks are suggested by [113].

In the first check, the measured input signals and the estimated parameter $h(i)$) are used to determine the model output $\hat{y}$.

Then, the prediction error $\epsilon = y_n - \hat{y}_n$, difference between the measured signal and the model output is then compared to the variations of the measured response by the following relation:

$$Q = 100 * \left(1 - \frac{\sqrt{\sum_{n=1}^{L} (y_n - \hat{y}_n)^2}}{\sqrt{\sum_{n=1}^{L} (y_n - \overline{y})^2}} \right) [\%] \tag{3.53}$$

The measured signal can be a part of the CFD data set which is not used for the identification procedure but only for the validation so that the model ability to reproduce fresh data sets from the process is evaluated

("cross-validation").
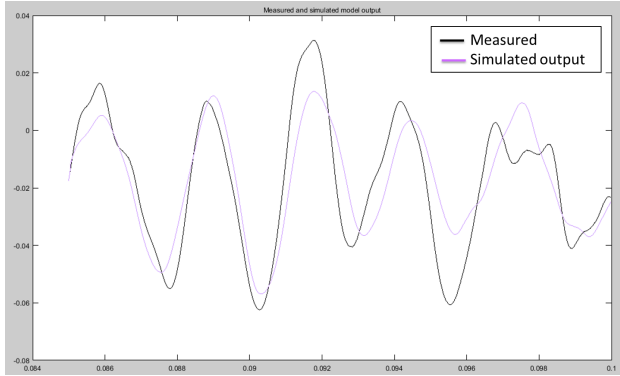
Figure 3.14: Measures and simulated model output.

Basically, Q is a measure of the area comprised within the two curves: the measures and simulated model output (see Figure 3.14). For this area tending to 0 Q tends to 100, and the measured signal is completely determined by the model.

Another check is to correlate the prediction error ϵ and the input signals $x^{(i)}$.

$$C_{\epsilon x(i)}(k) = \frac{1}{L - O + 1} \sum_{n=O}^{L} \epsilon_n x_{n+k}^{(i)}, \quad k = 0, ...O; \quad i =, ...; N_{input} \ (3.54)$$

With M model order and $O > M$ ([42]). Large correlations mean that there is still a part of the measured output y_n that originates from present and past input signals and the input-output relationship has not been properly identified by the model with order M [42].

To judge whether a value is small or still acceptable, the correlation can be compared to a 99 % confidence interval according to Ljung [113]:

$$ci_{x^{(i)}} = \sqrt{\frac{\sum_{k=-O}^{O} \Gamma_{e,k}\Gamma_{x^{(i)},k}}{N - 2O - 1}} N_\alpha, \quad i = 1, ..., N_{input} \tag{3.55}$$

where $\Gamma_{e,k}$ and $\Gamma_{x^{(i)},k}$ are the auto-correlation vectors of ϵ and $x^{(i)}$.

N_α represents the deviation of a normal distribution with expectation of 0 and a standard deviation of 1. For a confidence value of 99%, N_α amounts to 2.58.

3.2.4 Data Analysis

Finally, in this last section the data analysis techniques, implemented in this work and used in some of the studied case are presented.

Reading the results in term of Flame Transfer Function can give useful information on the global dynamics of the flame but, at the same time, it is not easy to provide physical explanation of the results. In particular, the computed Flame Transfer Function is usually given in terms of amplitude and phase as function of the frequency, as shown in Figure 3.13. Giving insight on the physical mechanism leading to the identified trends of amplitude and phase is definitely complex and not straightforward.

Looking at the mean results in terms of flame length, flame volume or mean heat release intensity peaks can only provide explanations on the global flame response but not a clear distinction of its response at different frequencies. For example, an increasing flame lengths can lead to more dispersion of perturbations along the flame and so decreased heat release fluctuation amplitude. Consequently, smaller amplitudes of the FTF might be expected for increased flame length. Similarly, a flame volume increase can reduces power density and should lead to smaller FTF amplitudes.

But giving explanation of amplitude peaks or phase behaviour occurring at different frequencies is not contemplated in this answers. In order to provide more insight many runs at a single frequency can be performed to acquire information on the whole spectrum.

Alternatively, starting from a series of images exported during the CFD calculation, together with the time-averaged picture of the flame, the flame behaviour can be condensed substantially by using Fast Fourier Transformation (FFT). Information can be acquired on those regions that activates at different frequencies as well as the intensity of the heat release fluctuations in the same regions.

Moreover, a sequence of "phase-averaged" images can be used to analyse the flame corresponding to the motion at a specified frequency.
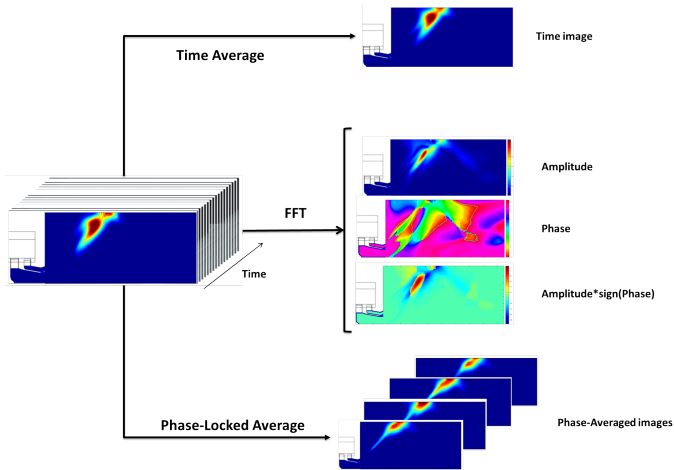
Figure 3.15: Velocity signal at the reference plane (blu) and the filtered component at the frequency of interest (red).

Figure 3.15 shows a schematic representation of the post-process workflow. In the following these post process techniques are briefly presented.

A set of data, e.g nodes ID, coordinates and variable of interest, such as heat release intensity, progress variable etc. are exported on a reference plane and given to the post-processor. A locally resolved flame transfer function can be calculated for each node. This technique is mainly adopted in experimental works such as [98, 141, 142, 143].

Like for the global FTFs, a signal serves as a reference, which is especially important for the phase. In particular, the velocity at the

burner mouth is, generally, used as reference signal. Being it a broadband
signal, as a consequence of the excitation imposed a the domain inlet
(see 3.2.2.4), a filtering operation is necessary to isolate the frequency to
be analysed. One way of doing this is by taking the Fourier transform
of the signal, then setting all frequencies outside the frequency band of
interest to zero, and then taking the inverse Fourier transform. A filter
is the implemented in Matlab following [144] and the reference signal is
determined (see Figure 3.16).
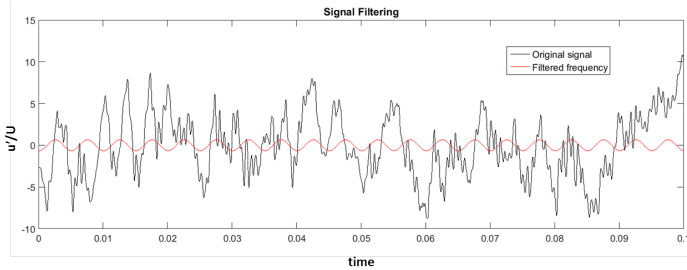
Figure 3.16: Velocity signal at the reference plane (blu) and the filtered
component at the frequency of interest (red).

The images are then post processed node by node and *Fourier trans-
formed*. The resulting amplitude image shows the regions of activity
within the flame, with the values being proportional to the intensity
oscillation amplitude at the investigated frequency. The corresponding
phase image represents the respective node phase angles, relative to the
reference signal. Also a combination of the former is used where the
picture is coloured with the product of the amplitude and the sign of the
phase. This visualization shows where the heat release oscillations are in
phase with the signal and their intensity at the same time. The operation
can be repeated at different frequencies (and for different variables) to
provide deeper insight on the response of the flame all over the frequency
spectrum.

Once the reference signal is known, for an image taken at the instant of
time t a relative phase can be associated. For all the images corresponding

to a specific phase-range can be averaged to obtain the *phase-averaged* pictures. In other words, a conditional average of the images is applied to the images corresponds to a certain phase-angle range. The operation is repeated for a number of phase ranges (e.g. the period of the oscillation can be divided into 10 phase-angles ranges).

The aim of the analysis to extract motion and intensity variation of the flame corresponding to one of the dominant frequency components. A sequence of these phase-averaged images can then be interpreted as a "movie" of the flame corresponding to the motion at the specified frequency.

Phase-locked average pictures can help shedding light on the unsteady behaviour of the flame at several frequencies, with the main advantage of being all post-process operations on of single CFD simulation where a broad band signal is imposed.

Chapter 4

Application to a Perfectly-Premix Lean-Burn Combustor

The identification strategy described in previous chapter is now applied to a lean premixed swirl-stabilized combustor, experimentally studied at Technische Universität in Munich [43, 95]. Measurements in terms of Flame Transfer Function are available for different operating condition of the experimental combustor.

The application of the identification procedure such perfectly premixed flame allowed the validation of the methodology. The effect of the thermal boundary condition on combustor walls is also studied here. Both adiabatic and non-adiabatic wall condition have been simulated. The obtained results are implemented into a finite element model of the combustor in order to analyse the stability of the system. Results are compared with available experimental data showing a satisfactory agreement. The advantage introduced by a more sophisticated model for FTF is further evidenced comparing the results with those obtained with analytical formulation found in literature.

4.1   TUM-BRS Combustor: Test Case Description

The configuration analysed herein is the BRS (Beschaufelter RingSpalt). Detailed experimental analyses on the flame dynamics of the premixed flame have been carried out by Komarek et al. [43, 95] at the Technische Universität in Munich, in the frame work of the KW21 European project.

The BRS combustor in Figure 4.1 is composed by a plenum section connected to the combustor by the feeding duct. Along the feeding duct it has an axial swirler, for the generation of the vortex breakdown and flame anchoring. The swirler has eight blades, that deviate the flow of 45$^\bullet$. for a total length of 30 mm. The CAD of the swirler has been generated from the sketches and pictures, available in literature [42, 43, 95, 116]. The derived swirler geometry is shown in Figure 4.2.
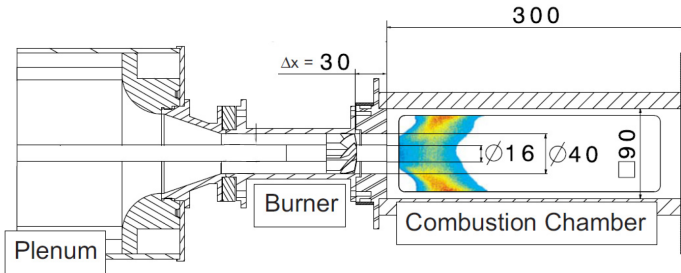
Figure 4.1: Schematic representation of the BRS experimental rig (adapted from [43].

The swirler is mounted on a centre-body at 30 mm upstream of the burner exit, an annular section with an inner diameter of 16 mm and an outer diameter of 40 mm. The combustor has a square section (90 mm x 90 mm) combustion chamber and a total length of 300 mm. With this combustor length, the test conditions were stable to perform OH chemiluminescence, flow field and FTF measurements. The combustor can be also increased to a length of 700 mm. The end of the combustion chamber is equipped with a perforated plate with 6 holes of 20 mm of diameter in order to create a low reflective acoustic boundary condition
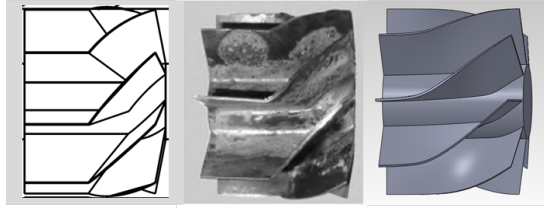
Figure 4.2: Scheme (left), real geometry (center) and reconstructed swirler geometry.

Table 4.1: Two operating condition investigated

Configuration	Inlet Velocity	Pressure Outlet	T wall
30 kW	11.3 $[ms^1]$	101325 $[Pa]$	600 $[K]$
50 kW	19.0 $[ms^1]$	101325 $[Pa]$	600 $[K]$

[86].

The BRS combustor is operated at ambient pressure with a perfectly-premixed lean mixture of air and methane ($\phi = 0.77$).

In tab. 4.1 the two operating condition experimentally studied and discussed also in [86] are reported.

To obtain the Flame Transfer Function, the velocity signal is obtained by Constant Temperature Anemometry (CTA) measurements. The position after the swirler was strongly affected by turbulent noise, making it not optimal for the measurement. Taking into account the acoustically transparent nature of the axial swirler (the amplitude and phase of the acoustic waves are not significantly affected by the swirler) and after verifying its acoustically compactness, even at the maximum excitation frequency for the identification of 500 Hz, the CTA probe would be positioned 10 mm upstream of the swirl generator, which corresponds to a distance of 70 mm to the burner exit [86].

A remark is to be made at this point: while for the 30 kW configuration measurements of the Flame Transfer Function only were available, for the 50 kW case also particle image velocimetry (PIV) data of the flow fields from non-reacting as well as reacting flow simulations (without

excitation) were available. However, for this last case, difficulties in the numerical reproduction of the flame dynamics and FTF identification have been found by other authors (see [86] [95]) due to the development of a transversal eigenmode at 3920 Hz which matches with the first (fundamental) transversal eigenfrequency of the geometry.

For this reasons, in this work, the preliminary investigations to define the numerical setup, have been carried out on the 50 kW configuration, exploiting the mentioned measurement while the FTF identification procedure has been validated on the 30 kW configuration.

4.2   Numerical Setup
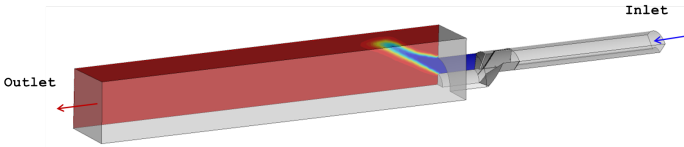
Figure 4.3: Exploiting the domain periodicity, the computational domain is reduced to 1/4 of the whole combustor.

The flame is simulated using Unsteady-RANS and the commercial software Ansys Fluent 15.0. The numerical settings employed are those described in Chapter 3.

A simulation time step of $2.5E-05s$ is used (accordingly to [42]).

Exploiting the domain periodicity just one quarter of the domain, shown in Figure 4.3, has been simulated. The numerical cost of the simulation is then reduced. At the lateral surfaces a periodicity condition is imposed.

At the outlet a Non-Reflecting Boundary Condition is adopted to avoid that flame dynamic behaviour and the identification procedure being influenced by wave reflected at the boundary.

As far as the inlet section is concerned, a velocity profile is imposed, accordingly to the experimental values in tab. 4.1, and maintained

constant during the first part of the simulation of stabilization, necessary for the intrinsic non-stationary phenomena to rise and propagate through the domain.

Mean values are then computed. Successively, a broadband excitation as described in 3.2.2.4 is superimposed at the inlet velocity. A maximum peak-to-average ratio of 20 % of the mean velocity is assigned during the excitation.

Tests with both reflecting and Non-reflecting inlet with acoustic excitation have been performed. In this particular case, in fact, the mixing tube has not a compact length (if compared with the wavelength in the frequency band considered) and a matching with a eigen-frequency during the excitation process is possible. A slight magnification of the frequency content of the recorded velocity signal is observed at frequencies around 450-500 Hz. Using the NRBC at the inlet the observed energy density is attenuated. It must be said that the final result was not affected by the mentioned phenomenon and similar results have been found for the reflecting inlet and NRBC condition, thanks also to the fact that the frequency magnified are at the limit of the investigated spectrum (0-500 Hz).

The mixture is introduced at an inlet temperature of 300 K and a mixture fraction of 0.04251 (meaning a $\phi = 0.77$).

The turbulence level of 5 % is considered at the inlet. Standard $k - \epsilon$ model is used to model turbulence.

At the combustor walls at lance tip, an adiabatic non-slip wall is considered at first. Successively the FTF is computed also with an constant wall temperature of 600 K.

A mesh sensitivity analysis has been carried out in order to select the computational mesh to be used for the following analysis. The mesh dimension is a compromise between computational costs, associated with the simulation, and an accurate reproduction of the flow feature: the main refinements are therefore realized in the first part of the combustion chamber and in the swirler region in order to catch the secondary flows which develop here as well as possible flow separation on the swirler

Table 4.2: TMesh elements for the three grids used in the mesh sensitivity analysis

Mesh ID	Num. of elements
M1	0.8782 E6
M2	1.3086 E6
M3	1.8134 E6

blades.
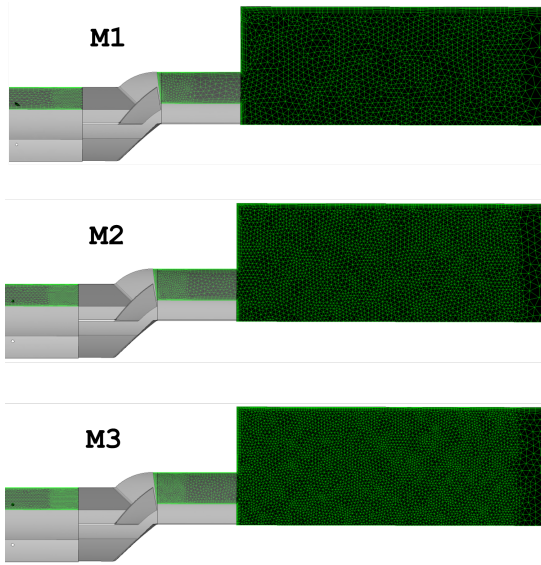
Figure 4.4: The three tested meshes: details.

Three different levels of mesh refinement have been test. The used meshes are shown in Figure 4.4. As it is possible to observe, hybrids tetrahedral-prismatic mesh is adopted. The regions of subsequent refinement can be also appreciated from the same picture. The respective number of elements is reported in tab. 4.2.

Comparisons in terms of velocity profiles are made with experiments for the 50 kW operating condition in reactive conditions. Profiles are

extracted at three axial location downstream the injector (30-60-80 mm downstream the burner outlet) shown in Figure 4.5.

From the plots in Figure 4.6 it is possible to see that the M1, with the lowest number of elements, is not suitable to reproduce correctly the experimental profiles. Increasing the mesh dimension, with both meshes M2 and M3 a good agreement is obtained. The profiles, obtained with the two level of refinement are basically overlapped everywhere but in the region close to the domain axis at the 60 mm plane. M3, with a higher number of elements, follow slightly better the experimental profile but, weighting up the improvement introduced and the increased computational costs associated with the more refined mesh, the M2 mesh is preferred and chosen to carry on the study.
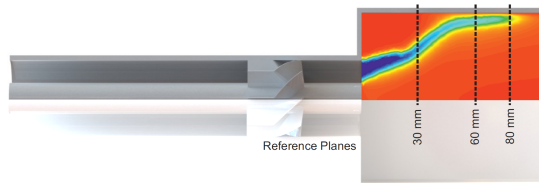
Figure 4.5: The three sampling section where the velocity profiles are extracted.
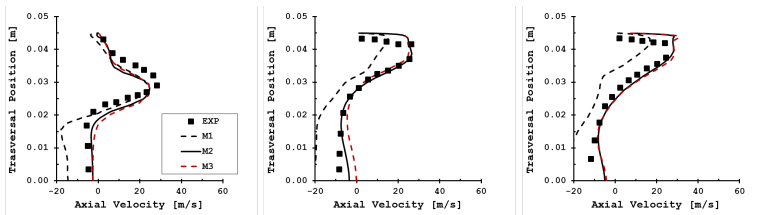
Figure 4.6: Axial velocity profiles, obtained for the tested meshes in tab 4.2, at three axial locations: 30 mm (left), 60 mm (centre), 80 mm (right).

4.2.1   Combustion Model Sensitivity

In order to choose for the most appropriate combustion model, a comparison between the Perfectly Premixed model with the classical Turbulent Flame Speed closure proposed by Zimont [145] and the Flamelet Generated Manifolds (FGM) model (see sec. 3.2.2.3) has been carried out. As far as the former model is concerned, an equation for the reaction progress variable c is solved, which completely describes the reaction in case of a premixed adiabatic flame. Heat-loss effect are, in fact, not taken into account in this model.

The progress variable source term is set proportional to the gradient of the mean progress variable and to a turbulent flame speed S_T that depends on the physical-chemical characteristics of the fuel mixture through its laminar flame speed S_L and on the local turbulence level:

$$S_T = A \cdot G \cdot u'^{3/4} S_L^{1/2} \chi_u^{-1/4} L_T^{1/4} \tag{4.1}$$

being u' the RMS of velocity fluctuations, L_T the integral scale, χ_u the thermal diffusivity. The model constant A is empirical and the suggested value is 0.52 for most hydrocarbon fuels [145]. To take flame stretching into account at very high turbulence intensity, a stretch factor G is introduced. This can be calculated as a function of the turbulent dissipation rate and of a the critical flame quenching rate that is obtained either from laminar flame computations or can be estimated from $g_{cr} \sim S_L^2/\chi$ [146].
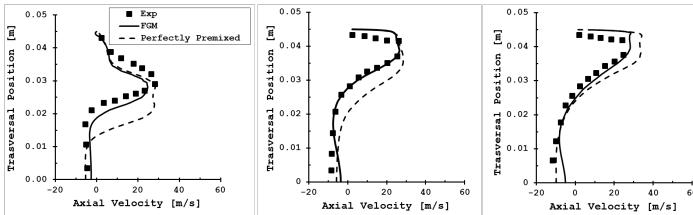
Figure 4.7: Axial velocity profiles, obtained for FGM and Perfectly Premixed combustion models, at three axial locations: 30 mm (left), 60 mm (centre), 80 mm (right).

In this first phase, an adiabatic condition is applied at the walls. The results obtained with the two models against experimental profiles of velocity at three axial locations, are shown in Figure 4.7. At all the three planes (30, 60 and 80 mm downstream the burner exit) the FGM catches better the flow-field inside the combustor. The position of the high speed jet as well as the velocity peak and the recirculation region are located better than in case of Perfectly-Premixed model. Probably, the inclusion of heat exchanges within the flame and the finite-rate effects accounted for in the FGM model allow a better reproduction of the flame structure. The FGM model is therefore adopted for the following analysis and for the FTF computation.

4.3   Results and Discussion

Thermal boundary condition as well as heat losses can influence the flame structure as well as the coupled flow-field and, in turn, the flame response to acoustic excitation. To analyse the impact of a change in this boundary conditions, two cases are considered varying the combustor and lance tip wall boundary condition: adiabatic wall and isothermal wall with temperature of $T_w = 600K$. Such value for the temperature is chosen accordingly to the experimental data provided in [95] and [116].

4.3.1   Mean Temperature and Heat Release
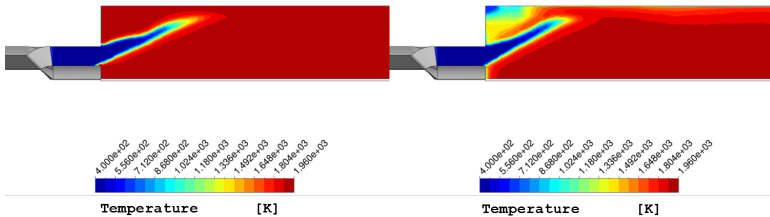
Figure 4.8: Temperature contours for the adiabatic run (left) and assigned temperature at the wall (right), plotted on one of the periodic surfaces.
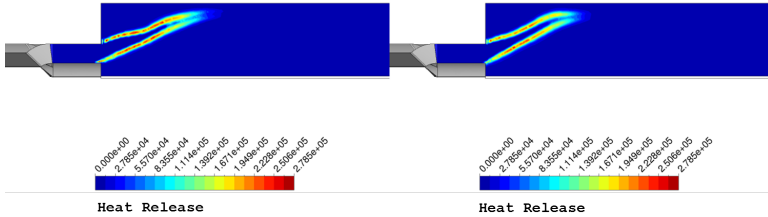
Figure 4.9: Heat release distribution for the adiabatic run (left) and assigned temperature at the wall (right), plotted on one of the periodic surfaces.

From temperature contours in Figure 4.8 the main differences can be appreciated. The influence of the cooled wall is evident in the corner recirculation region where lower temperature levels are predicted. Cooler gases are recirculated from this region into the flame so that a less intense reaction is developed in the outer shear layer, as seen in Figure 4.9. In [86] Chong made a similar comparison on the same test case, performing LES simulations. What he found is a change in the flame shape: the adiabatic flame assumed an M-shape configuration while with cooled walls the decreased reaction intensity in the outer shear layer of the flame let the flame change to an M-shape configuration. In the results presented here, such a change in flame configuration is not observed but the impact on the reaction rate of the wall temperature can be appreciated as well.

At the bluff-body tip, a change in the thermal boundary condition leads to a flame which is no more attached to the lance as in the adiabatic case but is moved downstream.

From the same pictures 4.8 and 4.9 it can be seen that also the flow-field is sightly modified and a wider jet angle is predicted with cooled wall, as an effect of a more intense and large recirculation region. The resulting flame is less projected forward than in the adiabatic case.

4.3.2   Computed Flame Transfer Functions

To identify the Flame Transfer Functions, the same RASW input signal has been adopted with a maximum peak-to-average ratio of 20 % (see Section 3.2.2.4). The flame is excited for $0.25s$ and the data are exported each time step (every $2.5E - 05s$).

The computed FTFs for the 30 kW case are depicted in Figure 4.10 in terms of gain and phase as function of the frequency.
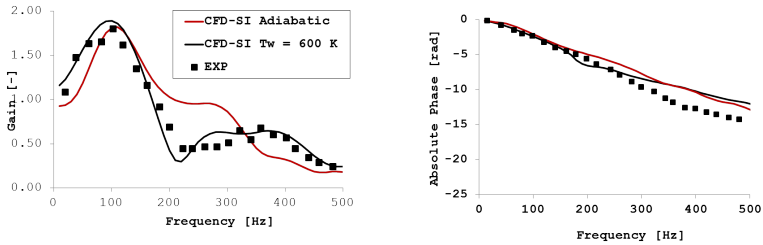
Figure 4.10: Computed Flame Transfer Functions for the analysed cases compared with the experimental one.

The obtained response shows the typical features of a perfectly premixed flame response. The theoretical limits for a premixed Flame Transfer Function are, in fact, observed: for zero frequency the gain tends to 1 while the phase correctly approaches to 0, that is due to the quasi-steady response of the flame so that any fluctuation in the mixture flow is translated into an equal fluctuation of heat release, as explained in section 2.2.1. At the other limit for $\omega \to \infty$, the dispersion of the perturbation is large, so that the flame does not follow the perturbation any more, and the gain of the FTF tends to 0: The flame is acting as a low-pass filter.

Comparing the numerical FTFs amplitude, a good agreement all over the range of frequencies is obtained with the non-adiabatic case. The peak location is caught by the model as well as the corresponding value. A minimum gain is predicted at around 200 Hz, then the curve follows the experimental plateau. The adiabatic FTF, instead, describe sufficiently

well the amplitude in the low frequency region while an overestimation of the gain is predicted from 200 Hz to 300 Hz, where the curve shows a plateau, and then decreases without a good matching of the experiments.

The phases of both the FTFs match the experimental data up to a frequency of 200 Hz. After that a small discontinuity is evident and the slope of the numerical curve is changed. In this second part of the frequency range experimental results are not perfectly matched and higher values are predicted for the phase. At higher frequencies, the phase of the adiabatic case follows better the experiments than the non-adiabatic case.
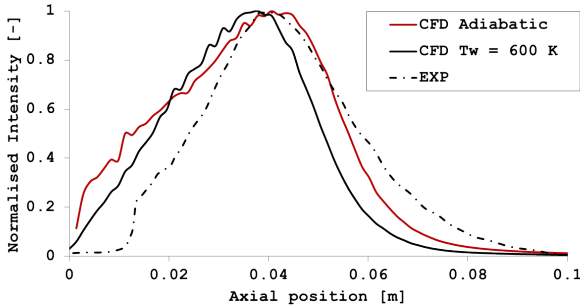
Figure 4.11: Normalised heat release (OH for experiments) intensity along the combustor.

Looking at Figure 4.11, where the normalized heat release is plotted against experiments (proportional to OH concentration), it is possible to see that the both adiabatic and non-adiabatic simulations predict the maximum heat release location with reasonable accuracy. For the non-adiabatic simulation, the predicted flame seems to be slightly shorter and moved upstream. The adiabatic case, instead, predicts correctly the location of maximum heat release but a more uniform heat release distribution then the experimental case is found, meaning higher weight of the first part of the flame on the global heat release.

The predicted phase is therefore smaller as the corresponding time lag that is, the response of the flame to the perturbation reduces with the flame length or when the inner part of the flame assume more weight on

the global contribution to the heat release.

From the analyses carried out and the direct comparison with measured FTF allow the validation of the procedure for FTF identification from CFD simulations. Good agreement is obtained for the identified Flame Transfer Functions in terms of both gain and phase. The predicted FTF shows the classical premixed-like shape and the theoretical limits are well respected.

For the following stability analysis the Flame Transfer Function of the non-adiabatic case is used as it is supposed to be more representative of the experimental tests.

4.4   Stability Analysis

The obtained results are implemented into a finite element model of the combustor in order to analyse the stability of the system. Results are compared with available experimental data.

Simulations are also performed with the analytical $n - \tau$ model so that a comparison can be made between the two flame models. When using the flame $n - \tau$ model, the interaction index n is set to a constant value of 1, while the time lag τ assumes local values equal to the convective time from the burner outlet to the flame point considered: $\tau = d/U_b$ where d is the axial distance of the flame point from the burner mouth and U_b is the velocity at the burner outlet.

A FEM model of the combustor, in Figure 4.12, is generated in COMSOL Multyphysics v 4.3b and solved with the *pressure Acoustic Module* [121].

The flame volume, in Figure 4.12, is imported in the FEM model from CFD data and identify the region where the source term of Helmholtz equation is applied

From the same picture ii is possible to observe that the swirler is eliminated from the model as it is replaced by its transfer matrix, computed following the procedure described in Section 3.1.2.3.

At the boundaries, no pressure fluctuations are imposed at both inlet
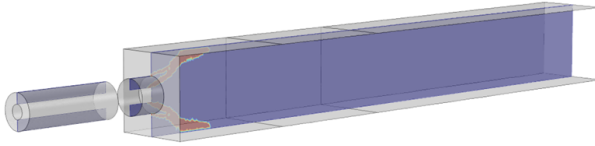
Figure 4.12: The flame region where the source term of Helmholtz equation is applied in the FEM model.

and outlet section $(p' = 0)$. The domain is then discretised with a computational mesh able to detect acoustic modes up to 2 kHz.
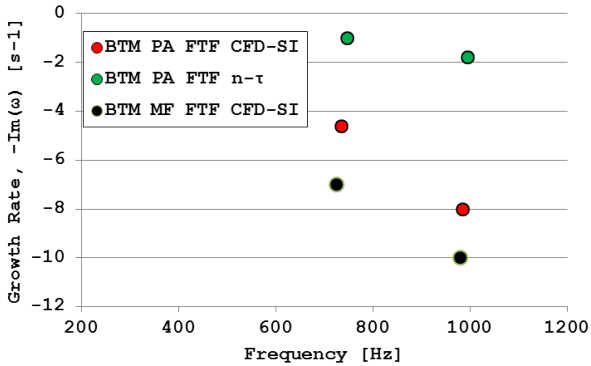
Figure 4.13: Results of the stability analysis for the combustor with length of 300 mm.

At first, the stability analysis for a combustor length of 300 mm is performed. With such a combustor no instabilities occurred experimentally and the FTF is measured [116].

In Figure 4.13 the computed modes are reported for three configurations. The two flame models are then compared. To assess the effect of a mean flow in the burner section, results with both two computed BTM are also discussed: when the mean flow is considered (BTM MF) and when only the pressure acoustics is considered (BTM PA).

As shown in Figure 4.13 no unstable modes are detected, accordingly

to experiments.

When changing from the $n - \tau$ (green dots) to the computed FTF (red dots), increased stability of the eigen-modes is found. Moreover a slight shift of the latter at lower frequencies is predicted. Changing the BTM formulation and including mean flow effects (black dots), maintaining the computed FTF formulations, a further effect of stabilisation is introduced, as a consequence of the change in the local acoustics in the burner section. Again, a slight shift at lower frequencies is predicted.

Successively, the analysis is extended to the domain with a combustor length of 700 mm. In this configuration the experiments predicted three system modes at 35 Hz, 101.3 Hz and 260 Hz. In particular, the first and the third mode were stable modes while at 101.3 Hz an instability occurred. The BTM formulation used for this second case include mean-flow effects.
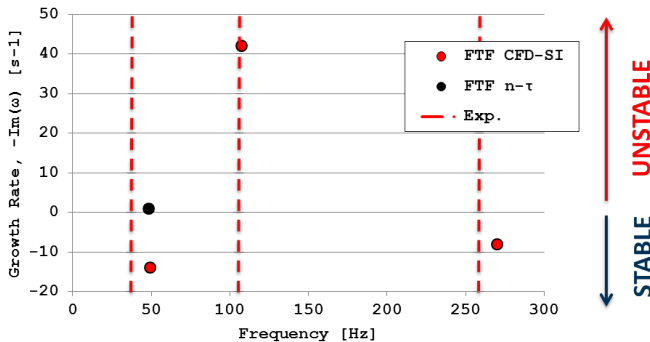
Figure 4.14: Results of the stability analysis for the combustor with length of 700 mm.

In Figure 4.14 the experimental results are compare with the results obtained with both $n - \tau$ and computed FTF flame model.

When the computed FTF is used, three modes are detected in the range 0-300 Hz where the measurements were available. In particular, one unstable mode is predicted at 107,3 Hz and two other stable modes, experimentally found at 35 and 260 Hz. The model is then able to identify the main modes as well as their stability properties. In case of using the

$n - \tau$ model only the first mode at 48.2 Hz was found as convergence issues arose when looking for the other modes. The main reason is that using the $n - \tau$ formulation (see equation 3.19) the unknown ω appear at the exponent so that the linearisation procedure results more complex and additional terms appear in the inversion matrix if compared with the alternative formulation (see equation 3.1.2.1) adopted when the computed FTF is exploited.

The adoption of a more refined model as the Flame Transfer Function computed from CFD data leads to improved results and introduce also a stabilisation in the solution procedure of the FEM code.

The application of of the numerical procedure to the perfectly premixed BRS combustor, experimentally studied at TUM University, allowed to assess the whole methodology from CFD simulation and Flame Transfer Function computation to the stability analysis with the FEM code.

The availability of the experimentally measured FTF as well the data on the eigen-modes in unstable operating conditions were precious to carry out this first part of the work. Moreover, several complexity that can be found in a typical gas-turbine combustor such as fuel injection and turbulent mixing that result in a non-uniform mixture at the combustor inlet are excluded thanks to the perfectly-premix nature of this flame

In the following Chapter 5, the procedure, validated on a perfectly-premixed flame is applied to a so-called technically-premixed flame of a real gas turbine combustor for industrial operations.

Chapter 5

Numerical Analysis Of The Dynamic Flame Response of a Technically-Premixed Gaseous Flame for Heavy-Duty Applications

In the present chapter a thermo-acoustic stability analysis of a lean-premixed gas-turbine full-annular combustor for heavy-duty gas turbine is presented. The flame response is computed with the methodologies described in previous chapters, exploiting system identification techniques. In particular, a sensitivity analysis onto flame temperature has been performed, studying two different operating conditions, aimed at replicating the dynamic response of the real flame and understanding the driving mechanism of thermo-acoustic instability onset as well. Successively, fuel mass flow fluctuations are included in the model to better understand the impact on the system stability and the improvements in the predictions lead by a Multi-Input Single-Output model of the flame. The identified Flame Transfer Functions (FTFs) are compared each other and the sim-

ulations results analysed in order to give more physical insight of the coupling mechanisms responsible for the flame dynamic response. The obtained results are implemented into a finite element model of the combustor, realized in COMSOL Multiphysics, to analyse the system stability. Numerical model affordability has been assessed through comparison with results from full-annular combustor experimental campaign carried out by GE Oil & Gas since the early phases of the design and development of a heavy-duty gas turbine. This allowed the discussion of the model ability to describe the stability properties of the combustor and to catch the instabilities onset as detected experimentally.

5.1   Combustor Description And Observed Dynamic Response

The object of the study is a lean-premixed combustor as tested by GE Oil& Gas in a full-annular rig. The combustor is equipped with 39 burners each one featuring discrete pilot fuel injections on nozzle tip.
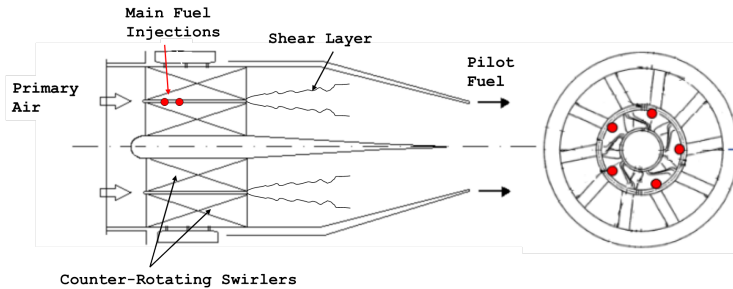
Figure 5.1: DACRS nozzle scheme

A schematic of the injector considered in this work is shown in Figure 5.1. It consists of a Dual Annular Counter Rotating Swirler (DACRS) followed by a converging duct and it features a transverse jet main injection onto the inner swirler. Such a fuel injection configuration revealed to be the most effective in keeping NOx emissions low over a wide operational

range, as observed within a single burner test rig [147].

Intense turbulence levels and mixing are guarantee by the counter rotating swirlers, as shown in Figure 5.2, results of numerical analyses, where a reliable numerical setup was assessed thanks to available experimental data (for further details refer to [148, 149]).
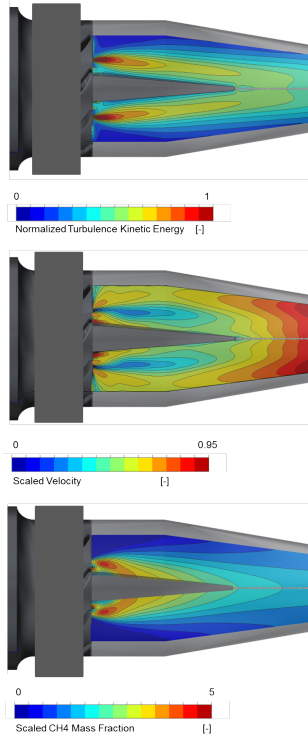
Figure 5.2: Velocity, turbulence kinetic energy and fuel concentration inside the premixer

From velocity and Turbulence Kinetic Energy (TKE) contours in Figure 5.2 the main features of the premixing system are evident, in particular, the high-turbulence region and low-velocity region of the shear layer generated by the interaction of the two swirling flows and the high.

It is in this region that the highest levels of turbulence are observed.

The fuel is injected close to the burner axis (red dots in Figure 5.1) generating a richer profile on the axis and a leaner mixture at outer radii interacting with the pilot flames (see CH4 contours in Figure 5.2). Such an injection strategy has been evaluated through numerical survey [150] in addition to the experimental campaign [147]], and selected among other design options (i.e. injecting fuel from outer swirler vanes or a more radially uniform distribution of injection holes along the swirler itself) as it showed the highest NOx abatement potential and good dynamic behaviour. The range of operability, determined in many conditions by limits on pollutants, is therefore wider and it must be analysed and characterized to prevent possible instabilities.
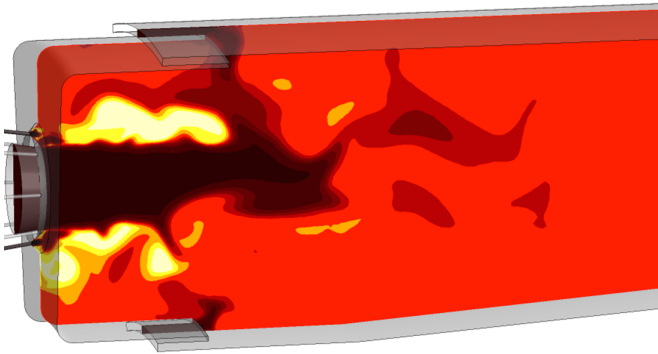
Figure 5.3: Sector of the the annular test-rig, studied where the injection system with the premixer, pilot injections and dome cooling are visible.

The current burner design follows LPC concept design, as it is based on a lean premixed flame surrounded by discrete pilot injection points which help to stabilize the flame, as it is possible to see from the reported combustor sector in Figure 5.3.

In terms of flame dynamics, the presence of the pilot flames and their interaction with the premixed one is a key aspect. Usual stabilization methods of pilot jet flames depends on the ratio between jet speed and laminar flame speed of reactants. Compared to the laminar flame speed of
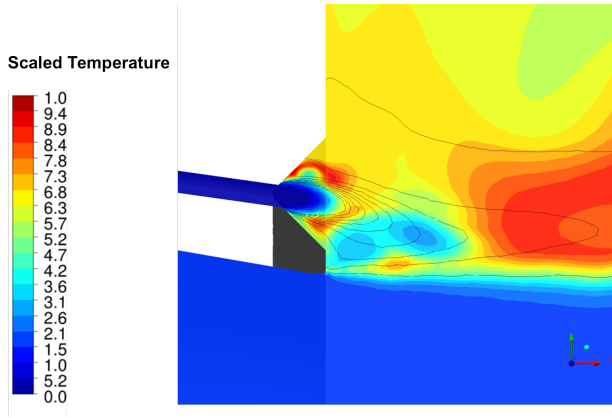
Figure 5.4: V-cut pilot exit section: scaled temperature contours and mixture fraction isoline.

a stoichiometric CH4/Air mixture, the injected fuel velocity is relatively high and more than 10 times, so that, accordingly [151], a stabilisation method is necessary and the corresponding regime cannot be identified in neither in a rim stabilised nor in a triple flame. In the investigated burner, the pilot jet flame is stabilised by the V-cut shape of the shroud in Figure 5.4 (result of a Scale Adaptive Simulation of combustor with a V-cut injection system). Basically, it acts as a dump geometry where turbulent structures and local recirculation of hot products ignites the jet flame that is also interested by an oscillating motion that make the flame anchoring intermittently on the outer and inner surface of the V. The jet is then dragged by the main swirled flux from the premixer, which gives the pilot a tangential component, and completes the mixing.

Despite this kind of interaction, both diffusive and premixed combustion modality coexist and can be considered separately for a large part of their evolution, as observed in [150] , and their interaction limited to the very first part of the flame. Anyway, the mutual influence between premixer and pilot constitutes an important aspect to understand the flame response (and NOx production).

The objective of this work is to setup and assess a numerical procedure able to catch the effects of such a complex flame on the stability properties of the system and to reproduce the effect of the main parameters on the instability onset as found experimentally.

Still from single burner experimental experience, larger amplitudes of pressure pulsations were observed as the flame temperature increases, while a more robust instability onset was obtained by reducing the pilot content. Despite the promising indications from single burner rig experience, the opportunity of modelling the dynamic response of the full annular combustor is considered a more reliable test bench for a design option, so that any numerical strategy should be able to model it instead.

A wide range experimental dynamic characterization against combustor inlet conditions, flame temperature and pilot content is anyhow a great opportunity to validate numerical approaches, as well as numerical analysis can give fundamental multi-scale information. Among the tested conditions, two test points have been selected in order to be representative of a Full-Speed Full-Load operation. In particular, attention has been focussed on the effect of the flame temperature (global equivalence ratio) on the stability of the second azimuthal mode. A tendency to destabilisation of the latter with flame temperature was, in fact, observed experimentally ("hot mode"). Starting from a stable condition (called TP145), different modelling strategies have been assessed where the main idea is to catch the instability onset provided by an increase of flame temperature (called TP145+).

As a second target, starting from the unstable condition, sensitivity on main physics based model parameters has been done to identify the most effective in abating the instability. In the following sections, the thermo-acoustic model of the combustor and the CFD setup, used to compute the FTFs are presented, followed by discussion of the obtained results.
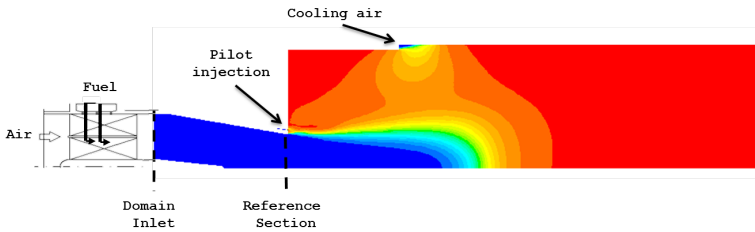
Figure 5.5: The computational domain with the main features introduced in the calculation and highlighted the reference section used for the velocity fluctuations export.

5.2 CFD Modelling And Numerical Setup

The computational model for the FTF computation is presented herebelow.

A single burner is simulated to derive the dynamic flame response. As it is not possible to find a common periodicity between the injector and the number of pilot injections, a full sector simulation should be realized. However, in order to carry on fast modelling and design evaluation over a number of operating conditions, a simplified configuration is adopted for the domain. An equivalent tubular combustor is considered and a 1 deg slice is simulated. Both dome cooling air and pilot injection are included in the domain, scaling the respective areas, as shown in Figure 5.5.

The combustor length has been chosen so that the outlet influence on the flame upstream is negligible. A non-slip adiabatic wall condition is assigned at the liner wall while rotation periodicity is assigned at the two cyclic surfaces.

At the outlet section a Non-Reflecting Boundary Condition is imposed to prevent resonances inside the domain which could eventually alter and deteriorate the FTF identification.

The velocity components mean profiles as well as the turbulence related quantities and mixture fraction (Z) ones are extracted from simulations of the whole premixing system where the air and fuel feeding ducts and

the swirlers were included, following the approach used in [148].

The computational mesh is depicted in Figure 5.6. It has a single element along the tangential direction and a total of 32000 hexahedral elements and 65000 nodes.
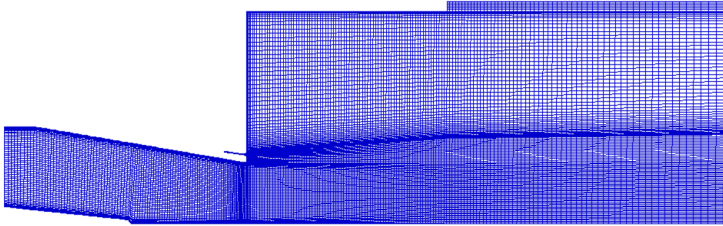
Figure 5.6: The computational mesh used to discretise the simplified domain.

Ansys Fluent 16.0 is used to perform the numerical simulations.

The partially premixed combustion model is adopted to model the flame. The laminar database is generated using the Flamelet Generated Manifold reduction technique as described in the dedicated section 3.2.2.3. The detailed GRI 3.0 mechanism for methane is used to generate to compute the laminar flamelet. The c equation is then closed with the Finite-Rate (FR) closure [139].

A second order scheme is adopted for the spatial and time (bounded second order) discretisation while for turbulence related quantities a first order upwind is adopted.

A time step of $2.5E-05s$ is used in the simulations. After a first stabilization period, necessary for the intrinsic non-stationary phenomena to rise and propagate through the domain, the mean values are computed. Successively, a broadband excitation is superimposed at the inlet velocity and the quantities for the FTFs identification are recorded.

The system input variables are excited with a Square Wave with Random variable Amplitude (RASW) signal, already presented in sec. 3.2.2.4. The excitation was deigned to have a maximum peak-to-average

ratio of 20 %. The system is excited for 0.25s and the data are exported each time step.

5.2.1 Results

5.2.2 General Flamaes Description

In Figure 5.7 the contours obtained with the numerical simulations are shown. The increased equivalence ratio of test point TP145+ is seen in mixture fraction contours where a richer zone in the pilot region is evident as well as the inlet profiles of the premixer. As said, a richer mixture is created along the burner axis and a leaner one at outer radii for the part that directly interact with the pilot flames. Turbulent mixing then makes the profile at the burner outlet more uniform. Form the contours of progress variable it is clearly visible the premix flame shape. In the pilot region an almost complete combustion is predicted. Pilot flames are directly fed by the premix air as well as by the cooling air that recirculates on the flame itself.

From PFR contours in Figure 5.7 the heat release distribution can be seen, together with the flame length (distance of the maximum heat release location from the burner mouth). The heat release distribution can also be appreciated from normalised heat release intensity along the axial distance in plot in Figure 5.8. The pilot peak is clearly visible and the location is almost the same for both the test points. A slight shift downstream is seen for TP145+ due to the enhanced jet penetration associated to an increased fuel mass flow. For the premixed flame the difference is more pronounced: Increasing the equivalence ratio at test point TP145+ a shorter and more compact flame is predicted.

Increasing the equivalence ratio at test point TP145+ a shorter and more compact flame is observed. Generally, an increased power density is associated with a shorter flame, as seen in heat release contours. This aspect leads to higher FTF amplitudes, so higher gains are expected for TP145+. Moreover, in a longer flame there is more dispersion of perturbations along it. Therefore, decreasing heat release fluctuation
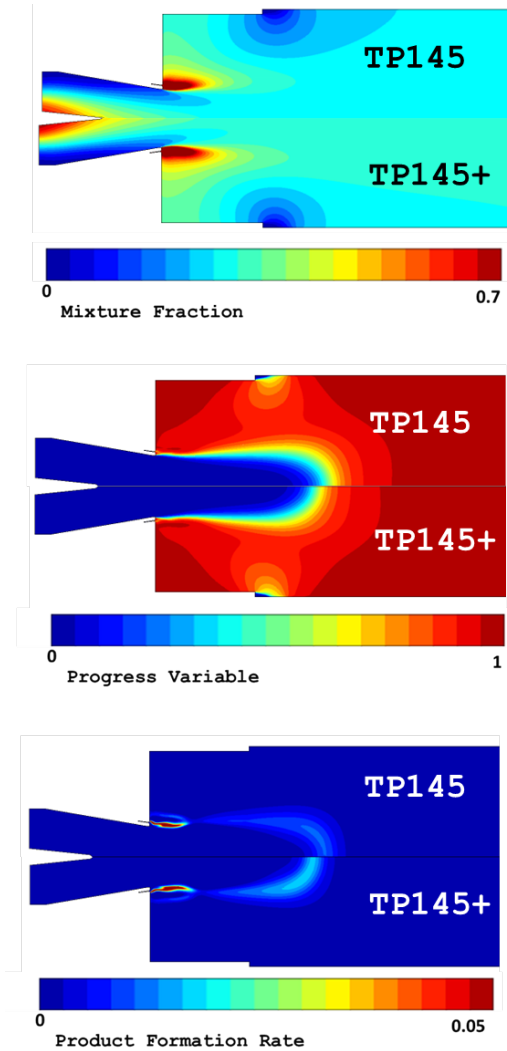
Figure 5.7: CFD contours for the simulated test points: mixture fraction (top), progress variable (centre), heat release (bottom).
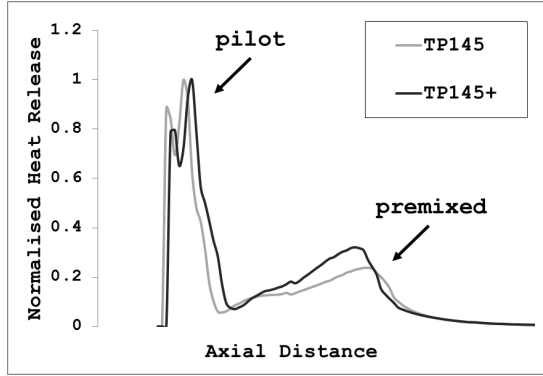
Figure 5.8: Normalised heat release intensity along along the domain for the two operating conditions.

amplitudes at higher frequency are observed. For what stated, smaller amplitudes of the FTF in the higher frequency range are expected for longer flames [152], such as TP145 ones.

5.2.3 Flame Transfer Functions

The dynamic response of a real combustion system, such as the one investigated in this work, can be described, in terms of heat release fluctuations which are influenced by several factors. Among these, the most important two are the air mass flow rate and fuel mass flow fluctuations. Therefore, generally, a flame system can be regarded as a Multi-Input Single-Output (MISO) system where the global response is the sum of the two contributions. In general, the fluctuating heat release of a system, where the air mass flow and fuel mass flow are injected from separated ducts, can be expressed, in linear regime, as the sum of the single contributions as:

$$\frac{Q'(\omega)}{\overline{Q}} = FTF_{CF}(\omega)\frac{u'_b(\omega)}{\overline{u}_b} + \sum_{i=1}^{N} FTF_{F_i}(\omega)\frac{u'_{F,i}(\omega)}{\overline{u}_{F,i}} \qquad (5.1)$$

Where the first term on the RHS is the response to air mass flow

fluctuations with choked fuel line FTF_{CF} (constant fuel mass flow), while the second one is the response to fuel mass flow fluctuations with constant air mass flow (FTF_F). The former contributions is related to the acoustic velocity fluctuation at the burner exit ($u'_b(\omega)$) while the second one depends on the acoustic velocity fluctuations at the i-th fuel line exit section ($u'_{F,i}(\omega)$).

Under the simplifying hypothesis of considering a stiff fuel line, fuel mass flow fluctuation may be neglected and heat release fluctuations are directly related to mass flow rate or velocity fluctuations. The flame system is, in this case, considered a Single-Input Single-Output (SISO) system and its response is governed by air mass flow fluctuations only as follows:

$$\frac{Q'(\omega)}{\overline{Q}} = FTF_{CF}(\omega)\frac{u'_b(\omega)}{\overline{u}_b} \qquad (5.2)$$

The physical evolution of the system is different from a perfectly-premixed flame where, a mass flow fluctuation is not followed by an induced equivalence ratio fluctuation. In a technically-premixed flame, in fact, together with the acoustic perturbation that propagates from the upstream sections, there is also an induced equivalence ration fluctuation is indirectly caused which propagates to the flame as well. A SISO flame transfer function can be sufficient to correctly predict the dynamic behaviour in many situations [153], where fuel mass flow do not induce important dynamics, thus highlighting the key role of air mass flow fluctuations in the global response. Where fuel mass flow fluctuations cannot be neglected and have an important influence on the flame dynamics, a MISO model has been shown to better represent the system [42, 152, 154, 155, 156].

5.2.3.1   Choked fuel line: FTFs

In the present work, initially the fuel line is considered choked therefore the flame is modelled as a SISO system.

The FTF is computed exploiting identification methods.

An unsteady-CFD simulation is performed, as described in the previous

sections, where a broadband excitation is applied at the inlet velocity. In order to reproduce a choked fuel flow, the mixture fraction profile is also excited so that, following the air mass flow fluctuation, the fuel mass flow remains constant. The time series of both the velocity fluctuations at the burner mouth (see the reference plane in Figure 5.5), and of the global heat release fluctuations on the whole domain, are recorded and the FTF_{CF}.
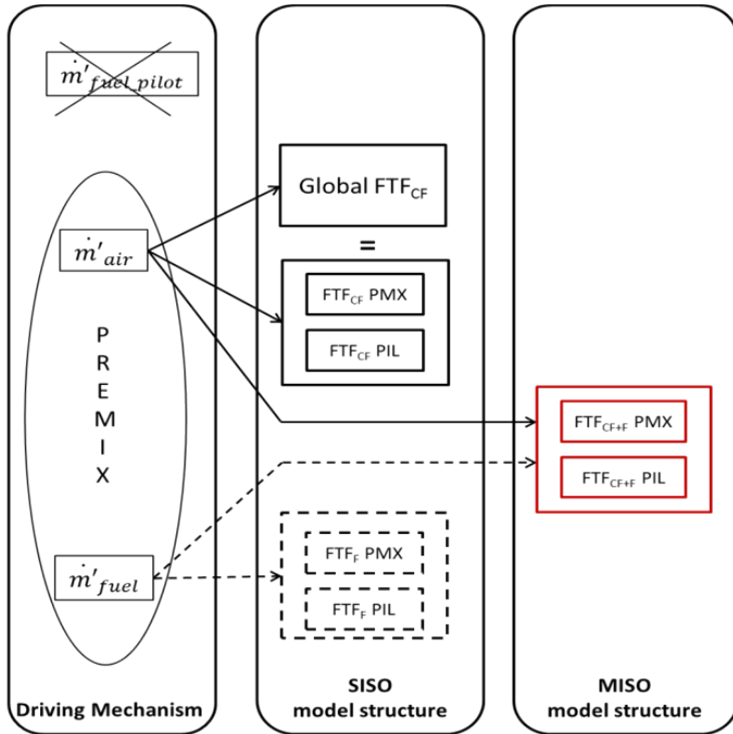
Figure 5.9: Scheme of the computed FTFs used in this work to perform the linear stability analysis in the FEM code.

Successively, in order to catch the particular behaviour of pilot and premix flame two separated FTFs are computed (see scheme in Figure

5.9).
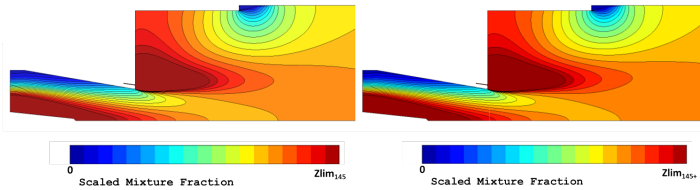
Figure 5.10: *Scaled Mixture Fraction contours for the simulated operating conditions: TP145 (left) and TP145+ (right).*

In the calculation the heat release is integrated separately for the two flames. The two regions are separated on the basis of the mixture fraction so that the pilot region is defined by the location with mixture fraction above a specific limit, arbitrary chosen to reasonably separate the two physics. In particular, the two limits are chosen such as that $Zlim_{145+} = Zlim_{145} * (Zref_{145+}/Zref_{145})$ assuming that the test point work in similarity. This is also confirmed looking at Figure 5.10 where the mixture fraction field are rescale with the respective $Zref$ of the burner, showing a similar distribution within the domains.

Once the strategy is assessed more refined criteria for to distinguish between the diffusion pilot flame and the premix-like evolution of the main one can be exploited (see i.e. the criterion proposed in [157]).
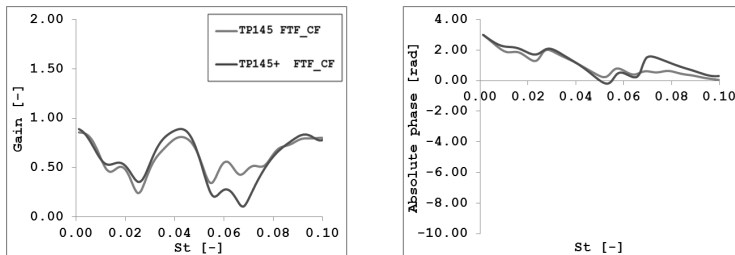
Figure 5.11: *Global FTF obtained assuming a choked fuel line.*

The flame response to air mass flow fluctuations with choked fuel line
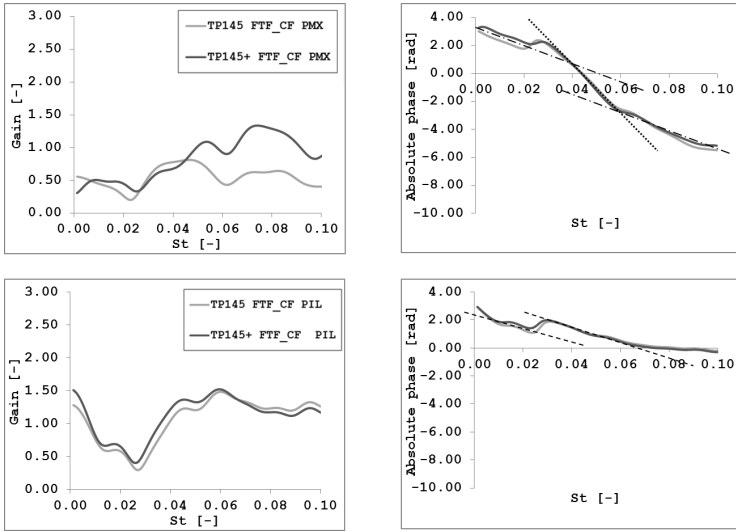
Figure 5.12: Premixed flame (top) and Pilot flame (bottom) FTFs obtained assuming a choked fuel line.

(FTF$_{CF}$ in Figure 5.9) obtained at the two simulated operating conditions are depicted in Figure 5.11.

Amplitude and phase are reported as function of the St number ($St = f/(cL)$) computed with the sound speed (c) at the relative flame temperature and with a L characteristic of the flame. In this way, the frequency of the mode of interest is around $St = 0.068$ for both the cases.

Looking at the global flame response in Figure 5.11, the amplitude presents three peaks, at zero frequency, at St 0.047 and St 0.09. The assumed values are always below unity. No particular distinction are found between the two test points except for the range between $0.05 \div 0.08$ where test point TP145 assumes higher values. As far as the phase is concerned, it starts at π and decreases for both the cases with no distinction but after St 0.06 where higher values are found for TP145+. Three ranges of different phase slope (time delay) can be identified: $0 \div 0.03$, $0.03 \div 0.06$ with steeper phase and $0.06 \div 0.1$ with a less steep

curve.

Looking at the FTFs obtained for the premixed part and pilot flames separately (FTF$_{CF}$ PMX and FTF$_{CF}$ PIL in Figure 5.9) it is possible to get more insight on the observed global behaviour.

In Figure 5.12 top the FTF for the premixed part is shown. The amplitude are similar in the trend for the two test point but higher gains are found for the TP145+, accordingly to the higher power density associated to the shorter premixed flame predicted. No distinction is found for the two phases. Three distinct frequency ranges are again clearly visible, with characteristic delay times. The phase starts at π and then, in the first range, till St 0.03, a constant delay time is followed. An increased constant time lag dominates in the second range of St 0.02 ÷ 0.06. Finally, the last part of the spectrum is characterized again by a lower time lag.
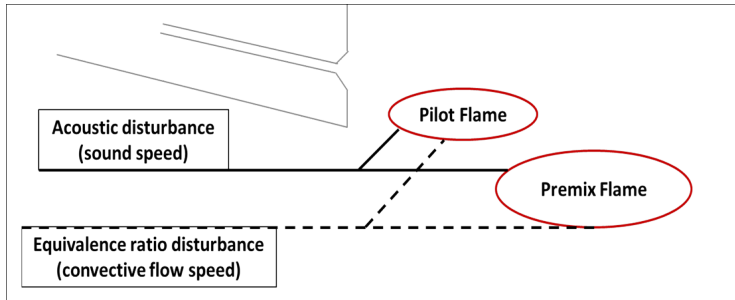
Figure 5.13: *Scheme of the influence of acoustic and equivalence ratio perturbation on pilot and premix flame.*

The central part of the spectrum is dominated by the equivalence ratio fluctuations, induced by a fluctuating flow rate at constant fuel mass flow, which propagates convectively, as schematically reported in Figure 5.13. In the other ranges, instead, acoustic perturbation, that propagates faster (local sound speed) dominates.

The pilot flame response is depicted in Figure 5.12 bottom. The amplitude shows that at frequencies close to zero and after St 0.05 the pilots respond to mass flow fluctuations while their response reduces in

the range between St $0.02 \div 0.04$. From the phase plot, another aspect emerges: the time lag of pilot flames relates to a fast response typical of an acoustic propagation of the disturbance. Equivalence ratio fluctuations, which propagates slower at the convective flow speed, as shown in Figure 5.13, seem not to affect the pilot dynamic. In fact, the part of the mass flow from the burner that interacts with the pilots is practically air, without fuel (see i.e. mixture fraction contours in Figure 5.7 left) so that almost no equivalence ratio fluctuations are present.

However, no distinction is observed between the two operating conditions. Therefore it can be concluded that, at the interested frequency at St 0.068, pilot flames cannot be responsible of the tendency to instability with the flame temperature, observed experimentally. If a different behaviour will be predicted numerically it has to be assigned to the difference in the premix flame response.

Finally, looking at the global flame response again in Figure 5.11, in the first part of the spectrum the pilot dynamic response is clearly observed. The second part of the spectrum, instead, presents a combination of both the premixed and pilot behaviours.

5.2.3.2 Introduction of fuel mass flow fluctuations

To derive the FTF_F a further simulation is performed where the mixture fraction profile is perturbed with the RASW signal, while the air mass flow is kept constant. The separated flame approach is used in for the following study so that independent FTFs are derived for pilot and premix flames. The obtained FTF_F relates the heat release to the inlet fuel mass flow fluctuations. The inlet section, in fact, can be reasonably considered coincident with the actual mixing section. The obtained FTFs for premix and pilot are shown in Figure 5.14.

From the plotted curves the effect of a fluctuating fuel injection is observed. A marked influence to this mechanism emerges especially for the premix flame. In both cases the FTF_F amplitude assumes values above unity for a large part of the frequency spectrum with a peak at around St $0.04 \div 0.05$. Then the amplitude decreases with an increase in
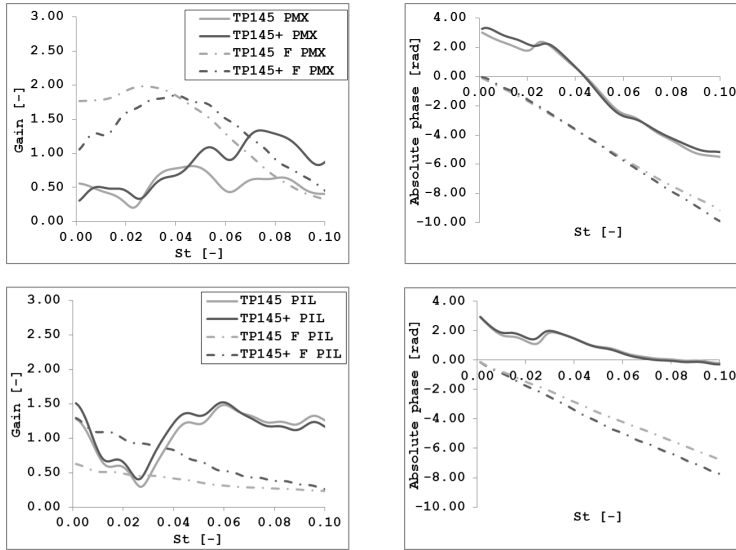
*Figure 5.14: Premixed flame (top) and Pilot flame (bottom) FTFs
relating the heat release to a fluctuating air mass flow (continue lines)
and to a fluctuating fuel injection (dashed-dotted lines).*

the frequency.

Pilot response shows a different amplitude trend: a fluctuation in the fuel injected in the premixer leads to a response that decreases in amplitude continuously with the frequency, due to increasing dispersion of perturbations along the path. Lower response are found for the TP145 pilot flame while, for premix flame higher values at low frequency are found compared with TP145+.

Looking at the phases plots a constant time lag is associated with a perturbation of the fuel mass flow. A higher time lag is predicted for premixed flame than pilot one due to a longer path the perturbation follow in the former case, before reaching the reaction zone.

In general, fuel mass flow and air mass flow fluctuations at the mixing section (M) may be out of phase and have different intensity. A particular case to be considered is when the two fluctuations are in phase and with

the same intensity. In this case:

$$\frac{u'_F}{\overline{u}_F} = \frac{u'_M}{\overline{u}_M} \tag{5.3}$$

Then, considering a compact burner the fluctuations at the mixing section can be identified with the fluctuations at the burner outlet:

$$\frac{u'_F}{\overline{u}_F} = \frac{u'_M}{\overline{u}_M} \sim \frac{u'_b}{\overline{u}_b} \tag{5.4}$$

so that equation 5.1 becomes:

$$\frac{Q'(\omega)}{\overline{Q}} = (FTF_{CF}(\omega) + FTF_F(\omega)) \frac{u'_b(\omega)}{\overline{u}_b} \tag{5.5}$$

and the two FTFs can be summed.

To verify this point the sum of the two FTFs, for TP145, is compared to the FTF obtained with a CFD simulation where the mixture fraction profile is kept constant while exciting the total mass flow rate, thus reproducing the described case.

Comparing the two FTFs a good agreement is obtained, confirming the validity of the assumption for both premix and pilot flame.

Before the stability analysis is presented in section 5.2.5, a physical interpretation of the discussed results is provided in the following section

5.2.4 Physical interpretation of the results

In order to get a physical interpretation of the results, it is possible to have a look at the UIRs caused by the acoustic velocity at the burner exit and by the fluctuating fuel mass flow at the domain inlet (mixing section) from which the presented FTFs come after being Fourier transformed (see sections 3.2.3 and 2.2.2).

Observing the response of pilot flames at an acoustic fluctuation at the burner exit, in case of choked flow line (UIR_{CF} PIL in Figure 5.16), an overshoot appears instantaneously as the burner outlet is coincident with the initial part of the pilot flame. Than and undershoot follows and the response disappear. As explained in sec. 2.2.1 the presence of an
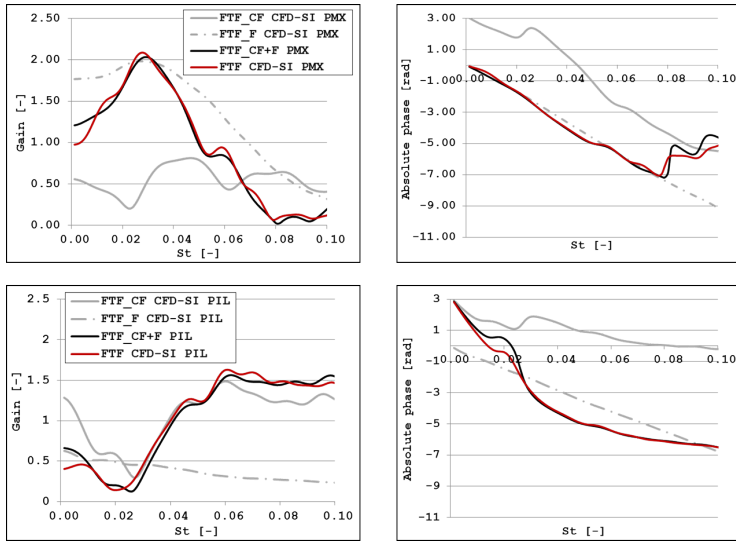
Figure 5.15: Premixed flame (top) and Pilot flame (bottom): comparison between the FTFs obtained from the sum of FTF_{CF} and FTF_F and the equivalent CFD-SI one.

undershoot leads to a FTF that can assume values above unity as it is actually seen in figure 5.12.

Looking at the UIR_F PIL, response to a fuel mass flow impulse, a different behaviour is observed. After a small initial response, due to spurious induced acoustic oscillations that follows a fluctuation of the fuel mass flow, an overshoot is visible. This comes after a delay time close to the convective time from the inlet section to the pilot flame peak location. Looking at the UIR amplitude the smaller entity of a fluctuation in the fuel mass flow, compared to the previous one, is clear. Moreover, no undershoot is observed so that no values above unity shoud result in the corresponding FTF, as it is possible to see in Figure 5.14.

When both fuel and air mass flow fluctuate simultaneously (UIR_U PIL) the predominant effect of the latter is clear (different scales in plots) and only a smaller contribution comes from fuel mass flow fluctuations.
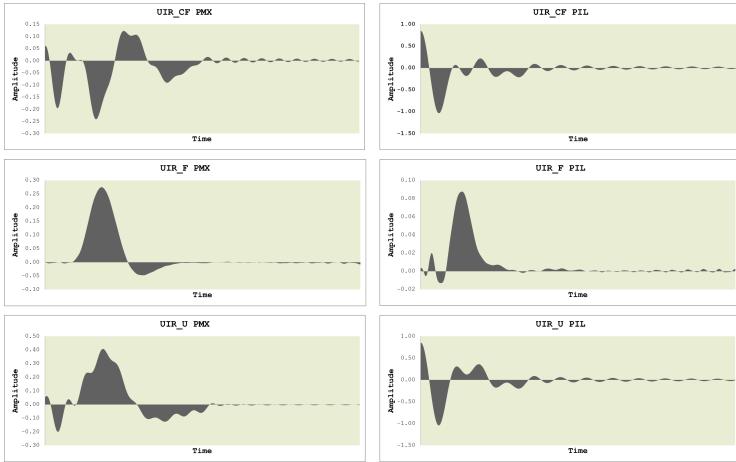
Figure 5.16: UIRs from which the FTFs (CF, F, CF+F or U) are derived, for both premixed (left) and pilot (right) flames.

Looking at the UIRs of the premixed flame in Figure 5.16 left, the differences in the flames behaviour emerge.

In the UIR_{CF} PMX a response is observed instantaneously that is probably to be associated to the part of the flame close to the pilots. A similar response of the pilot flame is, in fact, recognizable. Than an undershoot and an overshoot follow. Theses can be associated to the induced equivalence ratio fluctuations: a leaner mixture arrives at the flame front, corresponding to an increased air mass flow. Therefore, predicted response is substantially the opposite than the one obtained with a positive unit impulse of fuel mass flow: A negative peak appears after an equivalent time than a positive peak in the UIR_F PMX that is, after the convective time from the inlet section to the heat release peak of the premixed flame.

Differently from pilot UIR_F PIL, in this case there are both an overshoot and undershoot that allow the FTF to exceed unity, as seen in 5.14. This again agrees with the theoretical explanation provided in sec. 2.2.1.

In the UIR_U PMX the predominant effect of fuel mass flow fluctuations

is clear as the response is very close to the UIR_F PMX. Also here the initial contribution, of the flame part adjacent to the pilot is observed.

Finally, to better understand the specific behaviour within the flame, at the different frequencies, a phase-locked average post process and a FFT analysis (see sec. 3.2.4) are carried out.

<center>Increasing Fluctuations Amplitude →</center>
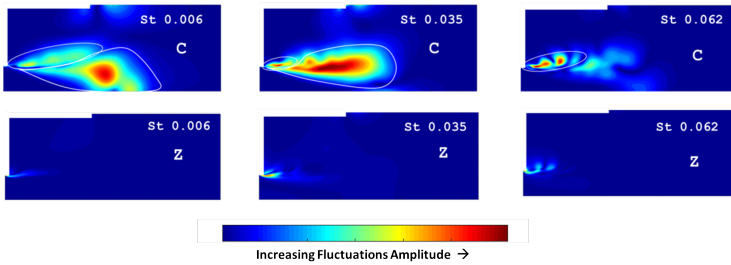
Figure 5.17: FFT amplitude for progress variable and mixture fraction fluctuations at three frequencies.

The frequency analysis has been carried out for the main variables of interest that may have a direct impact on the heat release response, such as progress variable and mixture fraction fluctuations, for the case when the air and fuel mass flow fluctuates simultaneously (FFT_u in previous discussion). Values for these are exported on one of the cyclic surface every 15 time steps. The time histories for the variables exported on the mesh nodes are then Fourier transformed and shown in Figure 5.17.

From progress variable fluctuations amplitude an interesting behaviour emerged. At low frequency (St 0.006) the main fluctuation are registered for the premix flame.

From phase-averaged images Figure 5.18 it can be observed that the premix flame front oscillated axially at this frequency while the pilot region seems substantially unaffected. This is again confirmed by the same picture in Figure 5.17 where progress variable fluctuations are found limited in this region.

Another interesting aspect is visible: the pilot flame and the premix
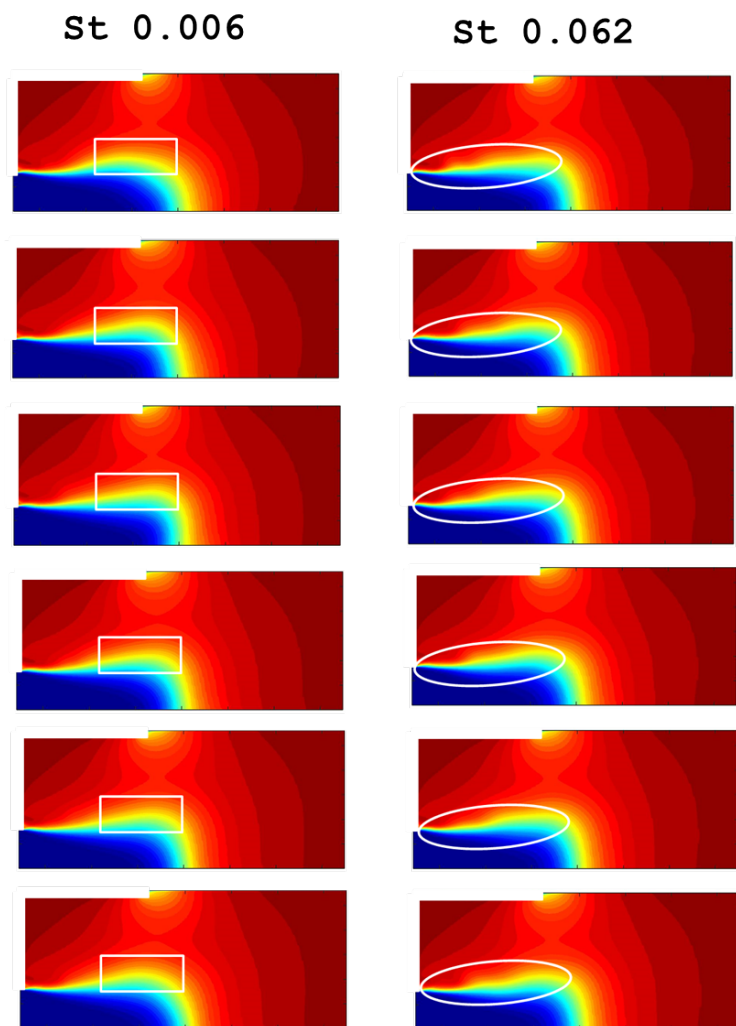
Figure 5.18: FFT amplitude for progress variable and mixture fraction fluctuations at three frequencies.

flame front seem to evolve in a separated manner and their regions of influence are well defined, a part from the common shear layer where an interaction is present. From progress variable fluctuations amplitude at St 0.035 the two regions are again visible but the pilot reduces to a smaller zone with higher intensity while the premixed part exhibits a predominant behaviour, especially in the later shear layer if compared with the flame head. The highest fluctuations are registered here. Finally, at St 0.062, close to the frequency of interest, important amplitudes are observed for the pilot flame only.

Again, from phase-average post-process in Figure 5.18 it can be observed a waving motion in this zone while the premix flame remains unaltered by the excitation.

Together with progress variable fluctuations amplitude mixture fraction fluctuations amplitude are shown in Figure 5.17. What emerges from this pictures is that mixture fraction fluctuations interest mainly the pilot region while in the premix part they have a lower amplitude. Moreover, increasing the frequency such fluctuations become more intense. At St 0.06 the mixture fraction fluctuation and progress variable fluctuation amplitudes show a very similar shape. This can be related to the fact that the pilots interact with the outer radii very lean mixture, so that a fluctuation at the premixer makes the mixture fraction in the pilot region fluctuate around the rich blow out limit of the mixture causing and intermittent state of complete and incomplete reaction, that is the cause of the progress variable fluctuations.

From this in-depth study it can be concluded that the unsteadiness of the heat release associated to premix part of the flame is mainly related to the fluctuation of the flame front and to the consequent variation in the surface of reaction. As far as pilot flame is concerned, the main cause of heat release fluctuation can be found in the mixture fraction variation which follows a fluctuating entrainment of the mixture from the premixer.

5.2.5 Stability Analysis

In this final section the stability analysis carried out on the full-annular combustor is presented.

The FEM model of the combustor is shown in Figure 5.20. In order to limit the number of element of the numerical mesh, all the smallest details which needs a large number of elements is necessary to be correctly reproduced, are eliminated. The main cavities are instead included in the model. The fuel line has been removed as well as the axial swirler blades after checking the limited effects of such a simplification. This is also confirmed by the observations of [6, 95] about the acoustically transparent nature of axial swirlers.

The resulting mesh and counts around 3.7E6 tetrahedral elements. The maximum element size is chosen in order to be able to detect acoustics modes well above the range of interest.
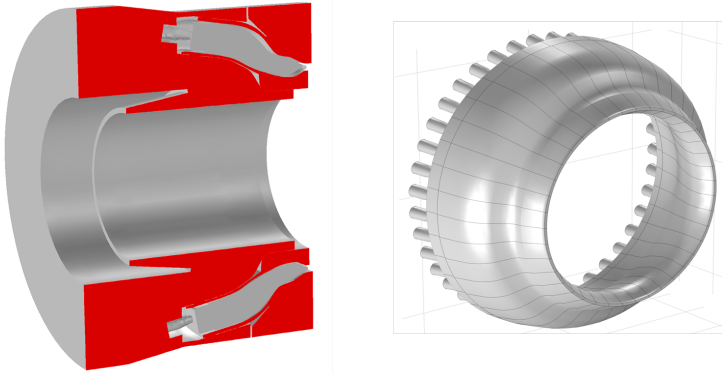
Figure 5.19: FEM model of the combustor (left) and particular of the burners and flame tube (right) divided in 39 sectors.

The flame region, where the source term assumes non-zero values, is imported in the FEM model from CFD results, defining it as the region of non-null rate of reaction (Product Formation Rate in the adopted combustion model). A non-uniform distribution of the source term,

defining a weighting function $(WF(\mathbf{x}))$, shown in Figure **??**, in the flame region, i.e. proportional to the PFR.
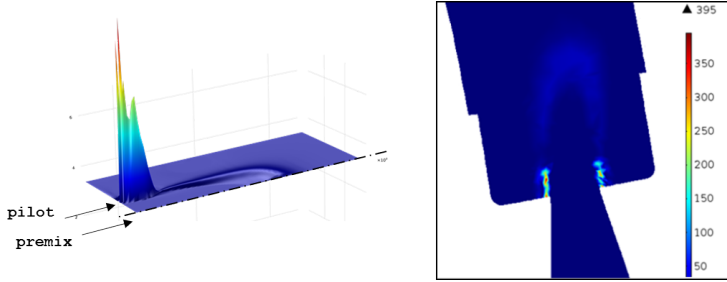
Figure 5.20: Weighting function of TP145 (left) and source term in COMSOL (right).

In this way, not only the differences in the flame shape and length are reproduced in the FEM model but also the change in the heat release distribution that can be observed at different operating conditions.

As shown in Figure **??**, a dedicated sector is assigned to each injector in order to limit the computational memory required during the solution, as described in section 3.1.2.1. The final expression for the source term is then given by 3.25.

The temperature distribution in Figure 5.21 is imported in COMSOL from the CFD results. Consequently, the density and the sound speed assumes local values, giving a more physical representation.

As far as the boundary condition are concerned, particular care has been put in replicating acoustic boundaries and operating conditions of the real engine in that rig. A plenum condition at the inlet and choked outlet are considered as boundary conditions.

COMSOL Pressure Acoustics module [121] is used to solve for the inhomogeneous Helmholtz equation in the frequency domain.

The thermo-acoustic model is fed at first with the global FTF, derived in case of choked fuel line. Successively, the simulation where each FTF, pilot and premix, acts on their respective region has been carried out.
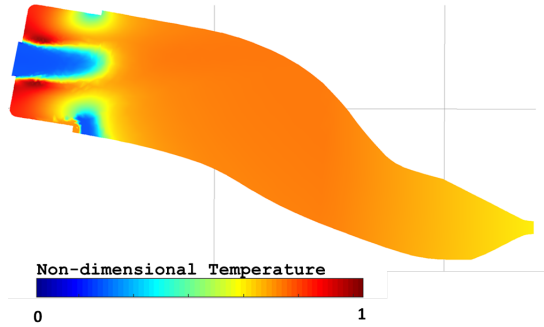
Figure 5.21: Temperature distribution imported in COMSOL from CFD data.
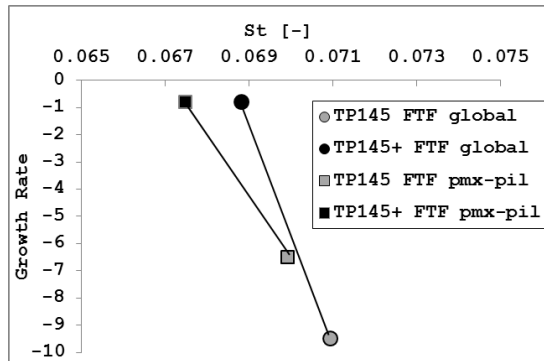
Figure 5.22: Results of the stability analysis with the FTFs obtained under the hypothesis of choked fuel line.

Attention was focussed on the second tangential mode of the flame tube, depicted in Figure 5.23.

The obtained results are shown in the plot in Figure 5.22. Both the simulations predict higher stability properties at TP145 and a tendency to instability increasing the flame temperature for TP145+. The experimental trend is, therefore, correctly observed though both the modes are stable modes in numerical results. When using the switching from
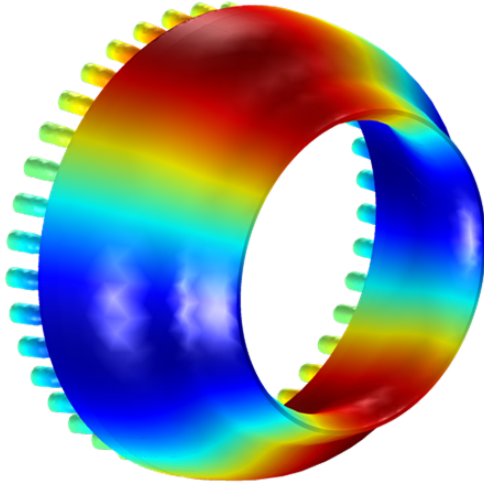
*Figure 5.23: Normalised absolute pressure within the flame tube for the
second tangential mode investigated.*

the global FTF to the separated zone treatment, similar growth rates are
found for TP145+ while TP145 is found to be less stable. Similar results
are obtained with global and separated FTF even if, in this second case, a
distinction of the respective region of activity and of the different under-
lying physics, allow a deeper understanding on the single contributions
and lead to less preventive results.

In order to understand the effect of fuel mass flow fluctuations on the
stability solution of the system also this two contribution is implemented
in the FEM code.

For simplicity it is assumed an equal intensity for the fuel and air
fluctuations so that:

$$|\frac{u'_F(\omega)}{\overline{u}_F}| = |\frac{u'_b(\omega)}{\overline{u}_b}| \tag{5.6}$$

A phase shift is then introduced between the fluctuations and a

sensitivity is performed to this parameter.
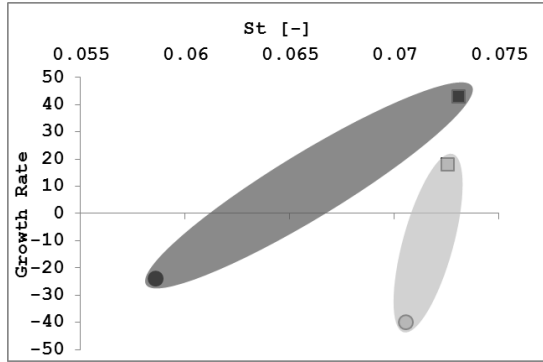
Figure 5.24: Results of the sensitivity analysis to the phase shift between fuel and air fluctuations for TP145 (light-grey region) and TP145+ (dark-grey region).

In Figure 5.24 the region of the solutions for the two investigated condition can be seen. The inclusion of fuel mass flow fluctuations can affect drastically the stability of the system, depending on the relative phase between air and fuel mass flow fluctuations.

Interestingly, both the test points TP145, TP145+ become unstable with particular values for the phase shift. TP145+ shows greater instability and becomes highly unstable at phase shift around $-\pi/2$ of delay between the air and the fuel fluctuation. TP145, instead, reaches the maximum values for the growth rate at around $-\pi$.

In both cases unstable conditions are found when fuel and air fluctuates out of phase. The maximum stability are found when both fluctuates in phase. Similar conclusions have been found in [47] on a simple experimental burner: In case of fuel and air fluctuating in phase, a damping effect is found in certain conditions while, whenever the former fluctuates out of phase they found always an amplification of the oscillations.

Their study showed, in fact, that the interaction between both effects have been found to be of major importance for the driving mechanism. Both, the total mass flow modulations at the burner exit and fuel mass

flow fluctuations, which are different in phase and magnitude have a very strong influence on the thermoacoustic feedback mechanism.

Therefore, the inclusion of the inclusion of the actual phase shift and relative intensity of the fluctuations can lead to the correct reproduction of the experimental founding. This means that it should be considered the inclusion of the fuel line in the calculation, or an equivalent model (transfer matrix, impedance etc.) for it.

From another point of view, the obtained results indicate that the system can be moved towards stable condition acting on the phase shift between fuel and air mass flow fluctuations, i.e. changing the burner length or the position of fuel injection within the premixer. A possible degree of freedom for stable design is therefore pointed out from this investigation.

It must be recalled that the interaction between the two flames, not considered in this simplified model, can also have a contribution. Also considering the effect of other driving mechanism on the dynamic response of the studied flame can have an impact on the solution, such as the fluctuation at the pilot fuel line. Therefore, in the following, additional consideration on the role of pilot flames are made.

5.2.6   Additional consideration on the pilot flame influence

A further in-depth study is made to better understand which is the impact of a different pilot penetration or, more in general, of an added delay time to the pilot response and of a fluctuating pilot injection on both premixed and pilot flames.

5.2.6.1   Pilot jet penetration

Concerning the CFD model adopted to compute the FTFs, additional evaluation are to be made to understand its ability to correctly catch the features and the evolution of pilots within the flame. Due to the complex and unsteady behaviour of pilots flame, related to the V-cut injection

geometry and to the interaction with premix and dome cooling flow, such a prediction is definitely a challenging aspect to be reproduced by CFD simulations.
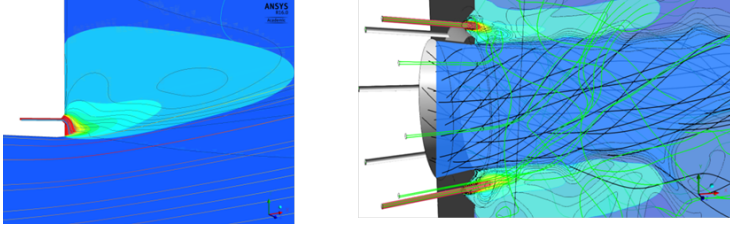
Figure 5.25: Pilot jet prediction obtained with the simplified domain (left), adopted for the FTFs identification, and obtained with a SAS simulation of a single sector of the combustor (right).

Comparing the CFD result obtained with the simplified domain with detailed SAS simulation of the same flame, the main discrepancies are found on the pilot jet penetration reproduction. Looking at Figure 5.25, the results of numerical simulations with the simplified computational domain described above and a SAS simulation of a single sector of the combustor are shown together. The pilot jet in the former solution does not penetrate with the same intensity than the SAS simulation. Possibly, considering the pilots as an equivalent slot instead that discrete injections does not represent the jet behaviour adequately.

A different pilot penetration prediction can impact positively the mode stability. There will be an impact also on the premix response but, due to the observations that led to the assumptions of almost independent behaviours for pilot and premix flame, this can be expected of minor entity and then neglected at first.

A simple test is then carried out in this part of the work, to simulate in a simplified way a different pilot jet penetration: An enhanced jet penetration of pilot jet is simulated adding a constant delay time to the pilot response. A sensitivity analysis is then carried out for different time lags (τ). As said, the premix flame is considered unaffected by such a
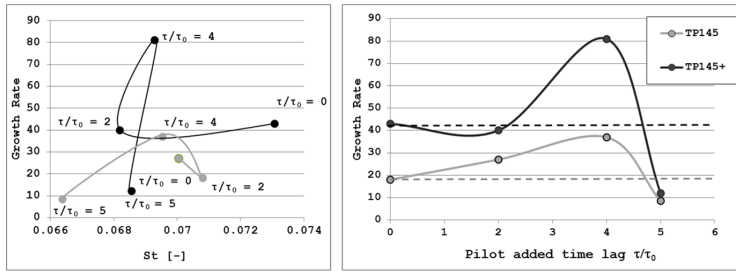
Figure 5.26: Obtained results varying the time lag added to the pilot FTF,
for the two operating condition TP145 (grey) and TP145+ (black).

change so that the FTFpmx is maintained the same used for previous
stability analyses.

The sensitivity is applied to the worst case (higher growth rate)
obtained from the sensitivity analysis presented in the previous section
5.2.5, for both the test points. Therefore, the starting point are two
unstable ones, with growth rate of around 40 and 18 for TP145+ and
TP145 respectively.

In Figure 5.26 the results of this last investigation are shown. The
added time lag is scaled with a reference delay time τ_0. An increase of
the time lag in the dynamic response of pilot tends to move the mode to
stability towards more unstable conditions at first, than a marked decrease
in the growth rate is observed. At τ/τ_0 of 5 a more stable solution than
the starting one is found for both the operating conditions. A drastic
beneficial abatement of the growth rate is predicted for TP145+ while a
lower reduction of the growth rated is found for TP145.

In general, from this investigation an interesting result is obtained:
acting on pilot flame time lag it is possible to change the investigated
mode stability till, eventually, stable conditions could be reached from
initially unstable ones.

Practically, this could be realised with a modified pilot injection where
the jet is no directed more axially in the combustor or changing the jet
momentum ratio (i.e. enhancing jet velocity).

5.2.6.2 Pilot fuel mass flow fluctuations

Finally, the effect of a fluctuating pilot injection is studied.

A CFD simulation is performed for the TP145, where only the pilot mass flow is excited with the RASW signal and a maximum peak-to-average ratio of the signal of 5 %. A lower maximum fluctuation is chosen for pilot injection than the previous cases where a RASW signal with a 20 % of peak-to-average ratio, to avoid having non-linear response that, for such a diffusion flame might be observed.

The pilot jet velocity is recorded within the pilot fuel channel while, heat release is recoded separately for pilot and premixed flames.

The same procedure is used for the calculation of the FTFs, as discussed in previous sections of this chapter.
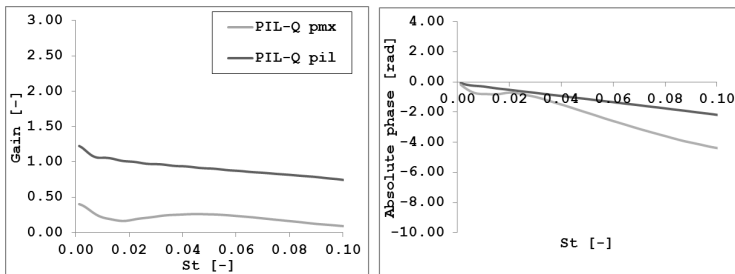
Figure 5.27: FTFs relating a fluctuation of pilot fuel mass flow to premix (grey) and pilot (black) heat release.

In Figure 5.27 the obtained FTFs are depicted. From the amplitude plot on the left the different impact that a pilot fuel mass flow fluctuation has on pilot and premix flame is seen. A marginal impact is found for premix response while it becomes a more important contribution for pilot flames, as expected. In this case, the Gain is almost unity all over the spectrum and a slow decrease with frequency is found.

As far as the phases are concerned, a constant time lag response is evident for pilot response. A higher time lag is correctly associated to premix flame due to the longer path that a fuel fluctuation has to cover

to reach this flame.
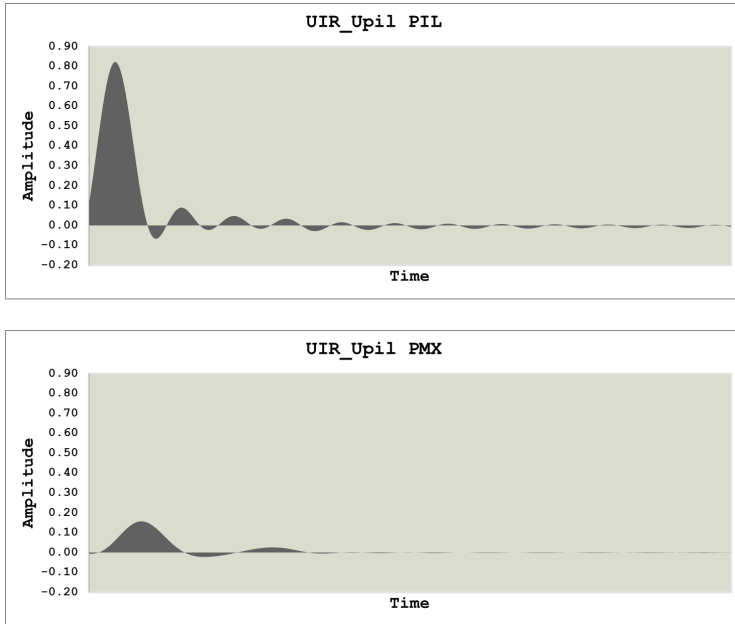
Figure 5.28: UIRs to a pilot fuel mass flow fluctuations of pilot and premix heat release.

To get a more physical interpretation of the result, UIRs to a pilot fuel mass flow fluctuations of pilot and premix heat release are reported in Figure 5.28. A similar response is obtained for the two part of the flame but higher amplitude is associated to pilots. The heat release response starts immediately as the reference section for the velocity and the pilot flame itself are very close. The peak is, instead, associated to the delay time between the reference section for the velocity and the location where a peak of the heat release is found. The premix response peak appear later and results in a less marked amplitude.

From this last analysis it can be concluded that pilot fuel mass flow fluctuations can have an important impact on pilot flame dynamics while

only a marginal effect is introduced for the premix one. The introduction of a further mechanism in the MISO model of the flame (together with the already contemplated air mass flow and premix fuel mass flow fluctuations), can make the thermo-acoustic model of the combustor even more representative.

In order to relate the heat release fluctuations to the new input, the inclusion of pilot feeding line should be considered. The possibility to model the latter with an equivalent impedance can be also taken into account for future developments of the model. Such an upgrade could lead to a proper evaluation of pilot fuel mass flow fluctuations effect and evidence other possibilities for alternative designs with an intrinsic higher induced stability.

5.2.7 Quality Checks
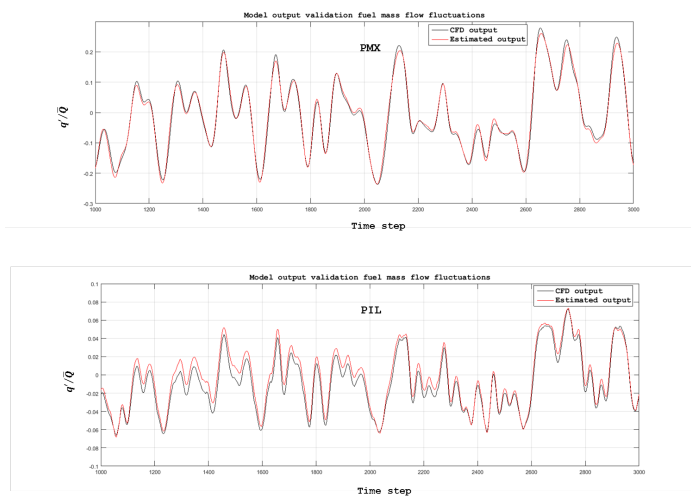
Figure 5.29: CFD and estimated outputs to fuel mass flow fluctuations at the premixer

Before the final remarks are presented in next section, few words are
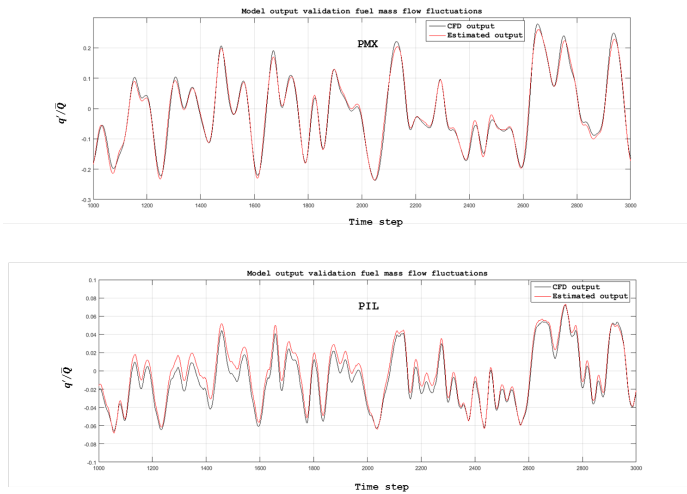
Figure 5.30: CFD and estimated outputs to pilot fuel mass flow fluctuations

due to the quality of the identified flame models.

In the next plots the CFD heat release fluctuation (best fit) is compared to the one predicted by the model when the same excitation signal than in the CFD simulation is given (estimated result).

When only fuel mass flow fluctuations from the premixer are considered (Figure 5.29), the estimated output well fit the reference CFD one, for both premix (top) and pilot (bottom) flames. This means that a model (FTF_F is able to well represent the effective situation in this case. Note the different entity of the response between premix and pilot flames. A fuel mass flow fluctuation at the burner does affect pilot flames as the premix one due to the fact that the former interact with the mixture from the outer radii that is practically pure air.

Also in case of a pilot fuel mass flow fluctuation only the model (PIL-Q in Figure 5.27) is able to describe the actual evolution as shown in Figure 5.30. The CFD results are fitted well for both pilot and premix flame. Note also in this case the difference between the entities of the response
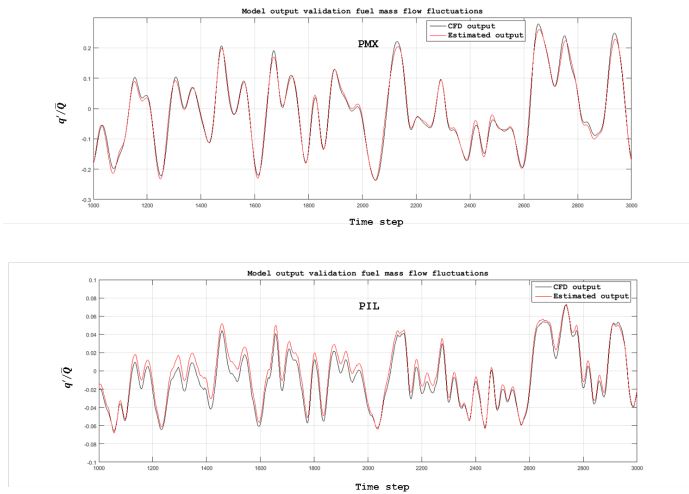
Figure 5.31: CFD and estimated outputs to air mass flow fluctuations at the premixer considering a choked fuel line

of the two flames: the premix one is definitely less sensitive to a pilot fuel mass flow fluctuation that the pilot one.

Finally, when only air mass flow fluctuations are considered two interesting aspects emerged from premix and pilot validations, in Figure 5.31. Concerning the premix flame (Figure 5.31 top), a model that relates the heat release fluctuations to mass flow (or acoustic velocity) fluctuations at the burner exit is not able to represent the real output. In fact, as already pointed out, together with air mass flow fluctuations also equivalence ratio ones are induced in case of a choked fuel line. The latter play a fundamental role in the flame response and the system should be described as a MISO one. Therefore, neglecting them lead to low quality models of a practical flame.

Concerning pilot flames (Figure 5.31 top), instead, a SISO model (FTF$_{CF}$ PIL) well describes the flame dynamics as pilot are not affected by equivalence ratio fluctuations at the premixer (as just mentioned above). What also emerged from Figure is the high sensitivity of the latter flame

to a fluctuation of the premixer mass flow and heat release fluctuations rates up to 0.45 are observed.

5.3   Final Remarks

Unsteady CFD simulations were performed to compute the flame transfer function of a GE Oil & Gas partially-premixed lean-burn combustor for two operating conditions, varying flame temperature. The direct comparison with results from full-annular combustor experimental campaign carried out by GE Oil & Gas allowed the model assessment and helped understanding the results.

The main features of the flame, composed by pilot diffusion flame and a main premix one, were investigated introducing two independent FTFs for pilot and premix flames.

When implemented into FEM model, it allowed understanding the effects of both the combustion modality on the system stability. The effect of fuel mass flow fluctuations are ten introduced in the thermo-acoustic model of the combustor as further driving input, showing that they can affect drastically the stability of the system, depending on the relative phase between air and fuel mass flow fluctuations.

A Multi-Input Single-Output model of the flame is therefore mandatory to catch the actual stability properties in case the fuel mass flow fluctuations play an important role in the flame dynamics.

The result also indicates that possible solutions for more stable designs can be realised changing such a phase by acting on the burner length or on the position of fuel injection within the premixer.

Additional consideration on the pilot flame have been carried out through a sensitivity analysis to a time lag added to pilot flame response, thus modelling an enhanced jet penetration. Valuable indications are obtained from the analysis, precious for future in-depth studies and pilot system design optimization.

Finally, the impact of a pilot fuel mass flow fluctuations has been studied showing the relative importance of the latter on pilot flame

response if compared with the premix one. Possible guidelines for future improvement of the model has been drawn which include premixer and pilot fuel lines inclusion in the FEM model, and an additional input to the MISO structure used to describe the flame.

A final note on the procedure to compute the FTFs related to each of the MISO inputs is due. In this work the inclusion of the various input came step by step and a distinct simulation has been carried out to compute the FTF associated to the input at issue. In a more fast way, the same result can be obtained in a single CFD simulation where all the input are associated, provided that the signal are uncorrelated and the inputs independent.

Chapter 6

Numerical Study of the Dynamic Response of a Liquid Fuel Flame for Aero-Engine Applications

6.1 Previous Studies and Main Features of PERM Injection System

The PERM (Partially Evaporated and Rapid Mixing) [158] injection system has been developed by GE AVIO for ultra low NOx (ULN) combustor core technology. It is addressed to achieve partial evaporation inside the inner duct and a rapid mixing within the combustor, optimizing the flame position and the stability of the combustion process. It is characterized by two radial co-rotating primary and secondary swirlers used to assign angular momentum on the two distinct inlet streams; before entering in the combustion region, the swirled flows are accelerated in the inner and the outer nozzles thanks to a conical internal body [159].

From Figure 6.1 the double swirler airblast atomizer concept design can be seen. The film of fuel is generated over the inner surface of the lip that separates the two swirled flows. As the film reaches the edge of the lip, through the action of the primary flow, primary atomization occurs: fine
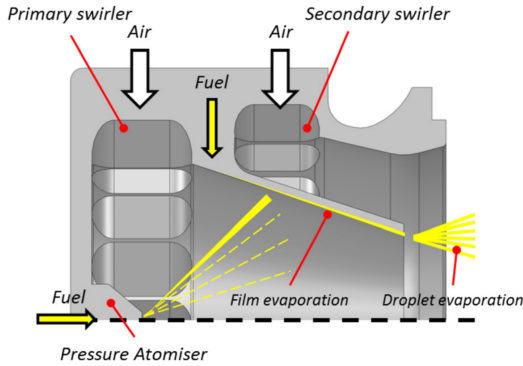
Figure 6.1: scheme of the PERM injector [160].

droplets and rapid mixing are promoted by the two co-rotating swirled flows generated by the double swirler configuration. Furthermore, in order to ensure a stable operation of the lean burn system, especially at low power conditions, the airblast injector is coupled with a hollow cone pressure atomizer (pilot injector), located at the centre of the primary swirler, which generates a pilot flame to stabilize the combustion process and it is usually active within the entire operating range with a variable fuel split between pilot and main stage [3].

PERM injector has been extensively studied in Heat Transfer and Combustion research group at the University of Florence.

A typical flow-field generated by a PERM injection system can be observed from the result of Andreini et al. [161], in Figure 6.2.

From the contours of velocity on the meridional plane passing through the injection system, it is possible to see how the recirculation zone generated by the swirler occupies almost all the combustion chamber. It is also evident the vortex breakdown, that provides the dominant flame stabilization mechanism, and is characterized by the existence of internal stagnation points and reversed flows, drawing hot gas towards the injection system.

Another typical features of the flow-field generated by swirling injectors
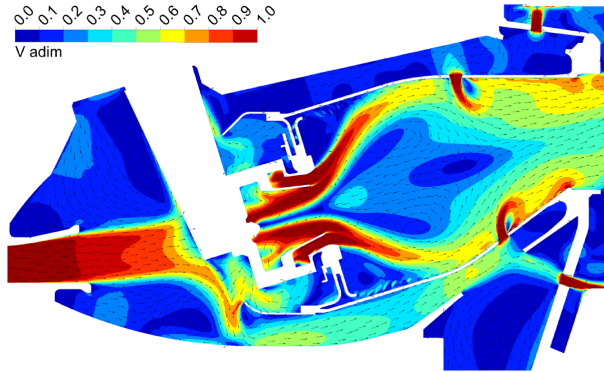
Figure 6.2: Cross-sectional view and flow field of a GE AVIO annlar aero-engine combustor chamber) [161].

is the so-called precessing vortex core (PVC), a three-dimensional unsteady asymmetric flow structure that develops when a central vortex core starts to precess around the axis of symmetry at a well-defined frequency. This phenomenon is usually linked to vortex breakdown and the associated recirculation zone in a high Reynolds number flow and strongly affects the flow and flame evolution in combustion systems [7].

In another work of the same research group [159, 160], the injector was studied with the main aim characterizing the flow field and the wall heat transfer resulting from the interaction of a swirling flow provided by the injector and the cooling system at combustor walls. In Figure 6.3 it is possible to see the PVC that develops along the high velocity jet, from the injector. The presence of a PVC also helps explain the occurrence of instantaneous negative azimuthal velocity in the region near the centreline of the chamber [7].

The PVC may improve combustion efficiency through its enhancement of turbulence intensity and mixing, but it also represents a largely undesired characteristic because of the possible resonant coupling with low-frequency acoustic oscillation in gas turbine combustors [7].

As the flow expands from the injector exit and evolves downstream,
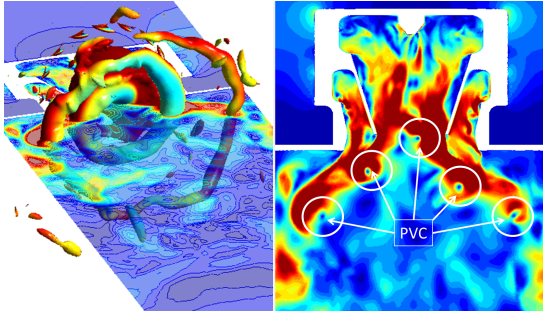
Figure 6.3: Results of a SAS simulation of the PERM: Two-dimensional velocity on the median plane (PVC visualized by a constant pressure isosurface) [159].

strong shear layers develop, due to the velocity difference between the jet flow and the ambient fluid. The high velocity jet expanding from the PERM injector can be seen in Figure 6.4, obtained with PIV measurement of the isothermal test rig at University of Florence [160].
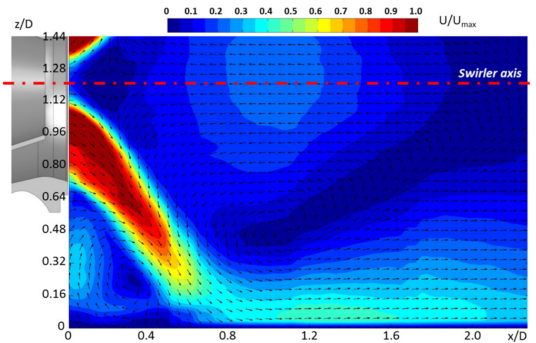
Figure 6.4: Results of PIV measurements of PERM flow-field: Particular of the high velocity jet impinging on liner wall [160].

As far as previous numerical studies of the PERM injector in reactive conditions, an example can be found in [161] where a sector of an annular combustion chamber is simulated.
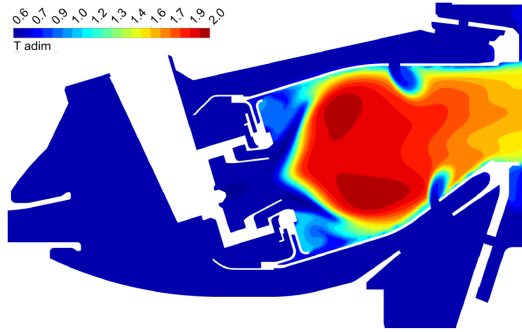
*Figure 6.5: Predicted temperature field in an annular combustion
chamber equipped with PERM injector [161].*

The predicted temperature field is reported in Figure 6.5. Again the
important role of role of central recirculation zone in flame stabilization
is evident. Along the shear layers between the annular jet of the swirler
and the main central recirculation a relevant mixing rate is induced by
local high turbulence intensity while hot gases, provided by recirculating
flow, assure the continuous ignition source.

6.1.0.1 Atomization and spray formation of liquid fuel

In premixed systems, the main tasks of a fuel atomizer are to produce
a large number of droplets with sufficiently large total surface area, and
to distribute the fuel droplets uniformly in the air stream to enhance the
mixing process. Therefore, liquid fuel preparation has a strong impact on
the combustion process and engine emissions since it directly influences the
air-fuel mixing and the fuel distribution inside the combustion chamber.

In order to properly predict the behaviour of aero-engine combustors,
particular care needs to put at the description of the most important
aspects related to fuel evolution and interactions with the gas-phase.

In his PhD work Giusti [3], devoted grat attention to the aspects
related to the film evolution and primary breakup developing proper
tools able to include liquid film modelling in industrial computations,

(a) Droplet dynamics   (b) Fuel mass fraction near the film
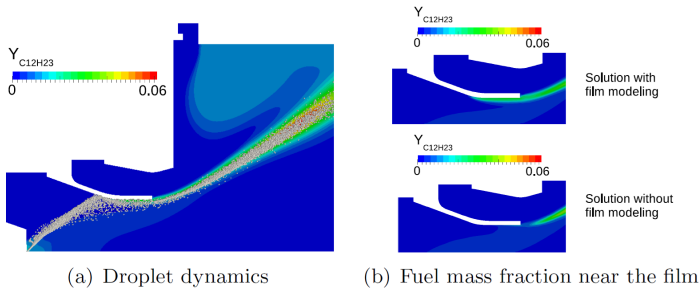
Figure 6.6: Multi-coupled solutions [3].

for the analysis of advanced prefilming airblast injectors to be used in standard industrial computations based on RANS (U-RANS) approaches (see Figure 6.6).

Finally, concerning the evaporation at different operating pressures, interesting results can be found in [162]. In Figure 6.7 it is possible to note that in some operating conditions, in particular at idle or more in general at low pressure with a high pilot/ main fuel split, droplets injected through the pressure atomizer could reach the lip promoting the formation of the liquid film. In these cases the aspects related to the modelling of wall/film-droplet impact are fundamental to determine the amount of fuel added to the liquid film by droplet impingement or droplets generated as a consequence of the impact with the film surface [3].

6.1.0.2 Thermo-acoustic investigations on PERM equipped combustors

Finally, to conclude this section, previous studies on PERM equipped combustor, carried out within the Heat Transfer and Combustion group at the University of Florence, are presented in order to draw the line of the state of the art from which the present work starts.

In [76] and in [77], within the context of KIAI and LEMCOTEC EU projects, the thermo-acoustic analysis of a full annular aero-engine
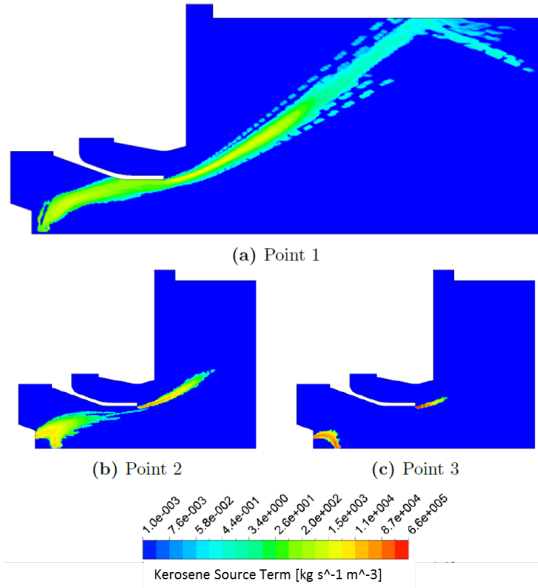
Figure 6.7: Kerosene evaporation rate at increasing operating pressure, from point 1 to point 3 ([162]).

combustor equipped with GE AVIO PERM injector is performed. Combustor walls exploit multi- perforated liners to control metal temperature; these devices are also recognized as potentially effective sound absorbers, thus they could be used for both wall cooling and damping combustion instabilities. Multi-perforated liners were modelled by assigning to the corresponding surfaces an equivalent internal impedance. Different models for multi-perforated liner impedance have been assessed and evaluated by numerically reproducing an experimental test rig developed at the University of Florence to measure the adsorption properties of cylindrical perforated walls.

On the other hand, when the presence of the flame was considered, the the inadequacy of FTFs commonly used for premixed combustion was evidenced by comparisons with experiments. The thermo-acoustic analysis

in lean-burn aero-engine combustor suffers the lack of a Flame Transfer
Function able to completely describe the thermo-acoustic instability driv-
ing mechanisms that characterize a liquid fuelled combustor operating in
lean burn regime. Besides the typical driving mechanisms of premixed
flames that could be still present when rapid evaporation and mixing
are achieved, the complex physical phenomena the characterize liquid
atomization and droplet evolution could also interact with the acoustic
field determining a fluctuation of the local equivalence ratio and thus of
the heat release rate. Thus, in order to perform reliable thermo-acoustic
simulations, a more detailed comprehension of the physical phenomena
and thermo-acoustic driving mechanisms characterizing liquid fuelled
combustors was pointed as the main future development target.
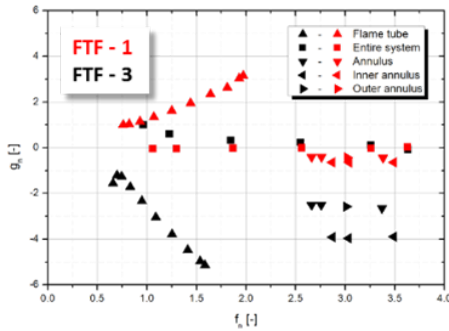
Figure 6.8: Eigenfrequencies of the active simulations: Effect of the FTF
[5].

Similarly, in [5], the same authors tested the capabilities of different
FTFs formulations in reproducing the complex phenomena characterizing
the coupling between heat release rate and acoustic field in lean burn
aero-engine combustors. They performed a thermo-acoustic analysis of a
tubular combustor equipped with a PERM injection system. Experiments
were also available in this configuration with combustor resonant frequen-
cies measured at several operating conditions characterized by different
mean pressure, air inlet temperature, fuel-air and pilot to total fuel mass

flow rate ratios. The thermo-acoustic behaviour of the combustors has been shown to be strongly dependent on operating conditions and that, again, simple FTF formulations seem to be inadequate to the study of the thermo-acustic stability in all conditions (see their results in Figure 6.8).

The work carried out in this thesis follows the previous analyses on PERM equipped combustors and the traced guidelines for the numerical modelling developments of lean-burn aero-engine combustors. In particular, the most incipient aspect of finding a proper description for the flame dynamics of liquid fuelled flames is taken on. The proposed methodology, that exploits unsteady CFD simulations where the liquid fuel evolution and its atomization, evaporation and mixing are reproduced, is considered a suitable tool to provide improved FTF formulations. Moreover, such instruments can also provide useful information on the physics of liquid fuelled flames together with a proper characterization of the injection system when acoustically perturbed.

At this regard, the following section introduces an acoustically analysis of the PERM injection system so that the latter aspect will be deeper investigated.

6.2   Acoustic Analysis of PERM injector

Before discussing the main results of this work, an acoustic investigation of the injection system has been performed to understand PERM behaviour when acoustically forced.

A tubular combustor equipped with PERM injector has been simulated. The feeding plenum included in the numerical simulation.

Exploiting the domain periodicity the computational domain is reduced to $1/16th$ and discretised with a hybrid tetra + prism mesh in Figure 6.9.

For the simulations the code Ansys Fluent 14.5 is used, performing Unsteady-RANS simulations. A second order scheme is adopted for spatial and temporal discretisation of the equations but for turbulence related quantities for which a first order upwind was, instead, used. Standard $k - \epsilon$ is adopted as turbulence model.
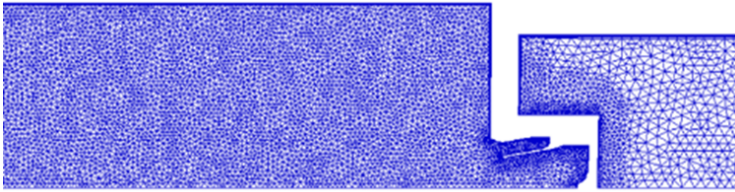
Figure 6.9: *Tubular combustor: mesh used to investigate the acosutic behaviour of the injector.*
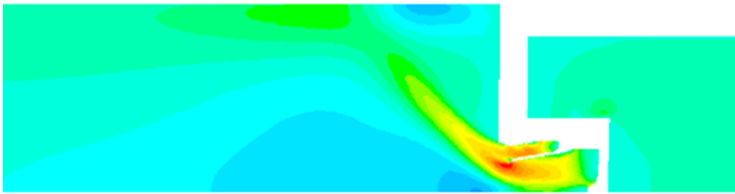
Figure 6.10: *Tubular combustor: axial velocity contours.*

A coupled Multi-Grid solver with a maximum Courant of 1 is exploited to solve for the equations.

In the resulting flow field (Mean Axial Velocity) depicted in Figure 6.10 the main features such as the main recirculation, the corner dome recirculation and the high velocity jet are observed.

A monochromatic excitation is superimposed at the inlet, for several frequencies: 150 Hz, 450 Hz, 950 Hz, 1350 Hz.

In Figure 6.11 are displayed the axial velocity fluctuation over a period of a 450Hz excitation. A region of increased velocity is visible initially at the injector exit region

These waves, generated by the flow oscillations at the entrance, are convected downstream along the direction identified by the swirled jet, the high velocity region identified by the air path from the injector exit (see Figure 6.11). The wavelength is inversely proportional to the forcing frequency, and shortens in the middle region of the injector due to the
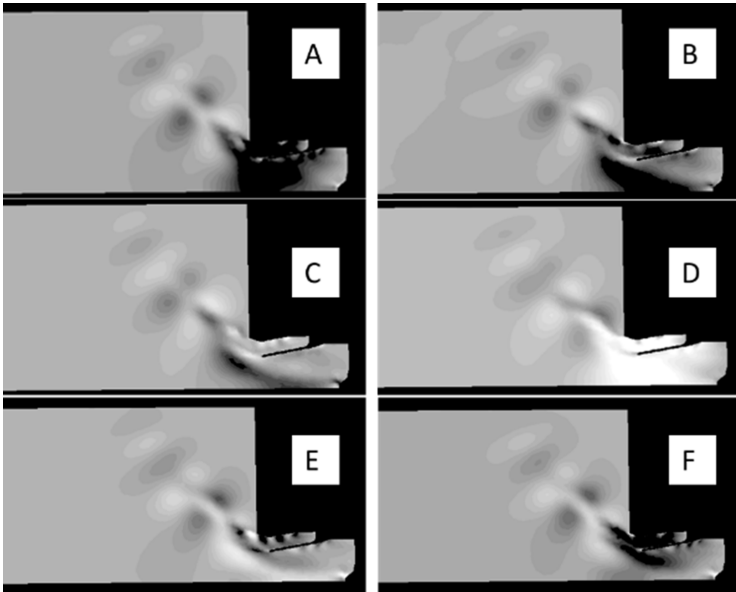
Figure 6.11: Axial velocity fluctuation over a period of a 450Hz excitation.

flow-turning effect, i.e., the flow direction turns in this region and the velocity component perpendicular to the wave front decreases.

The imposed excitation at the injector entrance can be further decomposed into two components in the azimuthal and radial directions. As observed by [7], the former generates a vortical wave due to the shear stress resulting from the flow oscillation in the azimuthal direction, and its dynamics are governed by the conservation of angular momentum. The latter produces an irrotational, travelling acoustic wave, and can be characterized by the pressure and stream-wise velocity fluctuations through mass conservation. While inside the injector the planar wave behaviour is clearly observable, when the excitation passes along the jet a slightly difference emerges between the three components. The radial velocity fluctuations develop along the jet direction (see Figure 6.12). In
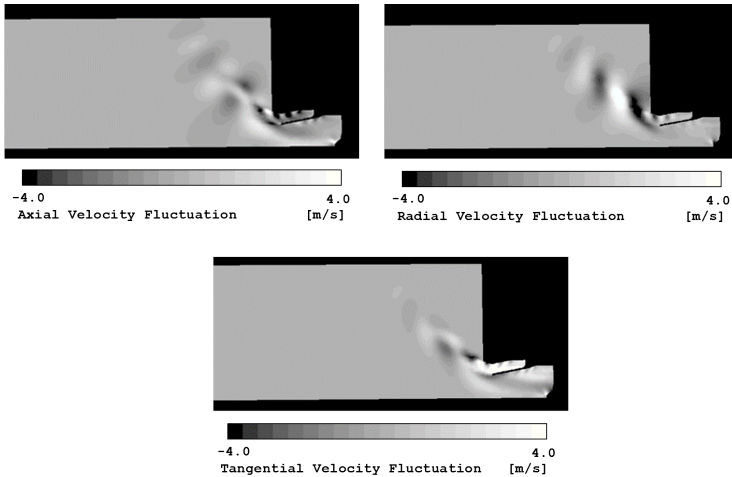
Figure 6.12: Contours of the velocity fluctuations: a) axial velocity fluctuations, b) radial velocity fluctuations, c) tangential velocity fluctuations.

the axial velocity fluctuations appear a combined evolution along the jet direction and along the direction perpendicular to the jet. In particular, two peaks are present in the first part of the jet, remembering the two feeding channel of the injector, that eventually merge in the final part of the jet, close to the liner wall. For the azimuthal velocity component, it seems that the waves that come from the two injector channels are out of phase, with a phase shift of 180 deg. The two perturbations propagate in an independent way, along the jet direction, till the final part where they merge.

The presented analysis gave an important insight on the physical behaviour of a PERM injector when an acoustic wave pass through it and more in general, on the acoustic behaviour of radial swirles.

It has been found that the main direction of propagation for the acoustic wave is the jet trajectory. The two channels form clearly distinguishable pathways and the two waves coming from these, propagates

independently. For axial and radial fluctuations they are in phase while for the tangential velocity (Figure 6.12) they seems out of phase. The plane wave hypothesis is, therefore, a stronger hypothesis for radial swirlers that axial ones and that might affect the practices developed for the used numerical tools employed in the study of the (thermo-)acoustic problems. As an example, when numerically computing the burner transfer matrix with a mean flow superimposed (see appendix A.1), such results should be considered to define a reliable numerical setup as well as to take into account the limitations of the mentioned technique. In particular, attention should be put when an excitation signal, as the one used in the two sources technique, as is not along the actual direction of propagation for of an acoustic wave passing through the injector.

Moreover, the presented analysis can gave interesting insight for the choice of the input signals to be used in the system Identification technique for the numerical determination of the Flame Transfer Function.

The common choice to characterise the FTF with the signal at the injector outlet, without distinction between the primary and secondary feeding channel, could be improved considering two separated input signal for the two injector vanes. Such aspects will be object for further verifications and analyses for future works.

After an introduction on the PERM injection system through previous studies and a in-depth investigation on its acoustic response to an acoustic fluctuation, in the following sections the identified test rig used to assess the FTF computation methodology and the main results are presented.

6.3   Test-rig description

An experimental test case where measurement were available as been identified for the assessment of the numerical methodology for the computation of the Flame Transfer Function .

In particular, the reactive test-rig of TUM University used by Gikadi in his PhD work [164] has been chosen (see Figure 6.13).
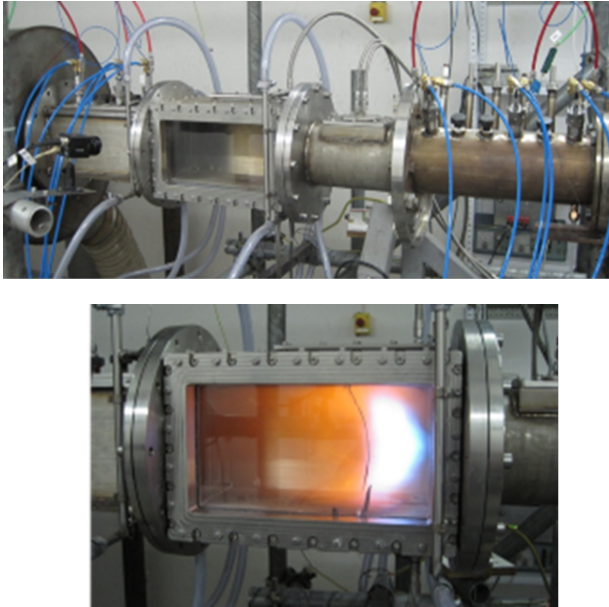
Figure 6.13: The reactive test-rig of TUM University used in KIAI EU
project [163].
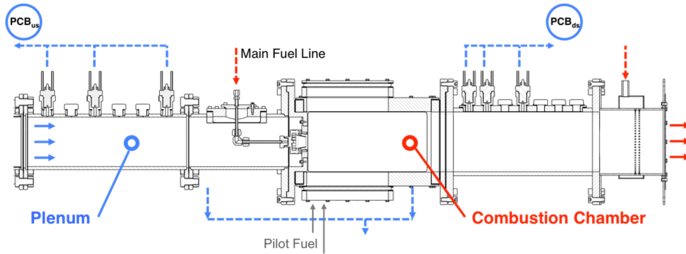
Figure 6.14: Scheme of the reactive test-rig of TUM University [163].

The test case description and the adopted measurement technique are
briefly reported in the following as presented in [164].

The available measurements consist in: FTF measurements and Injec-
tor Scattering matrix.

The atmospheric combustion chamber test rig is depicted in Figure 6.14. An upstream siren (not included in the figure) harmonically excites the air mass flow provided by a pre-heater.

The air crosses a circular plenum section of length 1.2 m and diameter 0.12 m and enter the PERM injection which produces a reactive mixture of vaporized kerosene and air. The mixture then discharges into the combustion chamber, where it is burnt. The combustion chamber has a rectangular cross section with edge length of 0.15 m and a total length 0.89 m. The combustion chamber is cooled from the outside using impingement air and is followed by an exhaust gas system.

The fuel line introduces a liquid kerosene film onto the atomizer lip and a pilot (centred atomizer). Under atmospheric conditions the atomiser could only be operated using the pilot fuel line.

For further detail on the experimental test-rig design please refer to [164].

In the adopted measurement technique, the flame is considered as black-box and conservation equations of mass, momentum and energy are formulated over the flame volume. When linearised, the conservation equations result in the famous Rankine-Hugonoit relations, which can be reformulated in a transfer matrix form.

To separate the transfer matrix of burner and flame, first the transfer matrix of the burner is measured without flame (BTM). Next, the transfer matrix of burner with flame (BFTM) is measured. Assuming that the burner transfer matrix remains unchanged in the presence of the flame, the desired flame transfer matrix (FTM) can be calculated as $FTM = BFTMxBTM^{-1}$ [124].

The BTM and BFTM transfer matrices are measured using the two-source technique [125]. For the four unknown coefficients of a transfer matrix, four linear independent equations need to be produced. This is done, by exciting the test rig once from upstream and once from downstream direction. Thereafter, the individual transfer matrices are constructed.

The frequency range considered is between 50-800 Hz with an increment

of 10 Hz. In order to create both unstable and stable condition, the outlet
boundary condition was changed case by case. The former useful to
assess acoustic code and perform validation of the unstable combustion
cooperation, is basically realised by mounting a fully acoustic reflecting
outlet at the exhaust boundary. However, under unstable conditions a
FTF cannot be measured. Therefore, at the same operating point the
combustion chamber needs to be stabilized. This is done, by introducing
a perforated screen at the combustion chamber outlet [163].
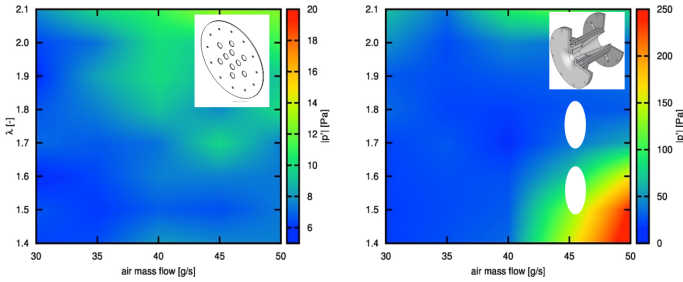
*Figure 6.15: Stability maps with perforated plate (left) and nozzle (right)
boundary condition [164].*

The measurement condition of the FTF presents a most likely unstable
condition at mair = 45 g/s and air-fuel ratio $\lambda = 1.6$ when the nozzle
boundary is used. When the perforated screen is used, instead, a stable
condition is realised and the FTF can be measured as shown in Figure
6.15.

Therefore, in this condition the FTF can be measured while, moving
to the nozzle boundary condition, the capabilities of numerical codes to
predict the stability behaviour could be assessed.

For further detail on the used experimental methodology and obtained
results please refer to [164].

6.4 Preliminary Investigations

6.4.1 Domain Selection

In order to take confidence with the test case and to find possible strategies to reduce the computational costs of the simulation, some preliminary investigations have been carried out. In particular, a perfectly premixed kerosene flame, with the same air-fuel ratio $\lambda = 1.6$ is simulated at first. Two numerical domains are tested in order to understand the impact of a reduced domain on the solution:

- 1/4th sector of the whole domain (compatible with both swirler minimum periodicity of 1/16th and of the squared combustion chamber)

- 1/16th of the domain so that only one of the 16 swirler inlet channel is simulated. A far as the combustion chamber is concerned, an axisymmetric tubular combustor is considered with equivalent effective area.

Such investigations are carried out for perfectly premixed gaseous flame in order to save computational time as, working with liquid fuel, the simulation become definitely more onerous.

In Figure 6.16 the numerical domain and meshes uses for the preliminary analysis to select the domain are shown. Tetrahedral-to-Polyhedral mesh conversion utility is exploited to generate the mesh. The resulting number of elements is 1.45E6 for the 90° domain and 5.2E5 for the 22.5° domain. As far as the meshing strategy is concerned, localised refinements are realised in the swirler section and in the first part of the flame tube where the main reaction rate and the flame location is expected. A further coarsening is then realised towards the outlet section.

In the 90° domain it is possible to see that the feeding duct that constitutes the plenum is shorten than the experimental apparatus, in order to reduce mesh sizes and the associated computational costs. The air is then introduced from the dedicated inlet section in the experimental conditions of 573 K and ambient pressure.
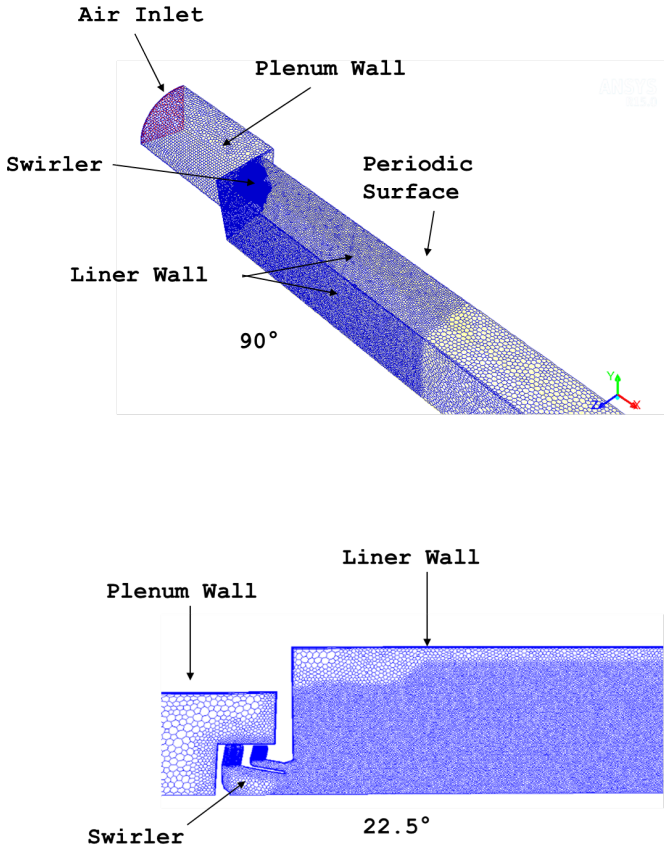
Figure 6.16: Numerical meshes used for the two domain with different periodicity.

At the lateral surfaces periodic boundary conditions are assigned while both plenum and liner walls are considered adiabatic walls.

At the outlet section a Non-Reflecting Boundary condition is assigned.

URANS simulation are then performed with Ansys Fluent 15.0.7.

$k - \epsilon$ standard with Scalable Wall Function is used as turbulence model.

The Partially-premixed combustion with Flamelet Generated Manifolds strategy to generate the laminar flamelet database is employed, as described in the dedicated section 3.2.2.3. For the laminar flamelet database, non-adiabatic premixed flamelet are solved, exploiting the JetAk99 mechanism for $C_{12}H_{23}$ hydrocarbon which is used as a surrogate for the JetA fuel. The mechanism counts for 16 species and 39 reactions.

For the progress variable closure, as the flame is a perfectly premixed one, a TFC/FR closure (see 3.2.2.3) is used. Taking the minimum between the Finite Rate source term and the Turbulent Flame Speed Closure with the Zimont formulation is used, the model should be able to correctly predict the flame front location as well as finite-rate chemistry effects. In particular the TFC should act in those region of the domain where the flame front should be located.
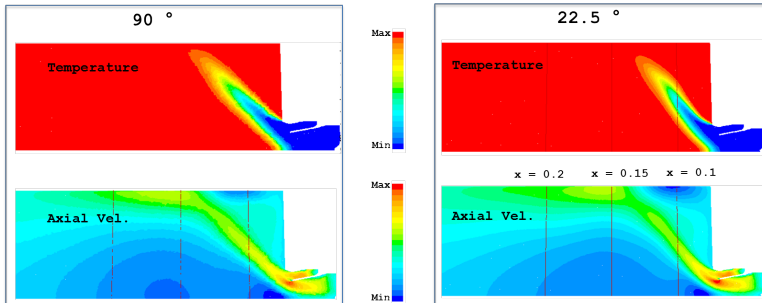
Figure 6.17: *Contours of temperature and axial velocity for simulated computational domains with different periodicity.*

In Figure 6.17 the contours of temperature and axial velocity are reported for the two cases. As it is possible to see from velocity contours, the typical flow field with the high velocity jet region that impinges on the wall and the main recirculation bubble, is found for both the cases. Looking at the predicted flame shape, similar configuration are predicted. A slightly more closed cone with a longer flame seems to appear for the 90° domain. However, looking at the profiles plotted against the scaled radius in Figure 6.18, more quantitative information can be obtained. At all
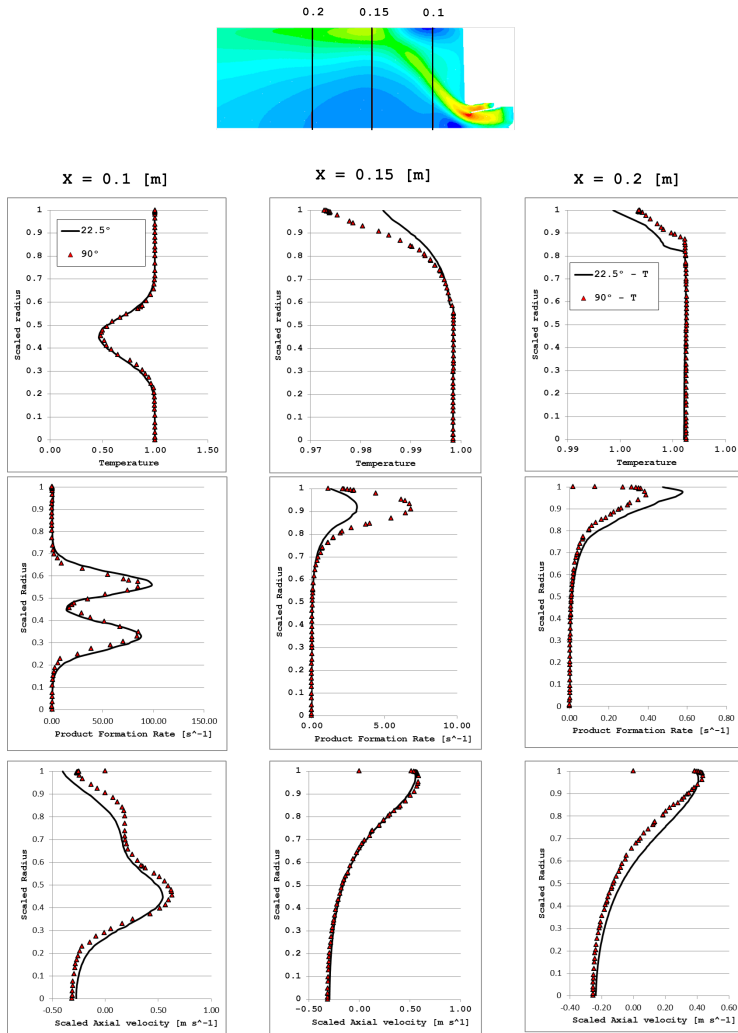
Figure 6.18: *Comparison between Temperature, Product Formation Rate and Axial Velocity profiles at three axial location, obtained for the 90° and the 22.5° domain.*

the sampled sections, similar behaviour is predicted for both the domains. Ath x=0.1 m the jet region is still visible with lower temperature levels and higher velocities. From PFR profiles two main region of reaction are found, with higher values, at the jet sides where inner and outer shear layers are generated, due to high velocity gradients. Moving downstream a complete combustion is predicted till the region closer to the wall where there is still a reaction is progress and lower temperature levels. It is in this region that the main differenced can be observed between the domains: the $90°$ shows higher formation rate at x=0.15 m and consequently lower temperature related to a slower attainment of the equilibrium. In terms of velocity, the two cases are practically equal.

From this preliminary instigation aimed at the definition of the computational domain that could lead to the lowest computational cost without compromise the physical solution, only slight differences emerged between the domains. Even if this might have an effect on the flame response to the acoustic perturbation the differences are considered negligible and, at least for the first phase of assessment of the numerical methodology and sensitivity analyses to the main parameters, the $22.5°$ domain is chosen to carry out the following investigations.

Moreover, lower computational costs are associated with such a domain that allow performing a large number of tests than the 1/4th sector. It should be also considered that the computational effort and time in case of liquid fuel and Lagrangian particle tracking is the bottleneck of such simulations and it is, basically, related to the number of droplet to track. In case of the 1/4th domain periodicity this number will be approximatively 4 times than the 1/16th domain and the impact on the simulation time would be definitely important.

6.4.2 Perfectly Premixed $C_{12}H_{23}$ flame FTF

Before studying a liquid fuel injection case, the FTF for the perfectly premixed case has been computed.

The inlet air mass flow is excited with the RASW signal, superimposed at the mean value. The cut-off frequency, defined by the period of the

square wave, has been chosen at 1000 Hz. The maximum wave amplitude is limited to the 20 % of the mean velocity.

The Non-Reflecting Inlet boundary is not used because, due to a short plenum duct, even if a resonance should be present, it will not affect the range of frequency of interest.

A Time step of 1E-05 s and a sampling time of 0.2 s are used in the computation.

The velocity fluctuation is recorded at sampling planes downstream the inlet and at the inlet itself as shown in Figure 6.19.
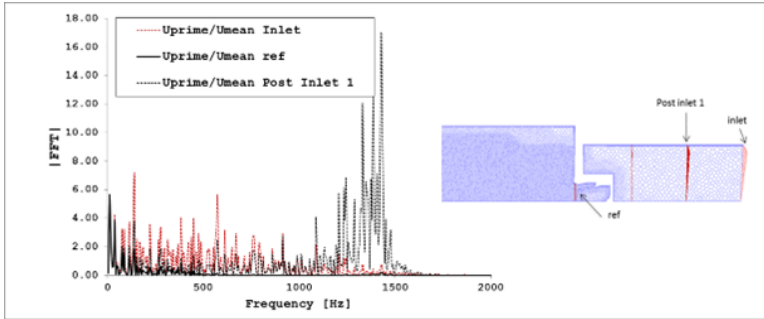
Figure 6.19: FFT of the velocity fluctuations at Inlet, Post Inlet 1 and ref planes

At the first plane downstream the inlet (Post Inlet 1), a group of frequencies around of 1300 Hz is magnified. Acoustic energy seems to be moved from low frequencies to higher ones. It can be a resonance effect due to the partial reflection at the swirler inlet. In any case, the frequency range where this phenomenon appears is pout of the range of measurements (0-800 [Hz]).

From the inlet signal FFT, it is possible to see that the selected signal allowed the direct control of the frequency range of the excitation and signal intensity without deteriorating its quality.

As far as the injector is concerned, it acts as a low-pass filter. After around 600 Hz the signal intensity is drastically reduced. In the same way, from the right plot in Figure 6.20, it is clear that also the flame acts

a low-pass filter. The flame response, in fact, decreases at around 400 Hz.
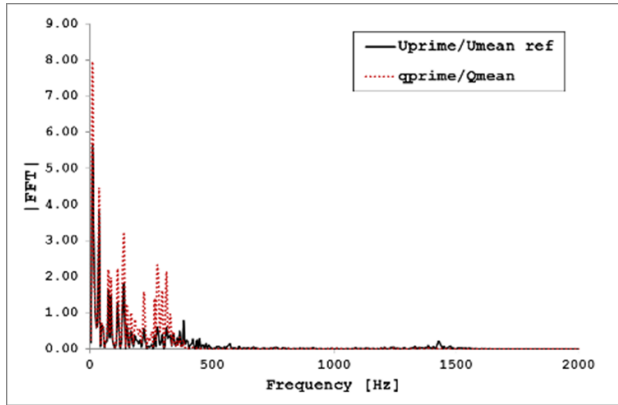
Figure 6.20: FFT of the velocity fluctuations at ref plane and fluctuations of heat release on the domain.

In Figure 6.21 the computed FTF for the premixed flame is plotted against the measurement, performed for a liquid flame. Obviously, the results are not directly comparable but it is interesting to see the similarity that might emerge as well as the differences.

The FTF module has the typical shape of a premixed flame: the low-pass filter behaviour of the flame, the response to acoustic excitation decreases with the frequency. The FTFs tend to values close to 1 when the frequency tends to 0 which, in case of premixed flame and neglecting equivalence ratio fluctuations is a theoretical limit as shown by Polifke [87] . For low frequencies. i.e. below 250 Hz, the two FTFs shows very different behaviours: the FTF for the premixed flame has a monotonic growing trend with the frequency while the experimental one start for valued exceeding unity at frequencies below 50 Hz and has a decreasing trend till a minimum is reached at around 150 Hz. A growing trend is then measured till the maximum at around 300 Hz. The maximum value of the module is similar for the two cases and it is obtained for the same frequency interval.
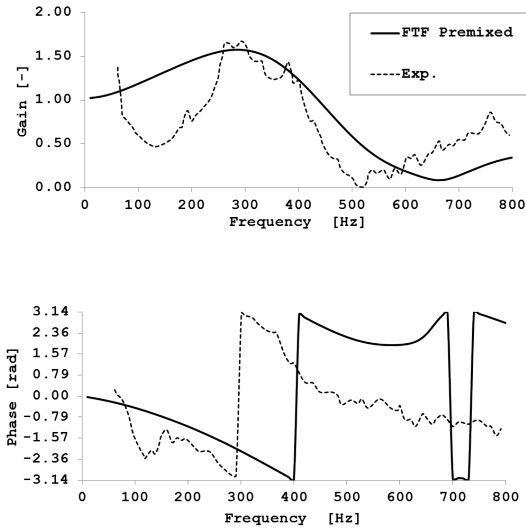
Figure 6.21: Numerically computed FTF for a perfectly premixed PERM flame against experimental FTF for the liquid fuel case.

As far as the frequency is concerned, the trend is similar in the first part of the range of interest while, for higher frequencies the numerical FTF for the premixed flame does not exhibit the same decreasing trend.

The numerical methodology for the computation of the Flame Transfer function has shown its potential. It has now to be adapted and tested when liquid fuel is injected.

The dynamic behaviour of droplet vaporization needs to be investigated. A series of modelling sensitivities analyses are carried out in order to upgrade the existing methodology with the aim of build a reliable and versatile modelling tool and understand the complex physics which lies behind liquid fuel flame dynamics.

6.5   Liquid Fuel Flame Investigations

6.5.1   Numerical Settings

Spray turbulent combustion is a very complex field since many physical phenomena could interact with each other determining the local and global flame structures. An essential characteristic of spray combustion is that the fuel is injected into the combustion chamber in liquid form and evaporation and diffusion of fuel vapour into the surrounding gas-phase precede chemical reactions between fuel and oxidizer. As a result, spray combustion shows features of both non-premixed and premixed combustion [3].

Moreover, as shown before in section 6.1 unlike what happens at high pressure operating conditions, at low pressures droplets do not completely evaporate close to the injection system and they are expected to cross the flame front. Diffusion and premixed combustion regimes are therefore expected.

As far as the numerical settings used in case of liquid fuel are concerned, the same numericals is maintained with respect of the premixed case except for the progress variable source term closure. In particular, instead of the TFC/FR closure the source term is modelled only with the FR one that is considered to be a more proper closure for the studied physics.

The Lagrangian discrete phase model in Ansys Fluent [139] is used to solve for the liquid phase. It follows the Euler-Lagrange approach. The fluid phase is treated as a continuum by solving the Navier-Stokes equations, while the dispersed phase is solved by tracking a large number of droplets through the calculated flow field. The dispersed phase can exchange momentum, mass, and energy with the fluid phase.

The dispersion of particles due to turbulence in the fluid phase is included using the Random Walk model.

For further detail on the solved equations please refer to [139].

As described in the dedicated section 6.3, the fuel in the experimental tests at ambient pressure is injected at the pilot injection only. However, at low pressure the pilot fuel does not evaporates suddenly and the droplet
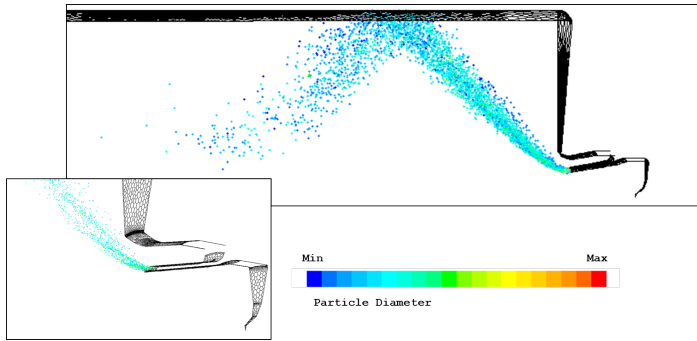
Figure 6.22: Droplet injection at the lip tip.

impinges on the lip bottom surface, creating a liquid film of fuel, as shown
in Figure 6.6. The physics that describes film evolution and its breakup at
the end of the surface (primary breakup) by the action of the shears that
are generated between the liquid film and the air, is very complex and
still object of research. Therefore, such phenomena are still a challenging
task to be simulated and advanced model are still under development. For
information on the topic and on modelling strategies of the film evolution
and breakup, the interested reader can refer to [3]. Alternatively, in the
condition of the experiments a common practice is to inject directly from
the lip where the primary breakup occurs. Sensitivity on the injection
point and to injection strategies have been the subject of past work in
the research group. In his PhD thesis [3] Giusti tested three injection
strategies, reported in Figure 6.23:

- with droplets are directly injected in the primary flow, in front
  of the liquid film layer, the classical approach used in industrial
  computations (P)

- parcels are injected in front of the atomizing edge (C)

- a split injection where the parcels are directly introduced in both
  primary and secondary flows with a given mass flow rate split (S).

Injection in the primary flow (P)   Centered injection (C)   Split injection (S)
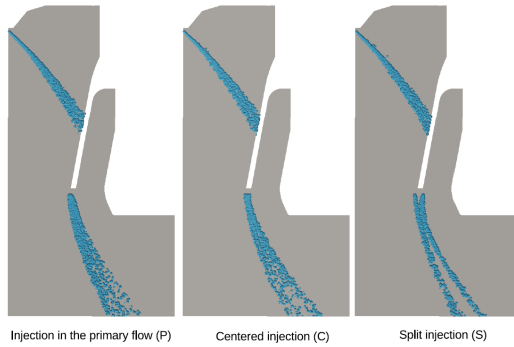
Figure 6.23: Application of different injection strategies to the PERM
injection system [3].

Therefore, following previous experiences and used internal practices,
in the present work the particles are injected at the lip tip center (see
Figure 6.22) onto a portion of this surface.

Because of the random nature of the atomization process, the popu-
lation of droplets generated by the typical injectors used in gas turbine
applications are characterized by a wide range drop sizes. The charac-
teristics of the spray have a strong impact on the combustor behaviour
since they directly influence the evaporation process and thus the fuel
distribution inside the combustion chamber [3].

In numerical simulations injected droplet are described by a statistical
distribution of droplet diameters. A widely used formulation in spray
applications is the Rosin-Rammler distribution. Such a formulation can
be defined as a function of the droplet diameter (X) such that 63.2 %
of the total liquid volume is contained in drops of smaller diameter and
q, a measure of dispersion of drop sizes. Another important parameter,
considered the most appropriate in combustion applications [165], since
it is the most relevant to the rates of evaporation, is the so called a D_{32},
usually called Sauter mean diameter (SMD).

The effect of both q and SMD on Rosin-Rammler distribution can be
appreciated looking at Figure 6.24.
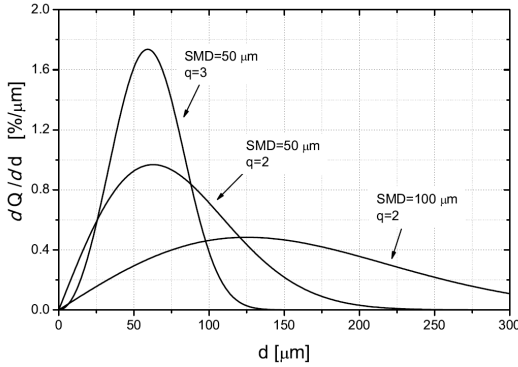
Figure 6.24: Example of Rosin-Rammler distributions: effect of q and SMD[3].

The injected particles follow a Rosin-Rambler distribution for which the following values are given for the Sauter Mean Diameter (SMD), spread factor (q) and Mean Diameter (X):

- SMD = 35.7 [mm],

- q= 2,

- X= 63.27 [mm].

The particles are injected with a constant velocity of 5 m/s.

As pointed out [3], the droplet diameter downstream of the atomizing edge is determined by both primary and secondary breakup. Secondary atomization becomes more efficient in the case of poor primary breakup allowing the reduction of droplet diameter downstream of the atomizing edge.

To model the secondary breakup the Taylor Analogy Breakup (TAB) model [139]. In this model the droplet distortion, caused by the interaction with the gas phase, is described as a one-dimensional, forced, damped, harmonic oscillation similar to the one of a spring-mass system, assuming that the droplet viscosity acts as a damping force and the surface tension as a restoring force.
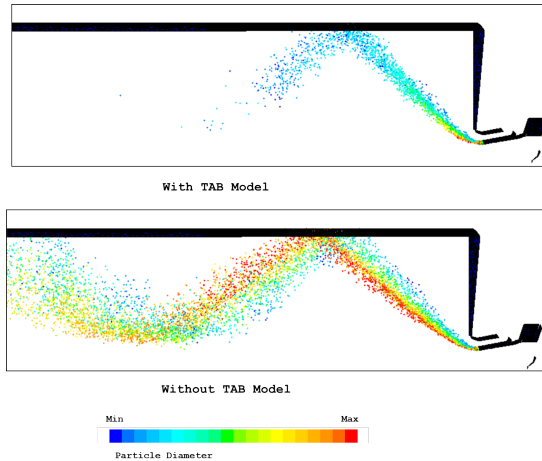
Figure 6.25: Particles inside the domain: effect of the TAB model.

Despite at low pressure the influence of the secondary breakup model should be negligible, in Figure 6.25 it is possible to appreciate the effect of the TAB model on the droplet histories. When the TAB model is disabled the particles reach the outlet section still with an non-physically high diameter.

6.5.2   Mesh Sensitivity

A mesh sensitivity analysis has been carried out at first in order to understand the effect of a finer mesh on spray behaviour and on the resulting temperature and flow-field distributions.

In Figure 6.26 the two meshes used in the simulations are depicted. The coarse mesh (M1) counts about 5.2 E5 elements while the fine one (M2) about 6.2 E5. In both the cases, polyhedral elements are used far from the walls where prismatic layer is instead realised. In M1 a 8-element layer is realised while only 2 elements are introduced in M2, considering the prismatic layer impact limited for this case studied and allowing a considerable saving in the resulting global number of mesh elements.
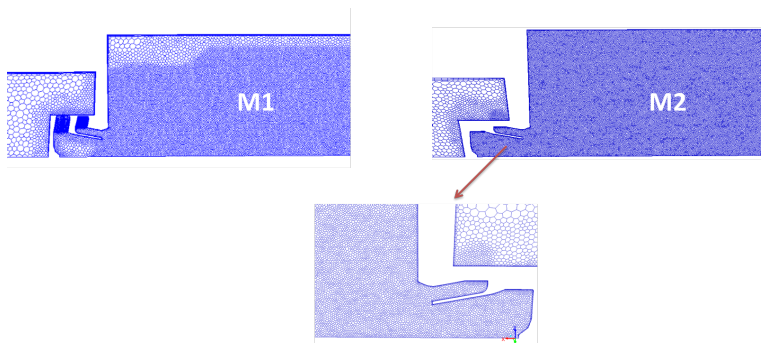
Figure 6.26: Pictures of the two meshes used for the mesh sensitivity analysis.

From the picture it is possible to appreciate the refinement strategy. A refinement is realised in the injector region with particular attention to the injection location. The first part of the combustor featured a global refinement as in this region the main evolution of the liquid fuel droplet is present. Moreover, a localised refinement has been realised in the near wall location. The liquid film, in fact, does not evaporates suddenly, as at higher pressures, and it arrives at the wall impinging on it. Therefore, the liquid phase evolution is expected to be more carefully predicted in this zone.

M2 has been also realised with attention on the element growth rate that has been reduced considerably where it is expected the presence of liquid fuel.

A progressive coarsening is then realised towards the inlet and outlet section.

In Figure 6.27 the results of the two simulation with M1 and M2 are shown. A coarser mesh leads to a wider spay jet. A more widespread distribution is obtained on M1 while the injected particles follow a more confined trajectory on M2. The particles diameter seems not to undergo a marked impact so that the secondary breakup model is supposed to act in a similar way and not being influenced by the mesh size.
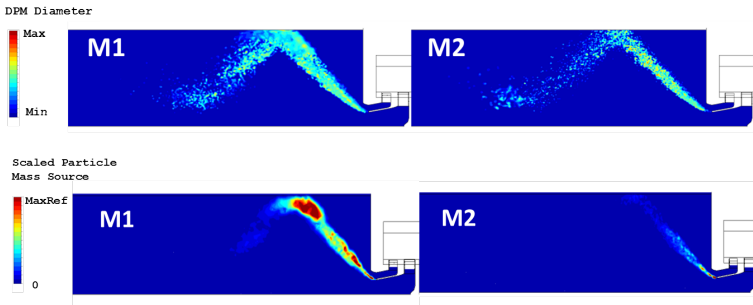
Figure 6.27: Contours of DPM diameters and prticle mass source: effect of the mesh refinement.

In both the cases the injected particles from the lip tip are suddenly trapped by the high velocity jet. An impingement on the liner wall is observed and the particles are then reflected. The greatest part of the evaporation is observed close to the wall and after the reflection a lower number of particles is seen.

As far as the particle mass source is concerned, the increased element dimension induce a smoother distribution and over a larger region. Refined elements make the evaporation more concentrated in the initial region of the spay. A large region with elevated mass source is predicted on M1 along the wall where the mesh element undergo a coarsening (see 6.26). The effect is definitely limited with a refinement in this region of M2.

The resulting evaporated fuel Mass Fraction distribution can be seen in Figure 6.28. A similar shape is obtained for the two meshes. In M1 a fraction of evaporated fuel with higher associated mass fraction is observed along the outer jet shear layer and appears before than in M2 case.

From the PFR maps in the same figure, the effect of the mentioned effect is seen in a branch where a reaction is already present while in M2 the reaction rate is still low. In any case, the highest heat release is predicted in the region before the liner wall and at the wall itself. M2 predicts two spots where the maximum heat release are presents while M1 only a single maximum at the wall.
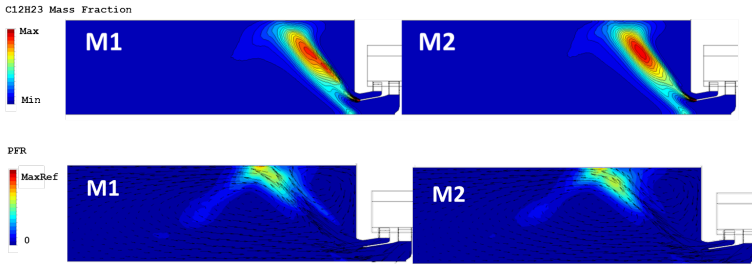
Figure 6.28: Contours of C12H23 Mass fraction and Product Formation
Rate: effect of the mesh refinement.

Possibly, a heat release peak closer to the reference section used to
sample the velocity could lead to a smaller time lag in the FTF (smaller
phase).
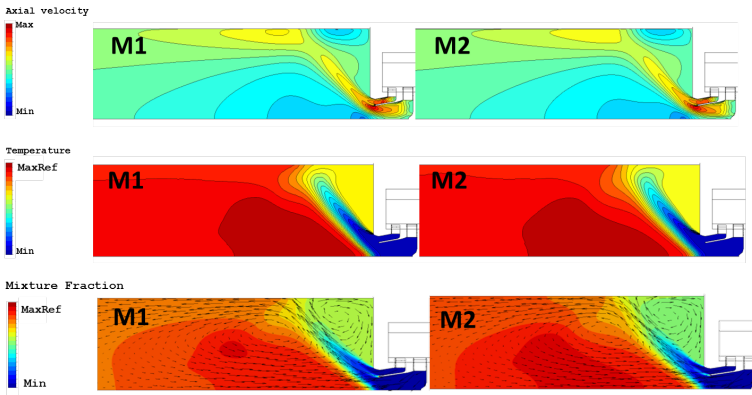
Figure 6.29: Contours of Axial Velocity, Temperature and Mixture
Fraction obtained with the two meshes.

It is worth to observe the effect of the mesh refinement on the temper-
ature and velocity fields. Interestingly, from Figure 6.29 it emerges that
the discussed differences in the DPM evolution does not impact the flow
evolutions (velocity axial). The mixture fraction distribution is similar,

with a leaner dome recirculation and a richer main recirculation bubble. A slightly leaner mixture is predicted for M1 in this zone. However, the corresponding variation on temperature are marginal.

The impact of a mesh refinement is therefore limited to the discussed effects and, despite it may have an impact on the resulting FTF, a similar response is expected for the two cases.
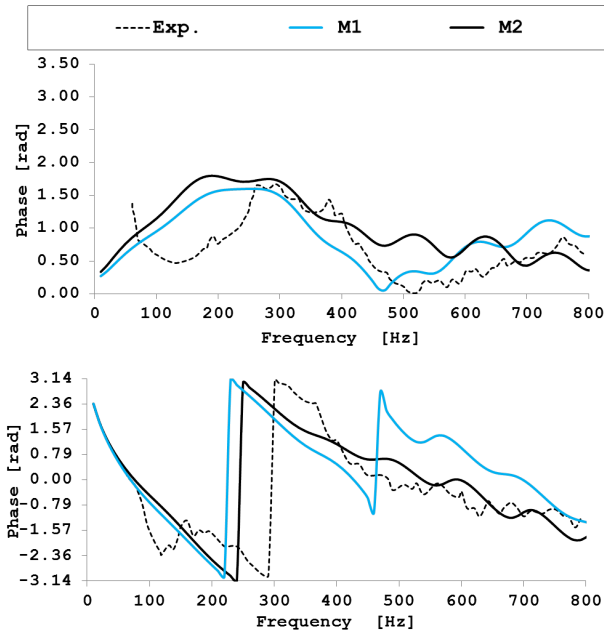
Figure 6.30: Computed FTFs with the two meshes.

The FTF is then computed for the two cases and the results in terms of amplitude and phase are shown in Figure 6.30. Looking at the Amplitudes a similar trend is predicted. The phase approaches 0 when the frequency go to 0. Then a region with maximum values is predicted at around 180-300 Hz, before a decreasing trend starts. On the M1 mesh a minimum Gain is predicted at about 480 HZ then it starts to grow again. A less marked and monotonic decrease is obtained with M2 in this second part

of the spectrum.

Comparing the results with the experimental FTF, at low frequency (50-250 Hz) a different behaviour emerges. The measured FTF, in fact, starts at about 1.5 at 50 Hz (minimum measured frequency) and than decreases to 0.5 at about 150 Hz. The FTF successively grows since maximum values are found for the range 280-400 Hz, with similar values than the numerical ones. The maximum appears shifted to higher frequencies. A minimum is reached at 520 Hz and then a slightly growing gain is measured.

M1 seems to catch better such a minimum and the amplitude in the higher frequency range. However, looking at the phase plot, representative of the time delay between the acoustic fluctuations at the injector exit and the following heat release response, improved results are obtained with the finer mesh M2. Higher time lag are associated with M1, possibly due to the heat release peak predicted slightly downstream in this case, as discussed before. A time lag close to the experimental one is instead found for the M2. To batter catch the result see Figure 6.31 where the absolute phases are plotted together.
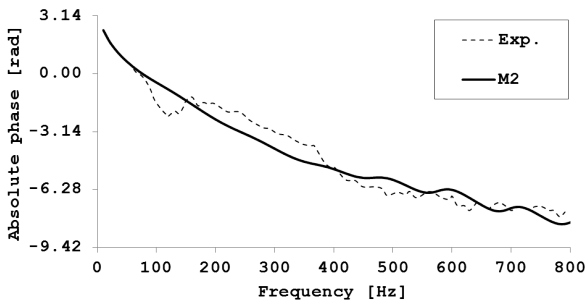
Figure 6.31: Absolute phase obtained with M2.

In the first part of the frequency spectrum, where also the measured gain is not completely followed, a higher time lag seems to characterize the experiments then, from 180 Hz the two phases are parallel, meaning that the measured time lag is found also numerically.

It seems that at low frequency a specific dynamics effect is not seen by the model and the FTF is therefore not representative in this range.

From the mesh sensitivity analysis, it is possible to conclude that the amplitude shows similar trends for both the meshes even if M1 appear to follow the experiments in a better way. The phase is, instead, better represented when the finer mesh is used. Considering this aspect of of prime importance the fine mesh is used to continue the investigation and the planned sensitivity analyses. It does not worth to further refine the mesh as a compromise should, in general, obtained also considering computational costs and the purpose of the investigations that, in this case, is to assess the methodology to numerically compute the FTF for liquid fuel flames understand the effects of the main simulation and modelling parameters. A good compromise is obtained with M2 mesh.

6.5.3 Liquid Phase Properties Sensitivity

A sensitivity analysis is carried out to the liquid phase properties. Variable properties with temperature are implemented in Fluent for:

- Density,

- Viscosity,

- Specific Heat,

- Surface Tension.

The implemented function comes from Jet-A properties used by GE-AVIO as a practice for numerical modelling of the fuel. In particular, the expressions for the polynomial fit is retrieved and the coefficients given as a input in Fluent.

The simulation is then repeated with the same settings for all the other parameters and the same excitation signal is used to perturb the inlet air mass flow.

In Figure 6.32 the effect of liquid phase properties changing with temperature on the spray behaviour is observed. A larger spray cone is
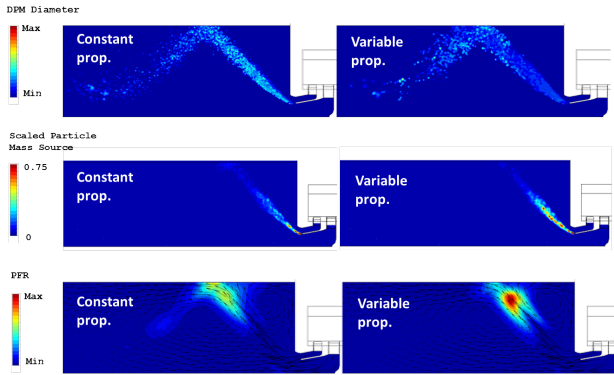
Figure 6.32: *Contours of Particle Diameters, Particle Mass Source and PFR: effect of liquid fuel properties.*
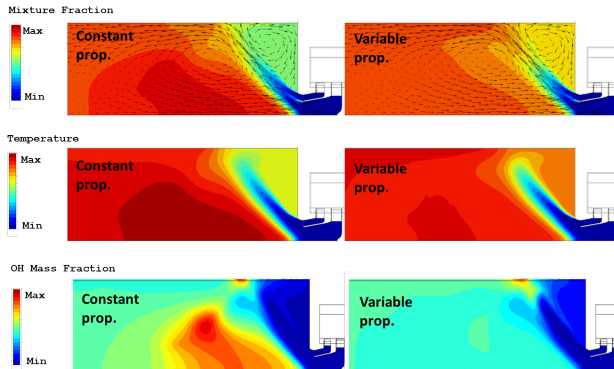
Figure 6.33: *Contours of Mixture Fraction, Temperature and OH Mass Fraction: effect of liquid fuel properties.*

predicted and the particle diameters decreases. Due to properties variation with temperature along the flame evolution, in fact, the conduction, surface tension and the viscosity tends to enhance the evaporation rate. Therefore large particles partially evaporates also in the first part of the jet, decreasing their diameter. This effect is also mirrored in an increased

particle mass source in the first part of the spray jet, close to the injection point.

Consistently, in Figure 6.33 it can be seen the effect on mixture fraction distribution: an earlier evaporation leads to a more uniform mixture fraction distribution. A leaner main recirculation zone is found while more evaporated fuel reaches the dome region thus enriching it. Consequently, also a smoother temperature distribution is observed and higher temperature at the dome.

As far as the product formation is concerned, in Figure 6.32 it can be seen that the reaction is moved upstream along the jet and the maximum is more marked and appears before the liner wall is reached. The branch of low reaction that with constant properties is seen after wall impingement is reduced with variable properties. The reaction does not continue in a significant way in this region nor in the main recirculation. This can be observed also from the higher presence of radicals in the main recirculation for the constant properties case (OH mass fraction distribution in Figure 6.33).

The effect on the computed Flame Transfer Function is important and can be appreciated in Figure 6.34.

Comparing the obtained result with the one obtained with constant liquid fuel properties, an increased amplitude is predicted. Similarly, the gain starts at 0 and has a growing trend since a maximum is reached at about 300 Hz. The peak location is this time at the same frequency than the experiments but with values more than twice. A relative minimum is obtained at 500 Hz, as in the experiments but the gain continues to decrease rather than follow the latter.

The low frequency range continues to show the larger discrepancies compared with experiments as if the mechanism governing the flame response in this range was not represented by the CFD model.

Interestingly, the predicted phase follows experiments in a good way. This is the most important result as a correct time lag governs the phase between the acoustic fluctuations and the flame response. Also in this case, the delay time of the mechanism affecting the response at low frequency
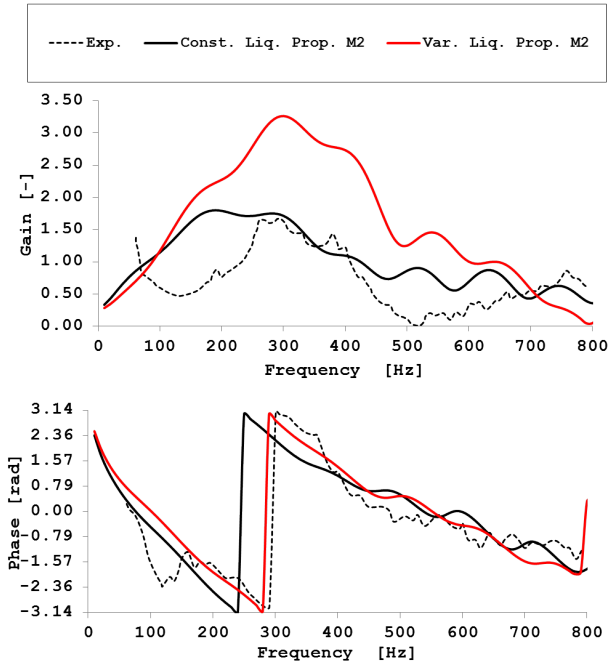
Figure 6.34: Flame Transfer Function computed with constant and variable liquid phase properties.

is not reproduced but, when the gain starts increasing again, the phase is correctly matched. A possible explanation is that, the acoustic fluctuations starts governing the flame response after 150 Hz and, in this range the model allow the reproduction of the correct flame dynamics.

6.5.4   Chemical Mechanism Sensitivity

A further investigation has been carried out to see the effect of a more accurate chemical mechanism on the result. In particular a validated change in the previously used chemical mechanism for JetAk99 is introduced as it is another GE-AVIO practice for the modelling of such a fuel reaction pattern.

The JetAk99 reaction rate for the C_12H_{23} and N_2 conversion to CH, H ans N_2 is enhanced varying the reaction order, reducing the coefficient α and β in the following expression:

$$\dot{\omega}_{C_{12}H_{23}} = KC_{C_{12}H_{23}}^{\alpha}C_{N_2}^{\beta} \tag{6.1}$$

where $C_{C_{12}H_{23}}$ and C_{N_2} are the molar concentration of jetA and nitrogen respectively and K the equilibrium constant.

The starting case is the one just analysed where variable liquid fuel properties are implemented. From the latter the only change made is in the chemical mechanism. The effect on the global solution can be seen in Figures 6.35 and 6.36.
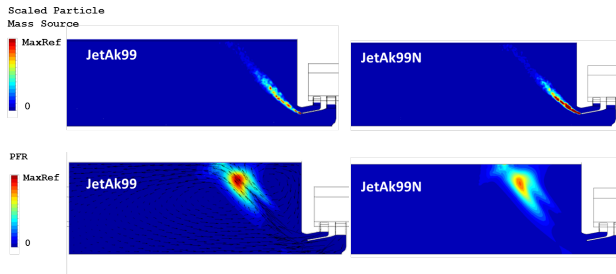
Figure 6.35: Effect of the chemical mechanism on particle mass source and PFR.
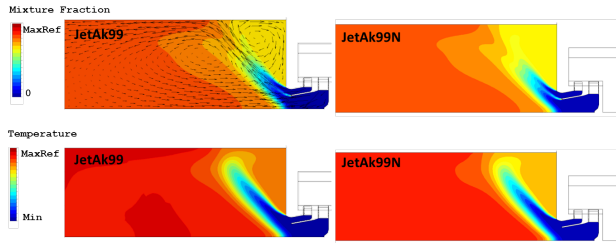
Figure 6.36: Effect of the chemical mechanism on mixture fraction and temperature.

The particle evaporation is further enhanced and higher sources are found in the region close to the injection point. The early evaporation have a double effect: it makes the evaporated fuel to mix earlier and therefore to uniform the global composition inside the domain and also let the reaction start earlier. The result on the product formation rate is that the peak seen in case of using the default jetAk99 model is smoothed and the reaction spread on a larger region.

Reduced amplitude are therefore expected in the FTF. The peak location is, instead, unchanged. No appreciable differences are instead expected for the phase.

Finally, in the temperature field in Figure 6.36, the more uniformity of the mixture is translated into a more uniform temperature distribution that no longer presents the high value in the recirculation region.

The computed Flame Transfer Function is depicted in Figure 6.37. As an effect of the reduced peak in the heat release, a lower FTF module is predicted. The peak location an the global trend remain the same already described for the FTF with JetAk99, with the peak at the same frequency.

Looking at the phase, a sightly increased time lag in the first part of the spectrum where a more steep phase curve is predicted. In the second part of the domain, instead, a lower time lag is found. However, no significant changes are evidenced, as expected.

6.5.5   Combustor Wall Temperature Sensitivity

The effect of wall boundary condition has been also investigated. Instead of adiabatic walls, the liner and the hot part of the dome are considered isothermal. As the actual wall temperature of the experimental apparatus, which is air cooled as described in section 6.3, a low temperature value has been assigned, the main aim being evaluate the impact of such a parameter on the flame response.

From Figure 6.38 the impact on the temperature field of such a boundary condition can be seen. The dome recirculation presents lower temperature levels as well as the region close to the combustor wall. The cooled flow then is brought in the recirculation region where, consequently,
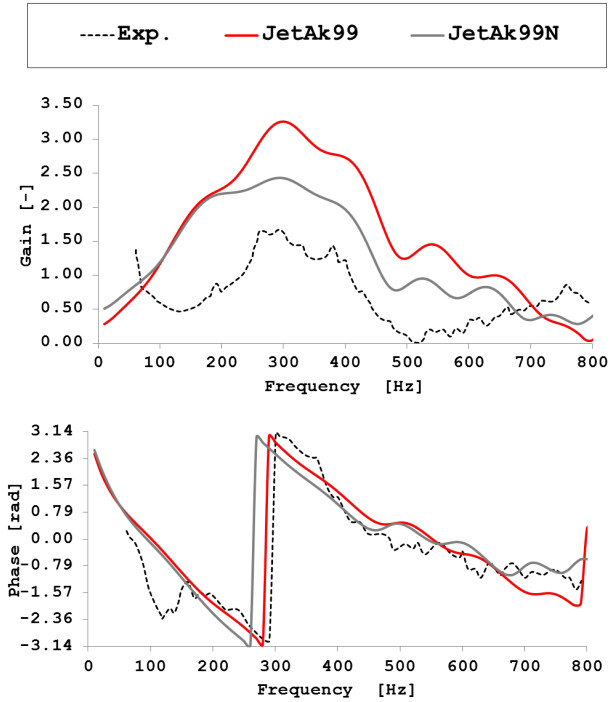
Figure 6.37: Flame Transfer Function computed using the modified chemical mechanism JetAk99N.
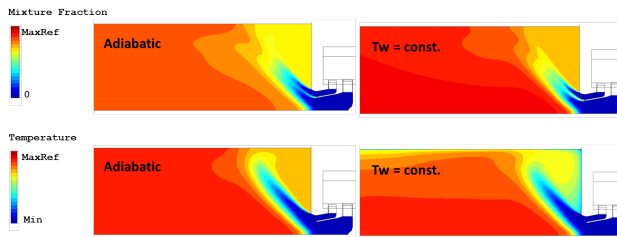
Figure 6.38: Mixture Fraction and Temperature contours in case of adiabatic and isothermal combustor walls.

lower temperature are predicted though a richer mixture is present if compared with the adiabatic case. Not only the recirculating bubble but all the fist part of the combustor appear richer than in case of adiabatic walls. This is, basically related to a different evaporation pattern: the droplet temperature close to the injection is lower as a consequence of the lower temperatures in the jet region. A lower evaporation is therefore present, as seen in Figure 6.39 and almost one order of magnitude of reduction is observed for the particle mass source. A slower evaporating pattern is present in case of isothermal combustor walls.
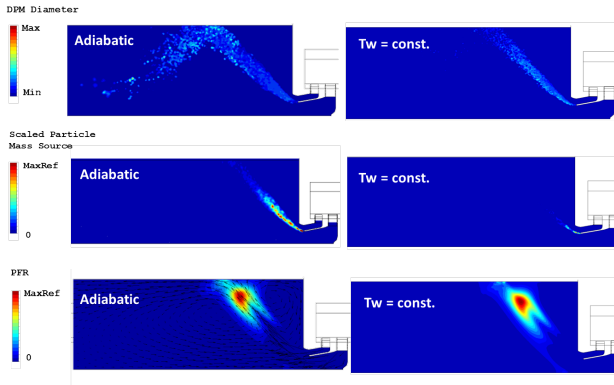
Figure 6.39: Droplet Diameter, Particle Mass Source and Product Formation Rate for the two cases with adiabatic and isothermal combustor wall.

Anyway, the effect on Product Formation Rate seems limited to a shift upstream of the high reaction intensity location but a similar shape and intensity is predicted for the two cases.

To understand the impact of an assigned constant wall temperature at the combustor wall on the flame response, the computed FTF is plotted in Figure 6.40. An interesting result emerged from this simulation: the experimental trend in the first part of the domain is correctly predicted by the model though higher amplitudes are found. An improvement in the trend seems to be introduced by the use of such a boundary condition
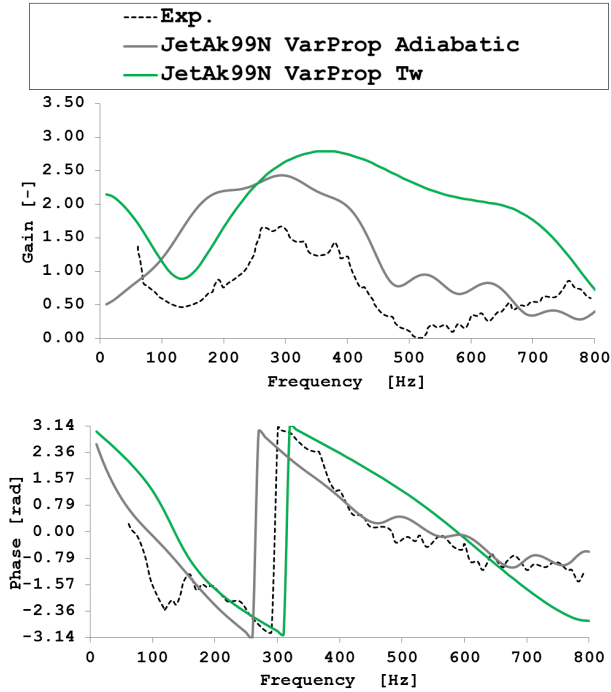
Figure 6.40: Flame Transfer Function computed with isothermal combustor walls.

if compared with adiabatic wall. However, a general overestimation of the experiments and a wrong trend is found in the FTF. Moreover, looking at the phase plot it is possible to see how the experimental response is not followed by the numerical FTF obtained with the isothermal wall. Probably the numerical value chosen for the temperature, used to stress and underline the effects of such a boundary, is too low and the consequent flame evolution is altered.

In general, form this result it can be said that the wall temperature might have an effect on the filtering behaviour of the flame and, in particular, on the filtered frequency. It also might have an important role

on the mechanisms that govern the flame response at low frequency.

6.5.6   Frequency Analysis

It is not easy to give a physical interpretation of the obtained results
in terms of FTF. Possible causes can be supposed by looking at the mean
field, product formation rated intensity, location and so on. However, in
order to provide a more physical insight of what happens at the different
frequencies within the flame, how do the regions of activation change with
the frequency of excitation a frequency analysis can be performed.

Single simulations with harmonic excitation could be performed as
well but with a much more computationally onerous procedure.

As explained in details in section 3.2.4, starting from the results of
an unsteady simulation where a broadband excitation is used to compute
the FTF, the effect of the single frequency can be analysed.

In order to underline some interesting feature observed for the investi-
gated case, the results of a post process of the simulations compared in
section 6.5.5, where the combustor boundary wall is considered adiabatic
in one case, isothermal in the other.

In Figures 6.41, 6.42 and **??** the normalised heat release fluctuation
amplitude, phase and and the product of the former times the sign of the
phase are shown for three frequencies: 50 Hz, 120 Hz and 300 Hz.

In particular, it worth to recall that the phase is relative to the filtered
component at the investigated frequency that forms the reference velocity
signal, used also in the FTF identification.

In Figure 6.41, looking at the amplitude at 50 Hz for the adiabatic case,
the main region of activation is coincident with the product formation
rate peak one (see i.g. Figure 6.39). Low activities can be appreciated
also along the path that the liquid droplet follows after the reflection at
the liner wall. The phase, that assumes reasonable values only where the
amplitude is non-zero, shows this aspect more clearly. The fluctuations is
positive and almost π in every point of activation.

At 120 Hz (Figure 6.42) the activation region is modified. The peak
location is always in the same region and in the impinging location of the
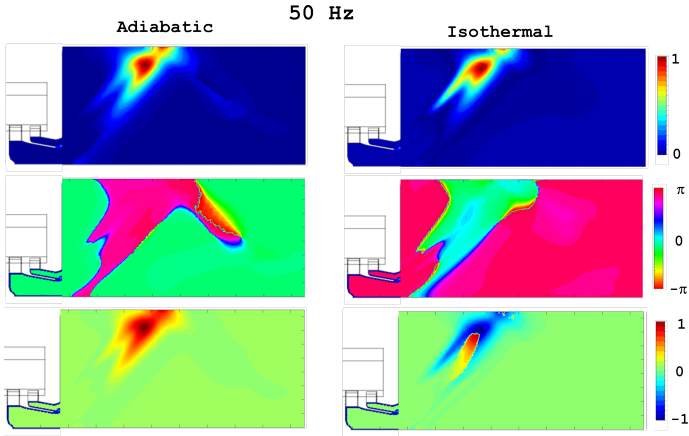
Figure 6.41: Normalised heat release amplitude (top), phase (center) and Amplitude times (sign(phase)) (bottom) for adiabatic and isothermal cases at 50 Hz.
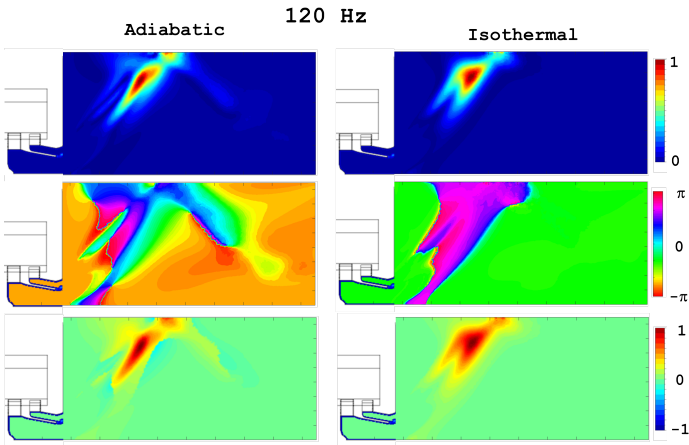
Figure 6.42: Normalised heat release amplitude (top), phase (center) and Amplitude times (sign(phase)) (bottom) for adiabatic and isothermal cases at 120 Hz.
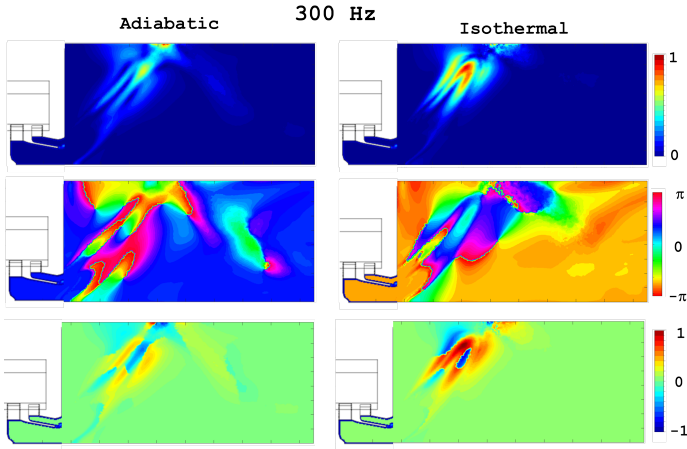
Figure 6.43: Normalised heat release amplitude (top), phase (center) and Amplitude times (sign(phase)) (bottom) for adiabatic and isothermal cases at 300 Hz.

droplet at the wall. A three-branch structure begins to delineate where the outer jet shear layer and the outer dome cooling begin to show signs of activity. Again, from phase contours it can be seen that the central region of the jet and the impingement location assume a lower phase shift, close to zero, and a distinct behaviour is recognised. Moreover, it clearly emerges that the region of activity follow the droplet pattern. From the Third picture, instead it is evident that the peak location continues to assume positive phase shift and therefore appear in red. It fluctuates in phase with acoustic velocity component at 120 Hz in the reference signal.

Moving to what happen at 300 Hz, that is where the a maximum is registered in the FTF amplitude, in Figure 6.43, the three-branch structure of the flame that starts delineating at 120 Hz is now well defined. The flame fluctuates along the inner and outer shear layers but the maximum of activity is still at the tip of the flame and in the impinging region. When the amplitude of normalised heat release fluctuations is multiplied times the sign assumed by the phase it can be seen that the central branch,

together with the region of activity at the liner wall, fluctuate out of phase with respect to the shear layers branches.

Some similarity can be found in case of an isothermal combustor wall. At 50 Hz, a similar shape then the adiabatic case is predicted for the region of activity. This time, from the last image at the bottom, it can be seen that the greatest part fluctuates out of phase with respect to the acoustic velocity at the injector mouth. The central part of the region, instead, fluctuates with positive phase shift. However, the values for the phase are close to zero.

Interestingly, at 120 Hz, where the FTF assumes a minimum, a configuration very close to the one described for the adiabatic case at 50 Hz is observed. At this frequency the latter case showed a minimum as well.

Moving to 300 Hz, where also in the isothermal case high values for the FTF amplitude are observed, in Figure 6.43 it can be recognised a structure of the region of activity with three main parts. The highest fluctuation are found i the central branch at the flame tip, while two other regions at the inner and outer sides of the jet shows important fluctuations as well. From the phase contours the independent evolution of the two jets from the primary and secondary swirlers are seen. At the dome recirculation and at the other side of the jet two other regions with independent evolution are seen. The result is a combination of region of activity with opposite phase, as shown in the bottom image.

To conclude this part, the presented frequency analysis allowed pointing out the main region of activity at different frequencies within the flame. It also evidenced the independent behaviour of the latter at some frequency.

Moreover, the flame response seems to follow exactly the liquid droplet evolution pattern, stressing the importance of the a right liquid fuel treatment in the modelling of such problems.

6.6   Quality Checks and General Observations

Before concluding this chapter, a note on the quality of the computed FTF is due.

In all the discussed cases, the quality of the estimated model, evaluated with the criteria discussed in section 3.2.3.3 is, in general, high.

The 99 % confidence interval is respected. The other quality check is the evaluation of Q parameter, that is a measure of how well the actual signal is reproduced by the model. In general not all the exported time series data are used for the identification procedure but only the 80-85 % is used for this purpose.

The remaining data are instead used to judge the model quality. In particular, the remaining part of the exported velocity time series is given as input to the computed model (computed FTF) whose output (the estimated q') is compared with the remaining part of the time series for q' coming from CFD.
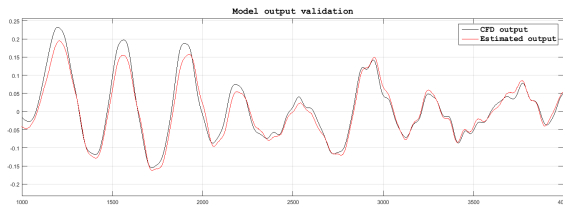
Figure 6.44: *Comparison between the estimated output and the "best fit".*

Q is a measure of the area comprised within the two curves and, for the application presented it ranged from the lowest values of around 60% to values close to 95% in other cases.

In Figure 6.44 one example of comparison between the estimated output and the "best fit" that is, the output from CFD, is shown for a $Q = 90\%$ estimation.

The good quality of the results is therefore indicative that a SISO model based on velocity at the injector outlet as input, may be adequate to reproduce the global flame response as in the CFD simulation.

The discrepancies in between the computed FTF and the experiments are, therefore, originated by a not suitable numerical modelling of the flame.

Once a numerical model is found that is able to reproduce with higher accuracy the complex spray flame evolution the SISO model presented for the flame is considered able to represent the flame dynamics and might be used to perform stability analyses of the combustor.

6.7 Final Remarks

The dynamics of a spray flame generated by a PERM injection has been numerically studied in this chapter. The CFD/SI method successfully applied at perfectly and technically premixed gas flame has been used to investigate a liquid fuelled flame.

The complexity of the problem together with the lack of a multitude of studies on the numerical studies of the dynamic of such flames make the topic of high interest and challenging at the same time.

After some preliminary studies aimed at understanding the response of the PERM injection system to acoustic perturbations, several sensitivities analyses have been performed to understand the impact of some modelling choices on the solution.

Comparisons with measured FTF in the same conditions allowed a direct evaluation of the results and modelling strategies.

The treatment of liquid fuel properties as constant or variable with temperature has been found to have a direct impact on liquid fuel the evaporation location and velocity. As a consequence of an earlier reaction, a different product formation rate intensity and location is predicted. On the FTF the main effects are seen on the values assumed by the amplitude while the phase is subjected to lower variations.

In the same way en enhanced reaction through a chemical mechanism change shows similar effects.

A more drastic effect is introduced by a change in the combustor wall thermal boundary condition, specifically changing from adiabatic to

isothermal wall.

The sensitivity analyses carried out in this work evidenced the marked and individual influence of several factors that compare in the numerical modelling of the spray flame.

Post process instruments have been applied to analyse the results. With a frequency analysis it has been possible to highlight the main regions of activity of the flame at the different frequencies. What is observed is that heat release fluctuates following the liquid particles path. Therefore, it is clear that an accurate flame response cannot be obtained if the liquid phase evolution is not modelled in an accurate way as well.

Other sensitivity analyses are possible, such as a different combustion model sensitivity. Anyway, what it should be carried out as more important investigations are those aimed at understanding liquid fuel behaviour under forced excitations. In the first place, for example, the injection modality and location should be considered to be moved at the pilot atomiser. In the experiments in fact, the fuel was injected at the pilot location only while in the simulation it has been simulated with a leap injection, mainly for stability reasons. If many studies, as discussed in the beginning of this chapter, shown that for the main behaviour it may be a reasonable modelling assumption, probably this is not valid in case of dynamic response to acoustic perturbation. The response of the particles to the latter can be significantly different in case of pilot and leap injection. Different would be, therefore, the flame response.

Tests have been performed with the simplified computational domain of $22.5°$ described in section 6.4.1, where the fuel was injected at the pilot location. Numerical instabilities led to divergences in the calculation whenever the fuel reached the axis location, following the acoustic perturbation at the burner, where pyramidal elements are present in the mesh. In order to analyse the effect of a pilot injection on the solution the use of an extended domain should be considered. As similar problems could be expected also on the $90°$ domain a simulation of the full test-rig becomes mandatory, with all the associated computational costs.

Moreover, the complex nature of a PERM generated flame, with all the

described fluid-dynamic features (vortex breakdown, PVC etc.) cannot be accurately represented by an U-RANS simulation. A reasonable future step to be planned is therefore the use of higher order simulations such as LES simulations or hybrid ones (SAS, DES) where a LES-like solution is performed. The mentioned phenomena and the high turbulence levels within the PERM would be properly solved an greater accuracy introduced in the dynamic flame response reproduction.

The present work constitutes a first important step in the study of PERM flames dynamic and sets the basis for future applications of the methodology to numerically compute Flame Transfer Function . It also has provided the numerical and mathematical instruments, such as the inversion algorithm to carry out the FTF identification and the advanced post processing tools for frequency analysis and phase-locked average investigations, which are necessary for a detailed analysis of the flame dynamics and to finally represent it in a simulation aimed at the thermo-acoustic stability prediction.

Chapter 7

Conclusions

Thermo-acoustic instabilities are one of the main issues affecting modern lean-burn combustion, which is the key technology to achieve the recent legislation limits on NOx emissions in gas turbine engines. Combustors' integrity as well as the range of operability under stable conditions can be limited by such phenomena and make their prediction fundamental, since the very earl design phases. In terms of thermo-acoustic stability analysis a physical understanding and an accurate description of the flame dynamics is essential.

The research activity presented in this dissertation is aimed at developing reliable tools to be used in the industrial design process, which are able to describe the complex interaction between the system acoustics and the turbulent flame. A methodology to compute the flame response from System Identification methods, based on correlation analysis of time series data and the inversion of the Wiener-Hopf equation, is set up.

To obtain the time data industrial Unsteady-RANS simulations (CFD) simulation where the system input are excited with a broadband, random-amplitude square-wave (RASW) excitation.

Preliminary investigations, carried out on simple test cases, allowed the definition of key aspects such as the impact of different type of excitation signal and the use of Non-Reflecting Boundary conditions for the inlet

and outlet sections.

Successively, the method was successfully validated on an experimental test case representing a perfectly-premixed swirled combustion system, where FTF measurements were available.

Once validated the methodology, the tool has been applied to investigate a practical industrial flame configuration of a GE Oil & Gas combustor. The flame presents a typical industrial technically-premixed burner surrounded by discrete pilot fuel flames. The flame is decomposed in two independent parts (pilot and premixed). The application of the methodology allowed a deep understanding of the physics governing the dynamic response to the single flame parts. In practical premixed combustion systems the flame responds to acoustic disturbances of the velocity at the flame holder and of the equivalence ratio, caused by fluctuations of the air and fuel ducts in the mixing location.

Fuel mass flow fluctuations at the premixer are included in the model together with air flow ones. Their impact on pilot and premix flame is analysed. The importance for a multiple-input single-output (MISO) model with more than one flame transfer functions, which relate the heat release rate of the flame to the various disturbances, is highlighted as mandatory to correctly predict the thermo-acoustic stability properties of real combustors. If fuel mass flow fluctuations play an important role in the flame dynamics, in fact, neglecting them can lead to significant errors. In the particular application, a great sensitivity to the relative phase between air and fuel fluctuations from the premixer has been detected, which can determine stable as well unstable operating points. In the same way, the effect of a fluctuating fuel mass flow injection and of a different pilot flame penetration has been evaluated.

From this investigations two valuable solutions emerged for the realisation of more stable designs:

- Through a change of such a phase by acting on the burner length or on the position of fuel injection within the premixer;

- Modifying the pilot injections through a jet no more axially directed

in the combustor or changing its momentum ratio (i.e. enhancing jet velocity).

A further application of the methodology, that is one of the few in literature, has been carried out to numerically study the liquid fuel flame dynamics generated by GE-AVIO developed PERM (Partially Evaporating and Rapid Mixing) injection system. Concerning this kind of flame, a series of complex physical phenomena acts together: liquid atomization, droplet evolution and their interaction with the acoustic field, which determines a fluctuation of the local equivalence ratio. A more detailed comprehension of them and of the effect of different modelling parameters used to reproduce this flame is provided thanks to the employment of the developed instrument for the dynamic flame response study. Advanced post-process of the results through frequency analysis of the main variables and phase-locked images of the solution allowed pointing out that the fluctuation of the heat release as well as its spatial intensity are strictly connected to the liquid fuel evolution path. However, despite the high quality of the results, affirmed by implemented criteria to evaluate the identification quality, the experimental FTF available for the investigated case where not adequately reproduced. This led to the main conclusion of the need for a more accurate modelling of the liquid fuel within the reactive process since the injection point.

Considering the starting point and the state of the art for liquid fuel flame dynamics characterization, the presented study constitutes a significant step forward in the numerical modelling for the thermo-acoustic analyses of GE AVIO lean burn combustors equipped with PERM injection system family.

Appendix A

Appendix 1

In this appendix, an application to validate the BTM computational approach when a Mean flow is included is presented. A simple test case where analytical solutions are present is exploited to carry out the investigations.

A.1 Investigation of Mean-flow Effects on Tubular Combustion Chamber Thermo-acoustics Using a Burner Transfer Matrix Approach

The simplified tubular combustor, studied by Dowling and Stow [72], is investigated. It is composed by three cylindrical ducts: plenum, premixer and combustion chamber. Details on the geometry and thermodynamic data are provided by Table 1 while a scheme of the combustor is in Figure A.1.

In the example it is assumed that, at the inlet, the flow is nearly choked while at the outlet an open end is considered. The thin flame zone is placed just downstream the premixer exit, at the inlet of the combustion chamber. A simple n-τ model is used, linking the fluctuating heat release to the acoustic velocity fluctuations at the premixer inlet.

The problem is solved in the COMSOL Pressure Acoustics module
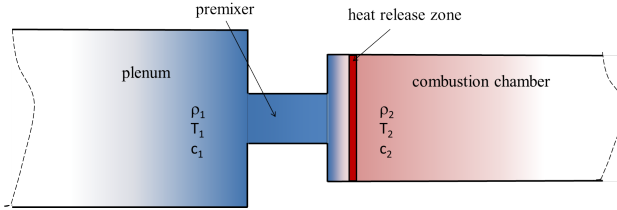
Figure A.1: Simplified scheme of the investigated combustor.

solving for the inhomogeneous Helmholtz equation in the frequency domain. No mean flow is therefore considered. In their analysis, Dowling and Stow, considered a mass flow of 0.05 kg/s. To recuperate the local effects of the mean flow, in this work, are accounted for in the BTM which replaces the premixer, excluded from the simulation.
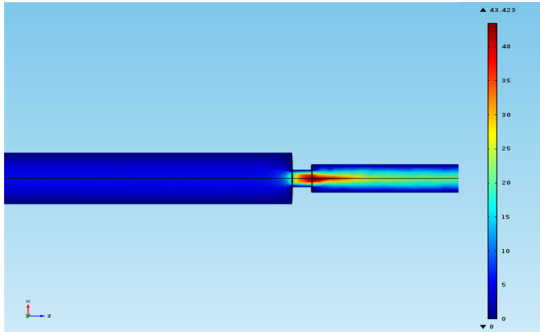
Figure A.2: Mean velocity field used for BTM computation for the 0.05kg/s case.

Three different flow rates are considered: the same mass flow adopted in [72] of 0.05 kg/s as well as 0.075 and 0.1kg/s. A laminar flow physics is introduced in the model and solved, assigning at the inlet the desired mass flow. In Figure A.2 it is possible to observe the flow-field for the 0.05 kg/s case. The system is simulated at first without heat release, that is, setting $n = 0$ in n-τ model.
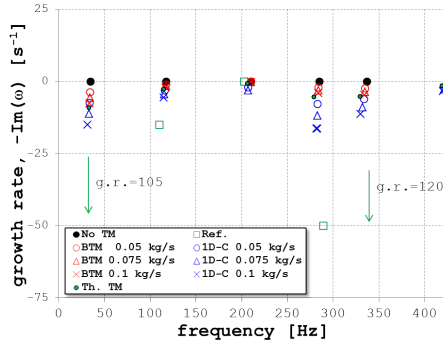
Figure A.3: Resonant modes of the combustor for no unsteady heat release (n = 0).

In Figure A.3 are reported the results obtained adopting the BTM, computed with the three tested flow rates (red). The blue symbols are, instead, the results obtained with the reference in-house 1D code (1D-C). Black dots are the case without TM while green squares the analytical solution by [72] (Ref.). The resonant modes found for the plenum are predicted at 116 Hz, 210 Hz, and 284 Hz while the first mode of the combustion chamber is at 335 Hz. The lowest mode at 34 Hz is the first of the entire combustor. The BTM approach is able to correctly predict the dissipative effect through a decreasing growth rate (g.r.) with an increasing mean flow. In all the cases a negative g.r. is found, meaning stable modes. Predicted g.r. are higher than the same computed with the 1D code. In any case, the values provided by [72] are not matched in most cases.

On the same plot in Figure A.3, are reported the results obtained with theoretically derived formulation for the BTM. The formulation has been proposed by Fanaca [123] and Alemela [124] for one-dimensional flow with low Mach number within a "compact element", variable cross section and pressure losses (Th. TM in the plot). It emerges that, acting on the model parameters in the Th. TM formulation (see [123, 124]), it is possible to find a setting able to reproduce the obtained trends for the

modes. A consideration must be done: the use of such a TM might reveal
very useful in a design phase, where the effects of the different parameters
is to be investigated. In case of analysis there might be too many degree
of freedom. In fact, without a reference point for the calibration of the
matrix coefficient, it is not straightforward finding a reliable setup. In this
last case, a computed transfer matrix approach might be more suitable,
as it does not introduce any modelling hypothesis, against the necessity
of computing a new TM for each operating condition.
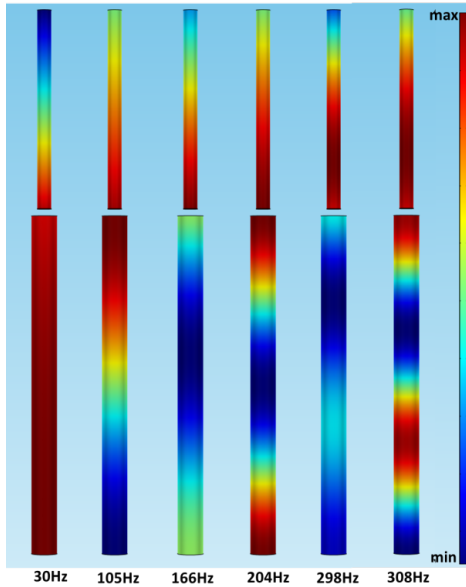
Figure A.4: Obtained modes for the BTM 0.05 kg/s case.

The unsteady heat release is then introduced, setting n=1. Simulations
are first performed maintaining a constant tau= 0.006 s, in order to
appreciate the effect of the only mean flow, in the presence of unsteady
heat release. The principal modes are well represented in COMSOL (see
Figure [?]), also for that family of modes related to the flame model, i.e.
166-Hz mode. As pointed out in [72], these modes are strictly connected

with the tau and their frequency is around $1/\tau$, $2/\tau$ etc.
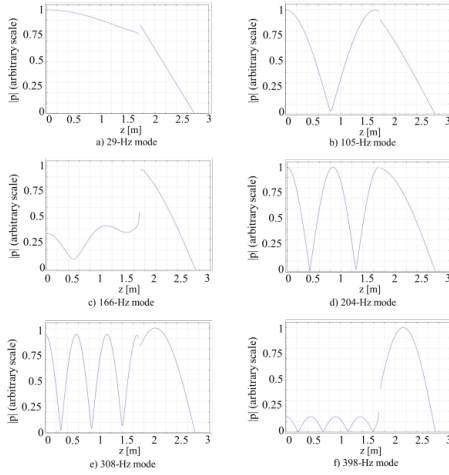
Figure A.5: Mode shapes of the computed modes for the case BTM 0.05 kg/s and $\tau = 0.006$ s.

The shape predicted by COMSOL model, for some of the computed modes, with BTM, 0.05 kg/s and $tau = 0.006$ s, are reported in Figures A.4 and A.5. It is clear that the mode b), d), e) belongs to the family of the plenum resonant modes. Mode c) and f) are the additional modes which are found in case of non-zero tau. The first mode of the combustor is the one predicted around 298 Hz

In Figure A.6 the shape of the first mode obtained for the cases Th. TM, BTM 0.05 kg/s and BTM 0.1 kg/s are compared with that computed analytically in [72]. It is possible to see how, increasing the flow rate from c) to d) the blockage effect at the premixer exit is increased. The effect of mean flow is to decouple the connected part of the plenum and combustion chamber. If compared with the analytical solution (a), case c) predicts a lower decoupling effect. This is likely to be due to the fact that, computing the BTM with the laminar solver, the effects of turbulence on the dissipation are neglected, thus underestimating the impact of the
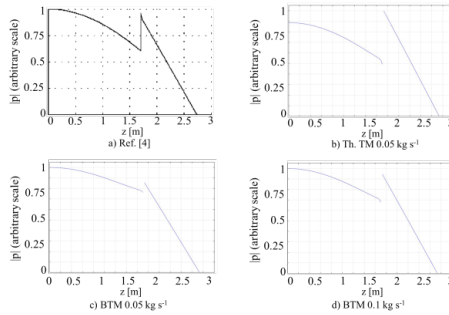
Figure A.6: First mode shape for three of the computed cases and
analytical solution [72].

mass flow. The theoretical TM b) predicts a higher blockage if compared
with the case at the same mean flow c). Calibrating the TM coefficient
the mode shape might have been better reproduced but altering (lowering)
the growth rate in the process.
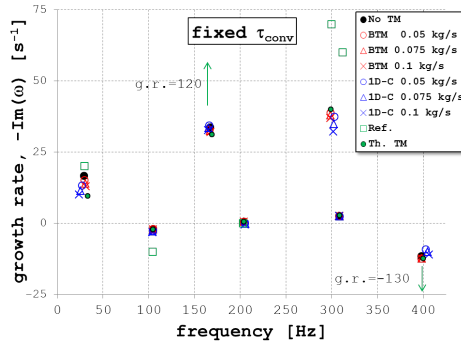
Figure A.7: Resonant modes for the combustor obtained maintaining a
fixed time delay ($\tau = 0.006$ s).

The stabilizing effect of the mean flow is properly predicted (Figure
A.7) and results are in line with the 1D code ones. As far as the first
frequency is concerned, a discrepancy emerges for the first mode between
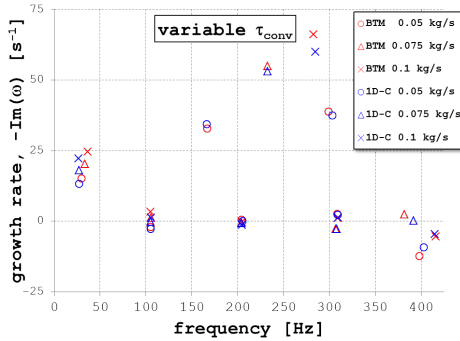
Figure A.8: Resonant modes for the combustor obtained varying the time
delay with the mean flow.

the solvers. In particular, when the flame effect is introduced, a different
trend for the value of the frequency is predicted. While the FEM solver
predicts a growing frequency with the flow rate, in the 1D code a slight
decrease is found. A possible explanation is in terms of entropy wave, not
solved in COMSOL, which, as stated, might have an impact on the lower
frequencies of the system. When no entropy is introduced in the system by
the flame (n=0 case in Figure A.3), in fact, both the simulations predict
the same trend.

In the last set of simulations the delay time, computed as a convective
time from the injection point to the flame region, is varied according to
the mean flow in the simulation. Again in Figure A.8, a good agreement
is observed with the reference simulation is achieved. The modes and
growth rates are well predicted. In contrast to the simulation at constant
τ, where the effect of an increased mean flow was a stabilization of all the
frequencies, now some of the mode is destabilized (i.e 34 Hz mode). In
other words, the effect of mean flow on the convective delay time has a
greater influence than the enhanced dissipation. BTM computed modes
are found to be more unstable than the 1D code predicted one. This is
likely due to some stabilizing effect, as the losses due to an area change,
not introduced in the FEM simulation by the BTM approach.

Bibliography

[1] Correa, Sanjay M. A review of nox formation under gas-turbine combustion conditions. *Combustion science and technology*, 87(1-6): 329–362, 1993.

[2] Lefebvre, Arthur H. *Gas turbine combustion*. CRC press, 1998.

[3] Mazzei, L. *Development of numerical tools for the analysis of advanced airblast injection systems for lean burn aero-engine combustors*. PhD thesis, University of Florence, Department of Industrial Engineering, 2014.

[4] Chu, Boa-Teh. On the energy transfer to small disturbances in fluid flow (part i). *Acta Mechanica*, 1(3):215–234, 1965.

[5] Andreini, Antonio, Facchini, Bruno, Giusti, Andrea, and Turrini, Fabio. Assessment of flame transfer function formulations for the thermoacoustic analysis of lean burn aero-engine combustors. *Energy Procedia*, 45:1422–1431, 2014.

[6] Lauer, Martin and Sattelmayer, Thomas. On the adequacy of chemiluminescence as a measure for heat release in turbulent flames with mixture gradients. *Journal of Engineering for Gas Turbines and Power*, 132(6):061502, 2010.

[7] Huang, Ying and Yang, Vigor. Dynamics and stability of lean-premixed swirl-stabilized combustion. *Progress in Energy and Combustion Science*, 35(4):293–364, 2009.

[8] Bahr, DW. Aircraft turbine engine nox emission abatement. In *Unsteady combustion*, pages 243–264. Springer, 1996.

[9] Ceccherini, G. and Malquori, D. and Petillo, G. and Falsini, M. Retrofitability of dln/dle systems. Technical report, GLOBAL SERVICES, GE OIL & GAS, 2013.

[10] Carrotte, Jon. Aerodynamics, unsteadiness and mixing. *Combustion in aero-engine*, 2012.

[11] Lyons, Valerie J. Fuevair nonuniformity-effect on nitric oxide emissions. *AIAA journal*, 20(5):660–665, 1982.

[12] Fric, Thomas F. Effects of fuel-air unmixedness on no (x) emissions. *Journal of Propulsion and Power*, 9(5):708–713, 1993.

[13] Polifke, Wolfgang. *Fundamental and practical limitations of NOx reduction in lean-premixed combustion*. ABB Corporate Research, 1995.

[14] Dunn-Rankin, Derek. *Lean combustion: technology and control*. Academic Press, 2011.

[15] Leonard, Gary and Stegmaier, James. Development of an aeroderivative gas turbine dry low emissions combustion system. *Journal of Engineering for Gas Turbines and Power*, 116(3):542–546, 1994.

[16] Ohkubo, Yoichiro. Low-nox combustion technology. *Target*, 20(35): 24, 2005.

[17] Cocca, M. A. and Marcucci, N. Performance and reliability improvements for ms5002 gas turbines. Technical Report GER-4171, GE Power Generation.

[18] Ceccherini, G., Malquori, D., Petillo, G., and Falsini, M. Retrofitability of dln/dle systems. Technical report, GE Oil & Gas, 2013.

[19] Thomas, L. L., Simons, D. W., Popovic, P., Romoser, C. E., Vandale, D. D., and Citeno, J. V. E-class dln technology advancements, dln1+. In *Proc. ASME Turbo Expo*, number GT2011-45944, 2011.

[20] Zajadatz, Martin, Pennell, Douglas, Bernero, Stefano, Paikert, Bettina, Zoli, Raffaele, and Döbbeling, Klaus. Development and implementation of the advanced environmental burner for the alstom gt13e2. *Journal of Engineering for Gas Turbines and Power*, 135 (6):061503, 2013.

[21] Ceccherini, A. *Design of Innovative Cooling Systems for Aero-Engine Combustion Chambers*. PhD thesis, University of Florence, Energy Engineering Department, 2009.

[22] Mazzei, L. *A 3D coupled approach for the thermal design of aero−engine combustor liners*. PhD thesis, University of Florence, Department of Industrial Engineering, 2015.

[23] General Electric. Taps II combustor final report - continuous lower energy, emissions and noise (CLEEN) program. Technical report, Federal Aviation Administration, June 2013.

[24] Lemcotec eu project web site. http: //www.lemcotec.eu, 2011.

[25] von der Bank, Ralf. Engineering the propulsion future. In *LEMCOTEC EU Kick−Off Meeting Presentation*, page 11. Rolls−Royce Deutschland, 2011.

[26] Zukoski, FE. *The aerothermodynamics of aircraft gas turbine engines. Air Force Aero Propulsion Laboratory*. Oates G, editor, 1978.

[27] Polifke, Wolfgang. Low−order analysis tools for aero− and termo−acoustic instabilities. *Advances in Aero-Acoustics and Thermo-Acoustics*, 2010.

[28] Barrere, M and Williams, FA. Comparison of combustion instabilities found in various types of combustion chambers. In *Symposium*

(International) on Combustion, volume 12, pages 169–181. Elsevier, 1969.

[29] Fernandes, Edgar C. and Litão, Ivo D. V. Rayleigh criterion: Theory and experiments. *Advances in Aero-Acoustics and Thermo-Acoustics*, 2010.

[30] Eckstein, Johannes. *On the mechanisms of combustion driven low-frequency oscillations in aero-engines.* PhD thesis, Universität München, 2004.

[31] Huang, Ying, Wang, Shanwu, and Yang, Vigor. Systematic analysis of lean-premixed swirl-stabilized combustion. *AIAA journal*, 44(4): 724–740, 2006.

[32] Rayleigh, J. S. W. *The Theory of Sound, Volume II*. MacMillan and Co, 1878.

[33] Lieuwen, Timothy C. *Investigation of combustion instability mechanisms in premixed gas turbines.* PhD thesis, Georgia Institute of Technology, 1999.

[34] Ducruix, Sébastien, Durox, Daniel, and Candel, Sébastien. Theoretical and experimental determinations of the transfer function of a laminar premixed flame. *Proceedings of the combustion institute*, 28 (1):765–773, 2000.

[35] Bohn, D and Deuker, E. An acoustical model to predict combustion driven oscillations. In *20th International Congress on Combustion Engines*, number G20, 1993.

[36] Boyer, L and Quinard, J. On the dynamics of anchored flames. *Combustion and flame*, 82(1):51–65, 1990.

[37] Dowling, Ann P. A kinematic model of a ducted flame. *Journal of fluid mechanics*, 394:51–72, 1999.

[38] Fleifil, M, Annaswamy, AM, Ghoneim, ZA, and Ghoniem, AF. Response of a laminar premixed flame to flow oscillations: A kinematic model and thermoacoustic instability results. *Combustion and flame*, 106(4):487–510, 1996.

[39] Schuller, Thierry, Durox, Daniel, and Candel, Sébastien. A unified model for the prediction of laminar flame transfer functions: comparisons between conical and v−flame dynamics. *Combustion and Flame*, 134(1):21–34, 2003.

[40] Cho, Ju Hyeong and Lieuwen, Tim. Laminar premixed flame response to equivalence ratio oscillations. *Combustion and Flame*, 140 (1):116–129, 2005.

[41] Shreekrishna, Hemchandra, Santosh, and Lieuwen, Tim. Premixed flame response to equivalence ratio perturbations. *Combustion Theory and Modelling*, 14(5):681–714, 2010.

[42] Huber, Andreas. *Impact of fuel supply impedance and fuel staging on gas turbine combustion stability*. PhD thesis, Universität München, 2009.

[43] Komarek, Thomas and Polifke, Wolfgang. Impact of swirl fluctuations on the flame response of a perfectly premixed swirl burner. *Journal of Engineering for Gas Turbines and Power*, 132(6):061503, 2010.

[44] Keller, Jacob J. Thermoacoustic oscillations in combustion chambers of gas turbines. *AIAA journal*, 33(12):2280–2287, 1995.

[45] Lieuwen, Tim and Zinn, Ben T. The role of equivalence ratio oscillations in driving combustion instabilities in low nox gas turbines. In *Symposium (International) on Combustion*, volume 27, pages 1809–1816. Elsevier, 1998.

[46] Sattelmayer, Thomas. Influence of the combustor aerodynamics on combustion instabilities from equivalence ratio fluctuations. *Journal*

of Engineering for Gas Turbines and Power(Transactions of the ASME), 125(1):11–19, 2003.

[47] Auer, MP, Hirsch, C, and Sattelmayer, T. Influence of the interaction of equivalence ratio and mass flow fluctuations on flame dynamics. In *ASME Turbo Expo 2005: Power for Land, Sea, and Air*, pages 249–257. American Society of Mechanical Engineers, 2005.

[48] Tong, AY and Sirignano, WA. Oscillatory vaporization of fuel droplets in an unstable combustor. *Journal of Propulsion and Power*, 5(3):257–261, 1989.

[49] Duvvur, A, Chiang, CH, and Sirignano, WA. Oscillatory fuel droplet vaporization-driving mechanism for combustion instability. *Journal of Propulsion and Power*, 12(2):358–365, 1996.

[50] Eckstein, J, Freitag, E, Hirsch, C, Sattelmayer, T, Von der Bank, R, and Schilling, T. Forced low-frequency spray characteristics of a generic airblast swirl diffusion burner. In *ASME Turbo Expo 2003, collocated with the 2003 International Joint Power Generation Conference*, pages 471–478. American Society of Mechanical Engineers, 2003.

[51] Lieuwen, Timothy C and Yang, Vigor. Combustion instabilities in gas turbine engines(operational experience, fundamental mechanisms and modeling). *Progress in astronautics and aeronautics*, 2005.

[52] Yu, KH, Wilson, KJ, and Schadow, KC. Liquid-fueled active instability suppression. In *Symposium (International) on Combustion*, volume 27, pages 2039–2046. Elsevier, 1998.

[53] De la Cruz Garcia, M, Mastorakos, E, and Dowling, AP. Investigations on the self-excited oscillations in a kerosene spray flame. *Combustion and Flame*, 156(2):374–384, 2009.

[54] Marble, FE and Candel, SM. Acoustic disturbance from gas non-uniformities convected through a nozzle. *Journal of Sound and Vibration*, 55(2):225–243, 1977.

[55] Polifke, Wolfgang, Paschereit, Christian Oliver, and Döbbeling, Klaus. Constructive and destructive interference of acoustic and entropy waves in a premixed combustor with a choked exit. *Int. J. Acoust. Vib*, 6(3):135–146, 2001.

[56] Eckstein, J, Freitag, E, Hirsch, C, and Sattelmayer, T. Experimental study on the role of entropy waves in low-frequency oscillations in a rql combustor. *Journal of engineering for gas turbines and power*, 128(2):264–270, 2006.

[57] Zukoski, EE and Smith, DA. Combustion instability sustained by unsteady vortex combustion. In *AIAA, SAE, ASME, and ASEE, Joint Propulsion Conference, 21 st, Monterey, CA*, 1985.

[58] Hegde, UG, Reuter, D, Daniel, BR, and Zinn, BT. Flame driving of longitudinal instabilities in dump type ramjet combustors. *Combustion Science and Technology*, 55(4-6):125–138, 1987.

[59] Dowling, Ann P. The calculation of thermoacoustic oscillations. *Journal of sound and vibration*, 180(4):557–581, 1995.

[60] Martin, Charles Etienne, Benoit, Laurent Jean-Louis, Sommerer, Yannick, Nicoud, Franck, and Poinsot, Thierry. Large-eddy simulation and acoustic analysis of a swirled staged turbulent combustor. *AIAA journal*, 44(4):741–750, 2006.

[61] Selle, Lartigue, Lartigue, Ghislain, Poinsot, Thierry, Koch, R, Schildmacher, K-U, Krebs, W, Prade, B, Kaufmann, P, and Veynante, Denis. Compressible large eddy simulation of turbulent combustion in complex geometry on unstructured meshes. *Combustion and Flame*, 137(4):489–505, 2004.

[62] Wolf, P, Staffelbach, G, Balakrishnan, R, Roux, A, and Poinsot, Thierry. Azimuthal instabilities in annular combustion chambers. In *Proc. of the Summer Program*, pages 259–269. Citeseer, 2010.

[63] Boudier, Guillaume, Lamarque, Nicolas, Sensiau, Claude, Staffelbach, Gabriel, Poinsot, T, and Moureau, V. Investigating the thermo-acoustic stability of a real gas turbine combustion chamber using large-eddy simulations. In *11th CEAS-ASC Workshop and 2nd Scientific Workshop of X3-NOISE 27–28 September 2007, Lisbon, Portugal*, 2007.

[64] Wolf, Pierre, Staffelbach, Gabriel, Gicquel, Laurent, and Poinsot, Thierry. Massively parallel les of azimuthal thermo-acoustic instabilities in annular gas turbines. In *Journal of Physics: Conference Series*, volume 180, page 012035. IOP Publishing, 2009.

[65] Wolf, Pierre, Balakrishnan, Ramesh, Staffelbach, Gabriel, Gicquel, Laurent YM, and Poinsot, Thierry. Using les to study reacting flows and instabilities in annular combustion chambers. *Flow, turbulence and combustion*, 88(1-2):191–206, 2012.

[66] Toffolo, Andrea, Masi, Massimo, and Lazzaretto, Andrea. Low computational cost cfd analysis of thermoacoustic oscillations. *Applied Thermal Engineering*, 30(6):544–552, 2010.

[67] Tiribuzi, Stefano. Cfd modelling of thermoacoustic oscillations inside an atmospheric test rig generated by a dln burner. In *ASME Turbo Expo 2004: Power for Land, Sea, and Air*, pages 475–485. American Society of Mechanical Engineers, 2004.

[68] Tiribuzi, Stefano. Very rough grid approach for cfd modelling of thermoacoustic oscillations inside an annular premixed combustor. In *ASME Turbo Expo 2006: Power for Land, Sea, and Air*, pages 11–21. American Society of Mechanical Engineers, 2006.

[69] Walz, Günther, Krebs, Werner, Hoffmann, Stefan, and Judith, Hans. Detailed analysis of the acoustic mode shapes of an annular combustion chamber. *Journal of engineering for gas turbines and power*, 124(1):3–9, 2002.

[70] Nicoud, Franck, Benoit, Laurent, Sensiau, Claude, and Poinsot, Thierry. Acoustic modes in combustors with complex impedances and multidimensional active flames. *AIAA journal*, 45 (2):426–441, 2007.

[71] Camporeale, SM, Fortunato, B, and Campa, G. A finite element method for three-dimensional analysis of thermo-acoustic combustion instability. *Journal of Engineering for Gas Turbines and Power*, 133(1):011506, 2011.

[72] Dowling, Ann P and Stow, Simon R. Acoustic analysis of gas turbine combustors. *Journal of propulsion and power*, 19(5):751–764, 2003.

[73] Campa, Giovanni, Camporeale, Sergio Mario, Cosatto, Ezio, and Mori, Giulio. Thermoacoustic analysis of combustion instability through a distributed flame response function. In *ASME Turbo Expo 2012: Turbine Technical Conference and Exposition*, pages 179–188. American Society of Mechanical Engineers, 2012.

[74] Campa, Giovanni and Camporeale, Sergio Mario. Prediction of the thermoacoustic combustion instabilities in practical annular combustors. *Journal of Engineering for Gas Turbines and Power*, 136(9):091504, 2014.

[75] Andreini, A, Facchini, B, Giusti, A, Turrini, F, and Vitale, I. Thermoacoustic analysis of an advanced lean injection system in a tubular combustor configuration. In *Proceedings of the COMSOL Conference 2012 Milan*, 2012.

[76] Andreini, A, Facchini, B, Giusti, A, Vitale, I, and Turrini, F. Thermoacoustic analysis of a full annular aero-engine lean combustor

with multi-perforated liners. In *Proceedings of the AIAA-CEAS Aeroacoustic Conference*, 2013.

[77] Andreini, Antonio, Facchini, Bruno, Giusti, Andrea, Vitale, Ignazio, and Turrini, Fabio. Thermoacoustic analysis of a full annular lean burn aero-engine combustor. In *ASME Turbo Expo 2013: Turbine Technical Conference and Exposition*, pages V01AT04A069–V01AT04A069. American Society of Mechanical Engineers, 2013.

[78] Nicoud and Wieczorek. About the zero mach number assumption in the calculation of thermoacoustic instabilities. *International journal of spray and combustion dynamics*, 1(1):67–111, 2009.

[79] Hubbard, S and Dowling, AP. Acoustic instabilities in premix burners. *AIAA paper*, 2272, 1998.

[80] Bellucci, Valter, Schuermans, Bruno, Nowak, Dariusz, Flohr, Peter, and Paschereit, Christian Oliver. Thermoacoustic modeling of a gas turbine combustor equipped with acoustic dampers. In *ASME Turbo Expo 2004: Power for Land, Sea, and Air*, pages 635–644. American Society of Mechanical Engineers, 2004.

[81] Hubbard, S and Dowling, AP. Acoustic resonances of an industrial gas turbine combustion system. *Journal of engineering for gas turbines and power*, 123(4):766–773, 2001.

[82] Lieuwen, Tim and Zinn, Ben T. Theoretical investigation of combustion instability mechanisms in lean premixed gas turbines. *AIAA paper*, (98-0641), 1998.

[83] Cho, Ju Hyeong and Lieuwen, Tim C. Modeling the response of premixed flames to mixture ratio perturbations. *ASME Paper GT2003-38089*, 2003.

[84] You, Danning, Huang, Ying, and Yang, Vigor. A generalized model of acoustic response of turbulent premixed flame and its application

to gas-turbine combustion instability analysis. *Combustion Science and Technology*, 177(5-6):1109–1150, 2005.

[85] Truffin, K and Poinsot, Thierry. Comparison and extension of methods for acoustic identification of burners. *Combustion and Flame*, 142(4):388–400, 2005.

[86] Hilares, Luis Roberto TayWo Chong. *Numerical Simulation of the Dynamics of Turbulent Swirling Flames*. PhD thesis, Universität München, 2012.

[87] Polifke, Wolfgang and Lawn, Chris. On the low-frequency limit of flame transfer functions. *Combustion and flame*, 151(3):437–451, 2007.

[88] Hirsch, C, Fanaca, D, Reddy, P, Polifke, W, and Sattelmayer, T. Influence of the swirler design on the flame transfer function of premixed flames. In *ASME Turbo Expo 2005: Power for Land, Sea, and Air*, pages 151–160. American Society of Mechanical Engineers, 2005.

[89] Palies, Paul, Durox, Daniel, Schuller, Thierry, and Candel, Sébastien. The combined dynamics of swirler and turbulent premixed swirling flames. *Combustion and Flame*, 157(9):1698–1717, 2010.

[90] Palies, P, Durox, D, Schuller, T, and Candel, S. Experimental study on the effect of swirler geometry and swirl number on flame describing functions. *Combustion Science and Technology*, 183(7): 704–717, 2011.

[91] Kunze, Klaas, Hirsch, Christoph, and Sattelmayer, Thomas. Transfer function measurements on a swirl stabilized premix burner in an annular combustion chamber. In *ASME Turbo Expo 2004: Power for Land, Sea, and Air*, pages 21–29. American Society of Mechanical Engineers, 2004.

[92] Polifke, Wolfgang. System identification for aero-and thermo-acoustic applications. *Advances in Aero-Acoustics and Thermo-Acoustics*, 2010.

[93] Huber and Polifke. Dynamics of practical premixed flames, part i: model structure and identification. *International journal of spray and combustion dynamics*, 1(2):199–228, 2009.

[94] Huber and Polifke. Dynamics of practical premixed flames, part ii: identification and interpretation of cfd data. *International journal of spray and combustion dynamics*, 1(2):229–249, 2009.

[95] Chong, Luis Tay Wo, Komarek, Thomas, Kaess, Roland, Föller, Stephan, and Polifke, Wolfgang. Identification of flame transfer functions from les of a premixed swirl burner. In *ASME Turbo Expo 2010: Power for Land, Sea, and Air*, pages 623–635. American Society of Mechanical Engineers, 2010.

[96] Crocco, Luigi and Cheng, Sin-I. *Theory of combustion instability in liquid propellant rocket motors*. Cambridge Univ Press, 1956.

[97] Polifke, Wolfgang, Kopitz, Jan, and Serbanovic, Ana. Impact of the fuel time lag distribution in elliptical premix nozzles on combustion stability. In *7th AIAA/CEAS Aeroacoustics Conference*, pages 2001–2104, 2001.

[98] Freitag, Ewald. *On the Measurement and Modelling of Flame Transfer Functions at Elevated Pressure*. PhD thesis, Universität München, 2009.

[99] Pankiewitz, Christian. *Hybrides Berechnungsverfahren für thermoakustische Instabilitäten von Mehrbrennersystemen*. PhD thesis, Universität München, 2004.

[100] Eckstein, Johannes and Sattelmayer, Thomas. Low-order modeling of low-frequency combustion instabilities in aeroengines. *Journal of propulsion and power*, 22(2):425–432, 2006.

[101] Gepperth, S, Koch, R, and Bauer, H-J. Analysis and comparison of primary droplet characteristics in the near field of a prefilming airblast atomizer. In *ASME Turbo Expo 2013: Turbine Technical Conference and Exposition*, pages V01AT04A002–V01AT04A002. American Society of Mechanical Engineers, 2013.

[102] Giauque, A, SELLE, Laurent, Gicquel, L, Poinsot, T, Buechner, H, Kaufmann, P, and Krebs, W. System identification of a large-scale swirled partially premixed combustor using les and measurements. *Journal of Turbulence*, (6):N21, 2005.

[103] Flohr, Peter, Paschereit, Christian Oliver, and Bellucci, Valter. Steady cfd analysis for gas turbine burner transfer functions. *AIAA Paper*, 1346:6–9, 2003.

[104] Flohr, Peter, Paschereit, Christian Oliver, van Roon, Bart, and Schuermans, Bruno. Using cfd for time-delay modeling of premix flames. In *ASME Turbo Expo 2001: Power for Land, Sea, and Air*, pages V002T02A057–V002T02A057. American Society of Mechanical Engineers, 2001.

[105] Krebs, Werner, FLOHR, PATRICK, PRADE, BERND, and Hoffmann, Stefan. Thermoacoustic stability chart for high-intensity gas turbine combustion systems. *Combustion Science and Technology*, 174(7):99–128, 2002.

[106] Hettel, Matthias, Habisreuther, Peter, Büchner, Horst, Bockhorn, Henning, and Zarzalis, Nikolaos. Urans-modelling of flame transfer functions of turbulent premixed jet flames. In *ASME Turbo Expo 2004: Power for Land, Sea, and Air*, pages 517–526. American Society of Mechanical Engineers, 2004.

[107] Giauque, Alexis, Poinsot, Thierry, and Nicoud, Franck. Validation of a flame transfer function reconstruction method for complex turbulent configurations. In *14th AIAA/CEAS Aeroacoustics Con-

ference (29th AIAA Aeroacoustics Conference), AIAA-2008-3046.
AIAA/CEAS, Vancouver, Canada, 2008.

[108] Kostrzewa, Krzysztof. *Advanced computational methods in identifi-cation of thermo-acoustic systems.* PhD thesis, Universität Stuttgart, 2011.

[109] Hermeth, Sebastian. *Mechanisms affecting the dynamic response of swirled flames in gas turbines.* PhD thesis, Toulouse, INPT, 2012.

[110] Hermeth, Sebastian, Staffelbach, Gabriel, Gicquel, Laurent YM, and Poinsot, Thierry. Les evaluation of the effects of equivalence ratio fluctuations on the dynamic flame response in a real gas turbine combustion chamber. *Proceedings of the Combustion Institute*, 34 (2):3165–3173, 2013.

[111] Hermeth, Sebastian, Staffelbach, Gabriel, Gicquel, Laurent YM, Anisimov, Vyacheslav, Cirigliano, Cinzia, and Poinsot, Thierry. Bistable swirled flames and influence on flame transfer functions. *Combustion and Flame*, 161(1):184–196, 2014.

[112] Bohn, Dieter, Deutsch, Gregor, and Krüger, Uwe. Numerical pre-diction of the dynamic behaviour of turbulent diffusion flames. In *ASME 1996 International Gas Turbine and Aeroengine Congress and Exhibition*, pages V003T06A024–V003T06A024. American So-ciety of Mechanical Engineers, 1996.

[113] Ljung, Lennart. *System identification.* Springer, 1998.

[114] Polifke, W, Poncet, A, Paschereit, CO, and Döbbeling, K. Recon-struction of acoustic transfer matrices by instationary computational fluid dynamics. *Journal of Sound and Vibration*, 245(3):483–510, 2001.

[115] Polifke, Wolfgang and Gentemann, Alexander. Order and realizabil-ity of impulse response filters for accurate identification of acoustic

multi-ports from transient cfd. *Int. J. of Acoustics and Vibration*, 9 (3):139–148, 2004.

[116] Tay-Wo-Chong, Luis, Bomberg, Sebastian, Ulhaq, Ahtsham, Komarek, Thomas, and Polifke, Wolfgang. Comparative validation study on identification of premixed flame transfer function. *Journal of Engineering for Gas Turbines and Power*, 134(2):021502, 2012.

[117] Yang, Yang, Noiray, Nicolas, Scarpato, Alessandro, Schulz, Oliver, Düsing, K Michael, and Bothien, Mirko. Numerical analysis of the dynamic flame response in alstom reheat combustion systems. In *ASME Turbo Expo 2015: Turbine Technical Conference and Exposition*, pages V04AT04A048–V04AT04A048. American Society of Mechanical Engineers, 2015.

[118] Zhu, M, Dowling, AP, and Bray, KNC. Transfer function calculations for aeroengine combustion oscillations. *Journal of Engineering for Gas Turbines and Power*, 127(1):18–26, 2005.

[119] Motheau, Emmanuel, Selle, Laurent, and Nicoud, Franck. Accounting for convective effects in zero-mach-number thermoacoustic models. *Journal of sound and vibration*, 333(1):246–262, 2014.

[120] Kovasznay, Leslie SG. Turbulence in supersonic flow. *Journal of the Aeronautical Sciences (Institute of the Aeronautical Sciences)*, 20(10), 1988.

[121] Multiphysics, COMSOL. Acoustics module user guide version 4.3b. *User's Manual*, 2013.

[122] Lehoucq, Richard B, Sorensen, Danny C, and Yang, Chao. *ARPACK users' guide: solution of large-scale eigenvalue problems with implicitly restarted Arnoldi methods*. Siam, 1998.

[123] Fanaca, Dan, Alemela, Panduranga Reddy, Ettner, Florian, Hirsch, Christoph, Sattelmayer, Thomas, and Schuermans, Bruno. Determination and comparison of the dynamic characteristics of

a perfectly premixed flame in both single and annular combustion chambers. In *ASME Turbo Expo 2008: Power for Land, Sea, and Air*, pages 565–573. American Society of Mechanical Engineers, 2008.

[124] Alemela, Panduranga Reddy, Fanaca, Dan, Ettner, Florian, Hirsch, Christoph, Sattelmayer, Thomas, and Schuermans, Bruno. Flame transfer matrices of a premixed flame and a global check with modelling and experiments. In *ASME Turbo Expo 2008: Power for Land, Sea, and Air*, pages 11–19. American Society of Mechanical Engineers, 2008.

[125] Munjal, ML and Doige, AG. Theory of a two source-location method for direct experimental evaluation of the four-pole parameters of an aeroacoustic element. *Journal of Sound and Vibration*, 141(2): 323–333, 1990.

[126] Campa, Giovanni and Camporeale, Sergio Mario. Influence of flame and burner transfer matrix on thermoacoustic combustion instability modes and frequencies. In *ASME Turbo Expo 2010: Power for Land, Sea, and Air*, pages 907–918. American Society of Mechanical Engineers, 2010.

[127] ANSYS. Fluent 15.0 user's guide. *User's Guide*, 2014.

[128] Thompson, Kevin W. Time dependent boundary conditions for hyperbolic systems. *Journal of computational physics*, 68(1):1–24, 1987.

[129] Thompson, Kevin W. Time-dependent boundary conditions for hyperbolic systems, ii. *Journal of Computational Physics*, 89(2): 439–461, 1990.

[130] Poinsot, T J&amp and Lele, SK. Boundary conditions for direct simulations of compressible viscous flows. *Journal of computational physics*, 101(1):104–129, 1992.

[131] Polifke, Wolfgang, Wall, Clifton, and Moin, Parviz. Partially reflecting and non-reflecting boundary conditions for simulation of compressible viscous flow. *Journal of Computational Physics*, 213 (1):437–449, 2006.

[132] Nguyen, Phuc-Danh, Vervisch, Luc, Subramanian, Vallinayagam, and Domingo, Pascale. Multidimensional flamelet-generated manifolds for partially premixed combustion. *Combustion and Flame*, 157(1):43–61, 2010.

[133] Vreman, AW, Albrecht, BA, Van Oijen, JA, De Goey, LPH, and Bastiaans, RJM. Premixed and nonpremixed generated manifolds in large-eddy simulation of sandia flame d and f. *Combustion and Flame*, 153(3):394–416, 2008.

[134] Ramaekers, WJS, Van Oijen, JA, and de Goey, LPH. Stratified turbulent bunsen flames: flame surface analysis and flame surface density modelling. *Combustion Theory and Modelling*, 16(6):943–975, 2012.

[135] Donini, Andrea, Martin, SM, Bastiaans, RJM, van Oijen, JA, and de Goey, LPH. Numerical simulations of a premixed turbulent confined jet flame using the flamelet generated manifold approach with heat loss inclusion. In *ASME Turbo Expo 2013: Turbine Technical Conference and Exposition*, pages V01AT04A024–V01AT04A024. American Society of Mechanical Engineers, 2013.

[136] Donini, Andrea, Bastiaans, Robert JM, van Oijen, Jeroen A, and de Goey, L Philip H. The application of flamelet-generated manifold in the modeling of stratified premixed cooled flames. In *ASME Turbo Expo 2014: Turbine Technical Conference and Exposition*, pages V04BT04A022–V04BT04A022. American Society of Mechanical Engineers, 2014.

[137] Oijen, JA van and Goey, LPH De. Modelling of premixed laminar

flames using flamelet-generated manifolds. *Combustion Science and Technology*, 161(1):113–137, 2000.

[138] Ramaekers, WJS, Albrecht, BA, van Oijen, JA, de Goey, LPH, and Eggels, RGLM. The application of flamelet generated manifolds in modelling of turbulent partiallypremixed flames. *Fluent Benelux User Group Meeting, Wavre, Belgium, Oct*, 2005.

[139] ANSYS. Fluent 15.0 theory guide. *Theory Guide*, 2014.

[140] Andreini, Antonio, Facchini, Bruno, Innocenti, Alessandro, and Cerutti, Matteo. Flame transfer function identification and thermoacoustic analysis of an annular heavy-duty gas turbine combustor. In *22nd International Congress on Sound and Vibrations, Florence, Italy*. International Institute of Acoustics and Vibration (IIAV) and Associazione Italiana di Acustica (AIA), 2015.

[141] Auer, MP, Hirsch, T, and Sattelmayer, T. Influence of air and fuel mass flow fluctuations in a premix swirl burner on flame dynamics. *ASME Paper No. GT-2006-90127*, 2006.

[142] De Rosa, Alexander J, Peluso, Stephen J, Quay, Bryan D, and Santavicca, Domenic A. The effect of confinement on the structure and dynamic response of lean-premixed, swirl-stabilized flames. In *ASME Turbo Expo 2015: Turbine Technical Conference and Exposition*, pages V04AT04A017–V04AT04A017. American Society of Mechanical Engineers, 2015.

[143] De Rosa, Alexander J, Samarasinghe, Janith, Peluso, Stephen J, Quay, Bryan D, and Santavicca, Domenic A. Flame area fluctuation measurements in velocity-forced premixed gas turbine flames. In *ASME Turbo Expo 2015: Turbine Technical Conference and Exposition*, pages V04AT04A039–V04AT04A039. American Society of Mechanical Engineers, 2015.

[144] Güthe, F and Schuermans, B. Phase-locking in post-processing for pulsating flames. *Measurement Science and Technology*, 18(9):3036, 2007.

[145] Zimont, V.L., Moreu, V., Battaglia, V., and Modi, R. Rans and les modelling of the ge10 burner. *Energy and Power engineering*, 3: 607–615, 2011.

[146] Flohr, P and Pitsch, H. A turbulent flame speed closure model for les of industrial burner flows. In *Proceedings of the summer program*, pages 169–179, 2000.

[147] M. Cerutti, R. Modi, D. Kalitan, and K. K. Singh. Design improvement survey for NOx emissions reduction of a heavy-duty gas turbine partially premixed fuel nozzle operating with natural gas: experimental campaign. 2015.

[148] Innocenti, Alessandro, Andreini, Antonio, Giusti, Andrea, Facchini, Bruno, Cerutti, Matteo, Ceccherini, Gianni, and Riccio, Giovanni. Numerical Investigations of NOx Emissions of a Partially Premixed Burner for Natural Gas Operations in Industrial Gas Turbine. In *ASME Turbo Expo 2014: Turbine Technical Conference and Exposition*. American Society of Mechanical Engineers, 2014.

[149] Andreini, Antonio, Facchini, Bruno, Innocenti, Alessandro, and Cerutti, Matteo. Numerical Analysis of a Low NOx Partially Premixed Burner for Industrial Gas Turbine Applications. *Energy Procedia*, 45:1382–1391, 2014.

[150] Innocenti, Alessandro, Andreini, Antonio, Facchini, Bruno, Cerutti, Matteo, Ceccherini, Gianni, and Riccio, Giovanni. Design Improvement Survey for NOx Emissions Reduction of a Heavy-Duty Gas Turbine Partially Premixed Fuel Nozzle Operating With Natural Gas: Numerical Assessment. *Journal of Engineering for Gas Turbines and Power*, 138(1):011501, 2016.

[151] Poinsot, Thierry and Veynante, Denis. *Theoretical and numerical combustion.* RT Edwards, Inc., 2005.

[152] Bade, Stefanie, Wagner, Michael, Hirsch, Christoph, Sattelmayer, Thomas, and Schuermans, Bruno. Influence of fuel-air mixing on flame dynamics of premixed swirl burners. In *ASME Turbo Expo 2014: Turbine Technical Conference and Exposition*, pages V04AT04A023–V04AT04A023. American Society of Mechanical Engineers, 2014.

[153] Yang, Yang, Noiray, Nicolas, Scarpato, Alessandro, Schulz, Oliver, DÃ¼sing, K Michael, and Bothien, Mirko. Numerical Analysis of the Dynamic Flame Response in Alstom Reheat Combustion Systems. In *ASME Turbo Expo 2015: Turbine Technical Conference and Exposition*, pages V04AT04A048–V04AT04A048. American Society of Mechanical Engineers, 2015.

[154] Huber, Andreas and Polifke, Wolfgang. Impact of fuel supply impedance on combustion stability of gas turbines. In *ASME Turbo Expo 2008: Power for Land, Sea, and Air*, pages 887–899. American Society of Mechanical Engineers, 2008.

[155] Huber, A and Polifke, W. Dynamics of practical premixed flames, part I: model structure and identification. *International journal of spray and combustion dynamics*, 1(2):199–228, 2009.

[156] Huber, A and Polifke, W. Dynamics of practical premixed flames, part II: identification and interpretation of CFD data. *International journal of spray and combustion dynamics*, 1(2):229–249, 2009.

[157] Knudsen, E and Pitsch, H. Large-Eddy Simulation for Combustion Systems: Modeling Approaches for Partially Premixed Flows. *Open Thermodynamics Journal*, 4:76–85, 2010.

[158] Kern, Matthias, Marinov, Svetoslav, Habisreuther, Peter, Zarzalis, Nikolaos, Peschiulli, Antonio, and Turrini, Fabio. Characteristics of an ultra-lean swirl combustor flow by les and comparison

to measurements. In *ASME 2011 Turbo Expo: Turbine Technical Conference and Exposition*, pages 321–330. American Society of Mechanical Engineers, 2011.

[159] Mazzei, Lorenzo, Andreini, Antonio, Facchini, Bruno, and Turrini, Fabio. Impact of swirl flow on combustor liner heat transfer and cooling: A numerical investigation with hybrid reynolds-averaged navier stokes–large eddy simulation models. *Journal of Engineering for Gas Turbines and Power*, 138(5):051504, 2016.

[160] Andreini, Antonio, Caciolli, Gianluca, Facchini, Bruno, Picchi, Alessio, and Turrini, Fabio. Experimental investigation of the flow field and the heat transfer on a scaled cooled combustor liner with realistic swirling flow generated by a lean-burn injection system. *Journal of Turbomachinery*, 137(3):031012, 2015.

[161] Andreini, A, Facchini, B, Mazzei, L, Bellocci, L, and Turrini, F. Assessment of aero-thermal design methodology for effusion cooled lean burn annular combustors. In *ASME Turbo Expo 2014: Turbine Technical Conference and Exposition*, pages V05CT18A012–V05CT18A012. American Society of Mechanical Engineers, 2014.

[162] Fondelli, Tommaso. CFD analysis of a low emissions aero-engine combustion system, 2011-2012.

[163] Jannis Gikadi, Thomas Sattelmayer. KIAI EU project, d2.2.1 experimental determination of flame transfer function, 2013.

[164] Gikadi, Jannis. *Prediction of acoustic modes in combustors using linearized Navier-Stokes equations in frequency space*. PhD thesis, Universität München, 2013.

[165] Lefebvre, Arthur. *Atomization and sprays*, volume 1040. CRC press, 1988.